1-1-2011

Control and Interface Design for Cost Reduction of a Low Power Grid-Connected Wind-Photovoltaic System

Shravana Kumar Musunuri

CONTROL AND INTERFACE DESIGN FOR COST REDUCTION OF A LOW POWER GRID-CONNECTED WIND-PHOTOVOLTAIC SYSTEM

By

Shravana Kumar Musunuri

A Dissertation
Submitted to the Faculty of
Mississippi State University
in Partial Fulfillment of the Requirements
for the Degree of Doctor of Philosophy
in Electrical Engineering
in the Department of Electrical and Computer Engineering

Mississippi State, Mississippi

April 2011

CONTROL AND INTERFACE DESIGN FOR COST REDUCTION OF A LOW POWER GRID-CONNECTED WIND-PHOTOVOLTAIC SYSTEM

By

Shravana Kumar Musunuri

Approved:

Herbert L. Ginn III Associate Professor of Electrical Engineering, University of South Carolina (Director of Dissertation)	Yong Fu Assistant Professor of Electrical and Computer Engineering (Major Advisor)
Randolph Follett Assistant Professor of Electrical and Computer Engineering (Committee Member)	Anurag K. Srivastava Assistant Professor of Electrical Engineering and Computer Science, Washington State University (Committee Member)
Sarah A. Rajala Dean of Bagley College of Engineering	James E. Fowler Professor and Graduate Program Director of Electrical and Computer Engineering

Name: Shravana Kumar Musunuri

Date of Degree: April 30, 2011

Institution: Mississippi State University

Major Field: Electrical Engineering

Major Professor: Herbert L. Ginn III

Title of Study: CONTROL AND INTERFACE DESIGN FOR COST REDUCTION OF A LOW POWER GRID-CONNECTED WIND-PHOTOVOLTAIC SYSTEM

Pages in Study: 175

Candidate for Degree of Doctor of Philosophy

The ever increasing demand for electricity has driven society toward the installation of new generation facilities. Concerns such as high costs associated with installation of new facilities, environmental pollution, higher transmission and distribution losses, depleting fossil fuels has created a lot of interest in exploring the renewable energy sources for generation, particularly near the load sites. Accordingly, emphasis has been put on Wind, and Photovoltaic (PV) energy systems. A study on the operational characteristics of these systems reveals that the power generation is high at certain optimal points and recognizing these optimum points and operating the system accordingly is an interesting and important part of the system design. Further, a hybrid Wind- PV system has higher reliability and generation capability when compared to either source alone, and as a result many such hybrid systems with an additional energy storage backup for increased reliability have been proposed. While the systems with energy storage are reported to have satisfactory performance, the energy storage component is typically found to incur the highest cost, requiring frequent maintenance and hence acts as a deterrent for increasing the renewable energy generation. Particularly,

for small grid connected applications like shopping malls, office buildings, etc. any additional power that could not be provided by the hybrid system could be provided by the grid, and in case the power generation is higher it could be sent to the grid. For cases like this, it would be ideal if systems could be developed without energy storage, and maximum possible power could be extracted from the hybrid energy sources. Also, the power quality concerns posed due to the random nature of the power generated from the hybrid system, is an important issue that must be addressed. The conventional control methods used typically require overly sized component ratings, resulting in the degradation of the dynamic performance while adding to the cost of the system. This dissertation addresses these issues by proposing faster maximum power extraction algorithms from the hybrid renewable energy system, and proposes new control architecture for improving the output power quality to the grid.

DEDICATION

This work is dedicated to my parents

ACKNOWLEDGEMENTS

First of all I would like to acknowledge God and my parents for guiding me throughout my life. I would like to express deepest gratitude to my dissertation director Dr. Herbert L. Ginn III for his support, guidance, and encouragement throughout this research. I would also like to extend my gratitude to Dr. Yong Fu for agreeing to be my major advisor, and to committee members Dr. Randolph Follett and Dr. Anurag Srivastava for serving on my committee to improve this work.

I would like to thank US Department of Energy (DoE) for providing the financial support.

I would also like to thank my brother and my friends for their support throughout my academic career without which I would not have dreamt about this. And very importantly I would also like to thank my wife Purnachandrika for her constant support and encouragement.

TABLE OF CONTENTS

Page

LIST OF TABLES

LIST OF FIGURES

CHAPTER I

INTRODUCTION

This chapter gives a brief background on the necessity of renewable energy systems and in particular the Wind and Photovoltaic renewable energy systems. Also, the objectives of this dissertation and the outline are mentioned.

1.1 Topic Background

Electrical energy has become one of the most important forms of energy that mankind finds very much required for his continuous growth. After the discovery of electrical power, mankind has made remarkable progress in his way of living and over the past century the electrical power generation and consumption has increased several manifolds. Figure 1.1 shows the increase in worldwide electrical energy consumption over the past three decades, with the worldwide installed electricity generating capacity expected to increase from 3,626 GW in 2010 to 5,495 GW in 2025 at the rate of 2.2-percent average annual growth rate [1].

As of 2008, about 30% of world total electricity demand is consumed by US and is expected to increase [1]. Moreover, the electricity demand from emerging economies like China and India is increasing even faster. To meet this growing demand for electrical power, more generation capacity worldwide and in US is necessary.

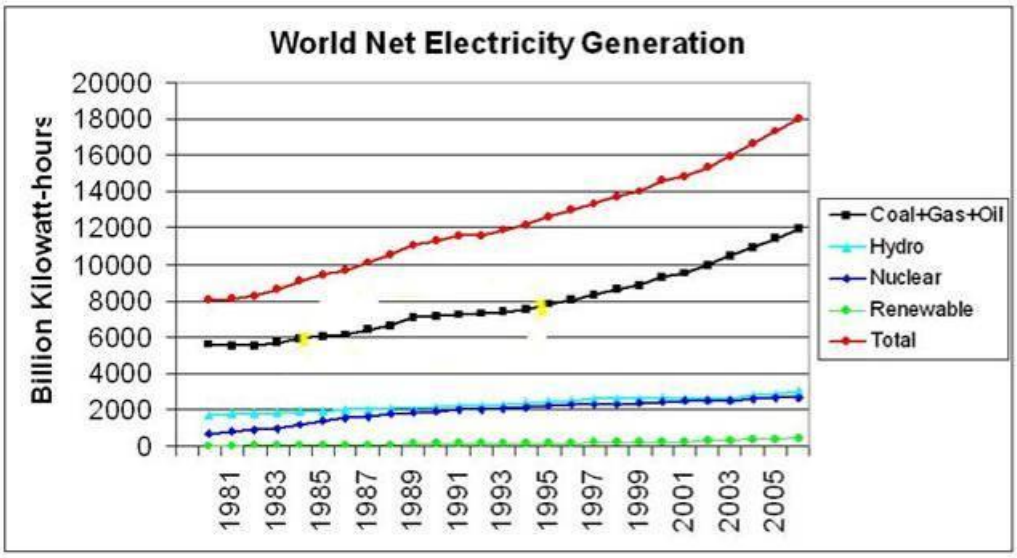

Figure 1.1 World Net Electricity Generation

Electricity can be generated in many ways from various energy sources. Electric power can be generated by conventional thermal power plants using fossil fuels like coal, oil, natural gas etc, hydropower stations, and other alternative power generating units such as wind turbine generators, photovoltaic arrays, fuel cells, biomass power plants, geothermal power stations, etc. Figure 1.2 shows the US net electricity generation by fuel type in 2010 [2].

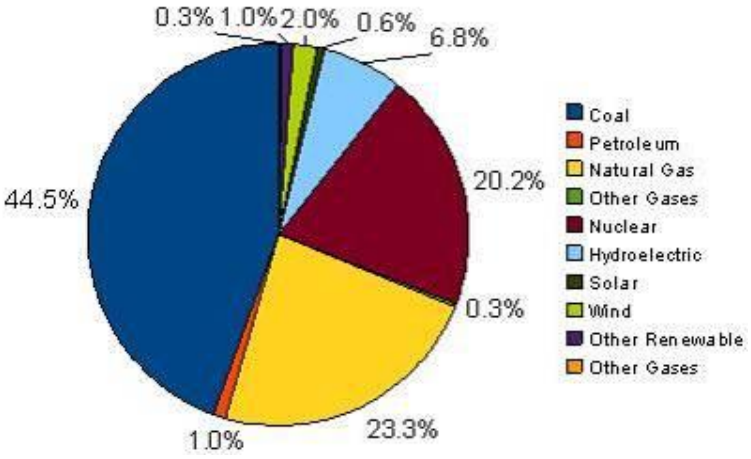

Figure 1.2 US Electricity Generation by Fuel Type

It is clear from this figure that more than 80% of US electricity generation is still contributed by the conventional fossil-fuel thermal power plants, nuclear and hydro power plants [2]. Compared to natural gas and oil, coal is cheap for electricity generation. However, if the cost for reducing emissions is taken into account, the actual price of generating electricity from coal would be much higher. The main problems associated with the fossil fuel based electrical power generation are the growing environmental concerns due to the harmful emissions as shown in Figure 1.3 [3], depletion of the existing resources, and certain fossil fuels (like oil, petroleum) are abundantly only in certain geographical regions in the world which is a cause of concern for political reasons. Further, growing concerns regarding increasing costs for installation of new facilities, safety concerns (for nuclear power plants), ecological damage and cost concerns (for hydro power plants) make them highly unattractive. Also, since many of these generating stations need to be located far from the actual load points (i.e., far from residential and commercial places), they involve higher transmission and distribution losses. Hence, recently much emphasis has been laid on the generation of power from alternate/renewable energy sources.

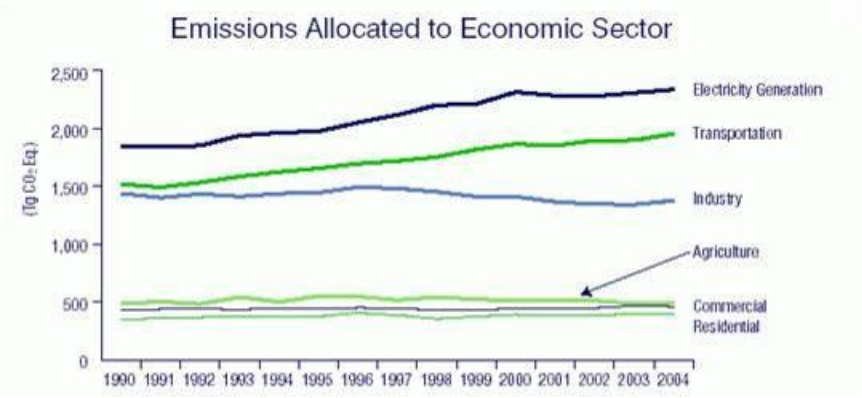

Figure 1.3 Harmful Emissions for Various Economic Sectors

On the other hand, compared with conventional electricity generation technologies, renewable energy resources are not only abundantly available but are also environmental friendly without causing any harmful emissions. Also, since the renewable energy sources are generally abundantly available, they are often located close to the actual load centers and hence the associated transmission and distribution losses, and costs involved are minimized. According to the data of 2000, the U.S. wind resources can produce more electricity than the entire nation would use [2] and the total solar energy from sun in a day at the earth surface is about 1000 times more than the all fossil fuels consumption [2]. Inspite of being that abundantly available, it could be seen from Figure 1.2 that the the portion of the electricity generated from renewable/alternative sources is very small.

Compared to the conventional centralized power plants, the generating stations that are close to the actual load site (Distributed Generation, DG) are smaller in size and typically are alternate/renewable energy based generating systems. Due to steady progress in power deregulation, utility restructuring, and tight constraints imposed on the construction of new transmission lines for long distance power transmission, DG applications are expected to increase in the future. Distribution generation systems are typically less than 30 MW and are often used in standby power, combined heat and power (CHP), peak shaving, grid support, and stand alone operation modes. Standby power is usually used for applications where any interruption in electrical power is unacceptable, like for hospitals, electronics manufacturing companies, water pumping stations etc. Those types of customers, such as large office buildings and hospitals, which can utilize both power and thermal energy from power generation process, make use of CHP. Peak shaving is a good solution for customers who need to reduce their

energy demand during high cost peak periods. Typical customers are industries that have a high cyclic power demand such as foundries. Grid support will be used to provide additional power support during peak power usage times and in some cases selling the excess power generated back to the grid thereby reducing the requirement for power generation from other conventional sources. Stand-alone DG systems are ideal for customers that are isolated from the power grid as in remote applications.

The most commonly used DG systems are microturbines, fuel cells, wind turbines, photovoltaics and small combustion turbines. Among these technologies, wind and photovoltaic systems are truly renewable and their resources are abundantly available in nature. As was mentioned before, inspite of being abundantly available in nature, the percentage of wind and photovoltaic generation systems in the world is still very small. This is mainly due to the intermittent nature of the wind blow, and the unavailablity of the sun radiation at nights and during cloudy or rainy days. This issue restricted the usage of these two sources for power generation. However, the improvements in the wind turbine and photovoltaic cell manufacture technologies, advancements in electric machines and power electronics control has made it possible for increasing their penetration into the power grid. Hence, this dissertation addresses these two renewable energy sources.

Electricity generation from wind turbines is an established technology with power generation ranging from small 1 Kilowatt systems at the distribution level to large wind farms of tens of Megawatts at the transmission level. Wind energy has been one of the fastest growing energy sources in the world and there have been many technological advances in the wind power industry, making this source of energy more affordable. The worldwide electricity generation capacity from Photovoltaics (PV) has been increasing at

an annual rate of 20% [3] with typical PV systems ranging from small 1kW system to large PV fields of hundreds of Kilowatts are used as a DG system.. Though the efficiency of a PV system is only around 11-15%, [4] and is expensive, the developments and breakthroughs in new cell materials and power electronics technologies has enabled its increasing usage. A study on the operational characteristics of the Wind and PV systems reveal that the power generation and efficiencies are high at certain optimal points which vary with the atmospheric conditions (wind blow or sun radiation). It was found in [4] [6] that by using advanced control methods about 10-15% more power can be obtained from both PV and wind systems respectively if they are operated at these optimum points. Hence, it is has become important to recognize these optimum points and operate the system accordingly.

While there are many Wind or PV stand-alone systems already in existence [6] [7], as mentioned before, one of the main issues with these renewable sources is that their power generation varies due to the intermittent nature of the wind and solar radiation. However, the complementary nature of the Wind and PV systems (since in the morning we have more sunshine and lesser wind in general, and at night more of wind and no sunshine) has created a lot of interest in adopting a hybrid Wind-PV system. The hybrid system has higher reliability and generation capabilities when compared to either source alone. As a result many such hybrid systems were proposed for stand-alone and grid connected operation with an additional energy storage backup for increased reliability and better power quality [8] [9] [10].

While the hybrid system with energy storage is reported to have satisfactory performance, the energy storage component is typically found to incur the highest cost. Of the various energy storage options available, like fuel cell, ultra capacitor, battery,

flywheel etc., battery energy storage is ideal for small hybrid power systems keeping in consideration the cost and performance. Battery selection is typically made taking into consideration the required battery capacity, number of charge/discharge cycles, operating temperature etc. Typically, for a small grid connected hybrid power system applications (for less than 100 kW) the popular battery technologies used are: lead acid, NiMH and Lithium Ion. Figure 1.4 shows the current energy storage cost estimates for various technologies. It can be seen from Figure 1.4 that the battery (Li-ion in this case) cost is about $1100/kW [11]. This would be a significant cost for a small grid connected hybrid power system like the one under consideration. The cost would further increase if the battery power converters, sensors etc. are considered. The cost of the system would further increase if the installations costs, annual maintenance costs, frequent replacements (which for a battery needs to be done once every 2 years for safety and improved performance) are considered which form a significant part [12]. All these costs add up to deter the benefits obtained from having increased renewable power generation into the distribution grid for small grid connected applications with energy storage. This increases the cost of the entire system and hence acts as a deterrent for increasing the penetration of renewable energy systems into the grid. Also, the frequent maintenance of the energy storage devices like batteries is problematic. Further, for applications where there are multiple generation sources like in Cooling Heat and Power (CHP) systems, or for small industrial grid connected systems like shopping malls, office buildings, small businesses etc. any additional power that could not be provided by the hybrid system without the energy storage could be provided by the grid and if the power generation from the sources is higher than the load demand it could be sent to the grid. For cases like this where the grid acts as a backup generation, it would be ideal if systems could be

developed without energy storage. This would help in reducing the cost of the system and it acts as an incentive for increasing the penetration of renewable energy into distribution systems and will justify the switchover from conventional to alternative ways for electric power generation.

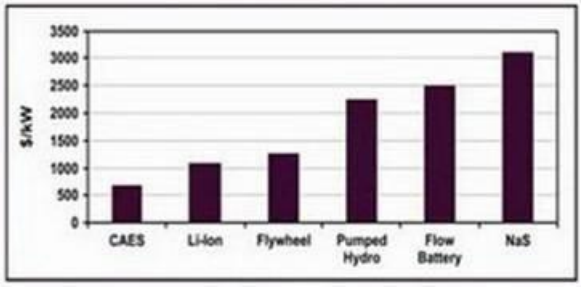

Figure 1.4 Energy Storage Costs Comparison [11]

In addition to this, the hybrid generation system has to meet the various grid interconnection standards as mentioned in the Appendix A before the system is connected to the distribution network. One of the issues with the random nature of the power generated from the Wind and PV systems is that the power quality concerns are a major problem and must be addressed. Further, the optimization of the component ratings of the hybrid system, especially the dc bus capacitor, is very important. The large electrolytic dc bus capacitors that are often used for interconnecting the hybrid energy system to the grid increases the cost and response time. Hence a proper design of the system that maximizes the power generation while addressing the power quality concerns and cost is very important.

1.2 Dissertation Objective

As was mentioned in the background section, it would be very beneficial if the Wind-PV hybrid system for grid connected small industrial applications and businesses

can be designed to operate efficiently, without any energy storage, by extracting maximum power from the renewable energy sources while optimizing the ratings of the system components thus reducing the cost of the system. Such a system will be an incentive for small businesses to opt for renewable energy sources thereby reducing the electricity costs incurred. From a power system perspective, this would allow the losses in the system to decrease and the reduction in harmful emissions from fossil fuel based generation. Thanks to the recent developments in the power electronics controls and power semiconductor technologies, easier and more flexible grid interconnection can be achieved using modern power electronics converters. Hence, the control architecture could be further improved to achieve these goals.

The goal of this research is to determine the appropriate system topology and control architecture for a hybrid Wind – PV system of 5- 50 Kilowatts power range to meet the requirements mentioned above. It is to be noted that the proposed control and interface design for the hybrid Wind-Photovoltaic system in this dissertation mainly addresses small grid connected individual wind turbine applications at the distribution side and not the large wind farm applications.

The main objectives and contributions of the dissertation are summarized in the following tasks:

Task 1: Hybrid Wind- Photovoltaic System Modeling and Simulation. Modeling and simulation of the Wind Turbine, Photovoltaic modules and determining the appropriate architecture, generator and converter topology for both Wind and PV systems.

Task 2: *Maximum Power Extraction from Hybrid System*. Review the existing algorithms and propose a modified maximum power extraction algorithm for the selected system.

Task 3: *Reduction of DC Bus Voltage Ripple Sensitivity*. Develop modified control architecture for reducing the sensitivity of dc bus voltage ripple caused by variations in the Wind – PV hybrid system, and local loads. This will reduce energy storage requirements and an optimal dc bus capacitor size will be investigated.

1.3 Dissertation Outline

The dissertation is organized as follows: Chapter II gives the background of wind energy system and the selection and modeling of various subsystems of the system. Chapter III gives the background of Photovoltaic energy system and the selection and modeling of various subsystems of the Photovoltaic energy system. Chapter IV highlights the selected architecture for the hybrid Wind – Photovoltaic renewable energy system. Chapter V deals with the algorithm development for maximum power extraction from the wind and photovoltaic systems. Chapter VI deals with the reduction of dc bus voltage ripple sensitivity. Chapter VII includes the conclusions and future work. The various grid interconnection standards and the discussion of various control strategies of the LCL filter are provided in the appendix.

CHAPTER II

WIND ENERGY SYSTEM MODELING

2.1 Background

Over the past several years, wind energy has been one of the fastest growing energy sources in the world. Wind energy not only has economical impact on our society, but it has a big environmental and social impact as well. The use of wind energy reduces the consumption of fossil fuels and the consequent harmful emissions. It also reduces the United States's dependence on foreign oil. This chapter gives a brief history of wind turbines and discusses the modeling and selection of various wind energy system subsystems.

2.2 History of Wind Turbines

Wind energy systems have been around for over a thousand years. The first windmills on record were built by the Persians in approximately 900 AD [13] where they were mainly used for mechanical tasks like water pumping, grinding grain etc. These early windmills had four blades and were built on posts so that the windmill could be turn to face the wind. Until before the industrial revolution, wind was a substantial source of energy, particularly in Europe. Even though wind energy popularity decreased after the industrial revolution, many of the earlier designs were later incorporated into electricity generating wind turbines in the 20^{th} century [13]. Over the last century, major improvements were made in the efficiency and operation of these windmills that benefitted the generation of electricity.

Before the beginning of the rural electrification program in the United States in 1920, there was some development of early wind turbine generator systems particularly in the rural areas which are not connected to the utility grid. These systems were used mainly for recharging batteries with a few kilowatts power range capability. After the rural electrification, the US central electrical grid was expanded and electricity was more accessible to rural places through long transmission lines from central power stations. This led to the decrease in wind power generation as electricity at a much lower cost was available from central power stations which were mainly fossil fuel, hydro power or oil based. However, the oil price shock in the 1970s resulted in the consensus to use lesser oil for generation and transportation purposes and this led to a renewed interest in renewable energy technologies, particularly the wind turbines.

While a lot of research has been done on the wind power generation since many years before, it was only since 1980s that the wind turbine, and generator technology has become mature enough to efficiently and reliably produce electricity. Since then, many wind energy systems have been developed and the technological advances have been phenomenal. In the last two decades, wind power market continued to grow at an average cumulative rate of nearly 30% [2], becoming one of the fastest growing markets in the world. Breakthroughs in the turbine operation, generator design and control, power electronics interface, governmental policies has resulted in the wind power generation to increase. In the past two decades, the global wind energy capacity has increased from 3.5 GW to almost 160 GW as shown in Figure 2.1.

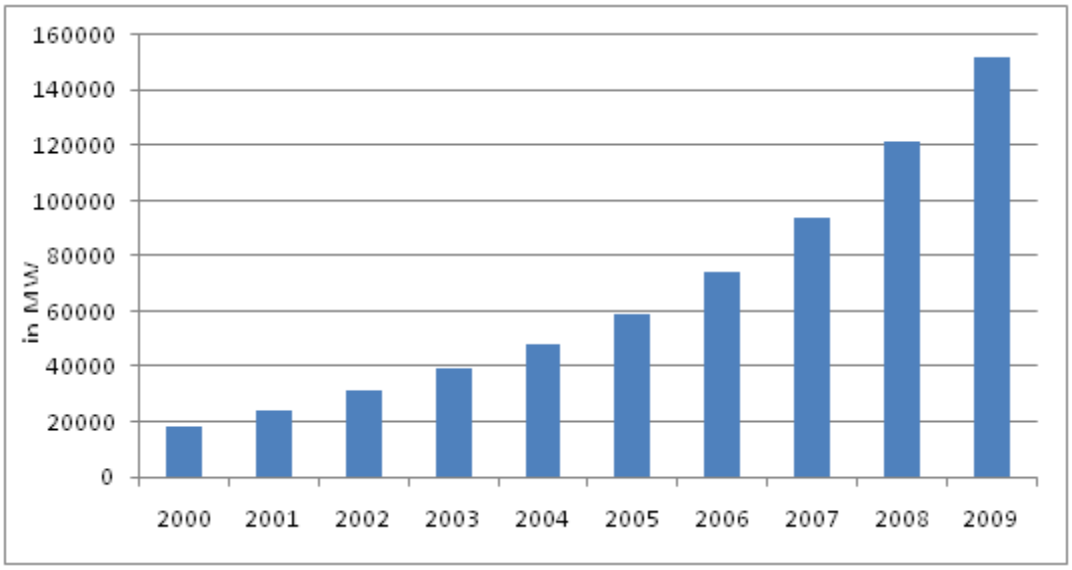

Figure 2.1 World Total Installed Wind Capacity in MW over the years

In the United States, wind power capacity in the last decade has increased from 2554 MW to 13149 MW as shown in Figure 2.2 accounting for approximately 18% [2] of the global wind power installations. In the present days, wind power generation can be commercialized and penetration into the present power systems is increasing particularly with interest in distributed generation, and the cost of electrical power from wind has dropped from $0.8/kWh in the early 1980s [2] to about $0.04/kWh today [2] for utility-scale turbines. An interesting observation that could be made from Figure 2.2 is that over the past few years, particularly from 2004, the installed wind capacity in USA has been increasing which is mainly attributed to the federal production tax credits [2] (unlike in prior years where when the tax credit is removed the installed capacity has dropped e.g., in 1998, 2000, 2002) and recognizing the capability and importance of wind power generation.

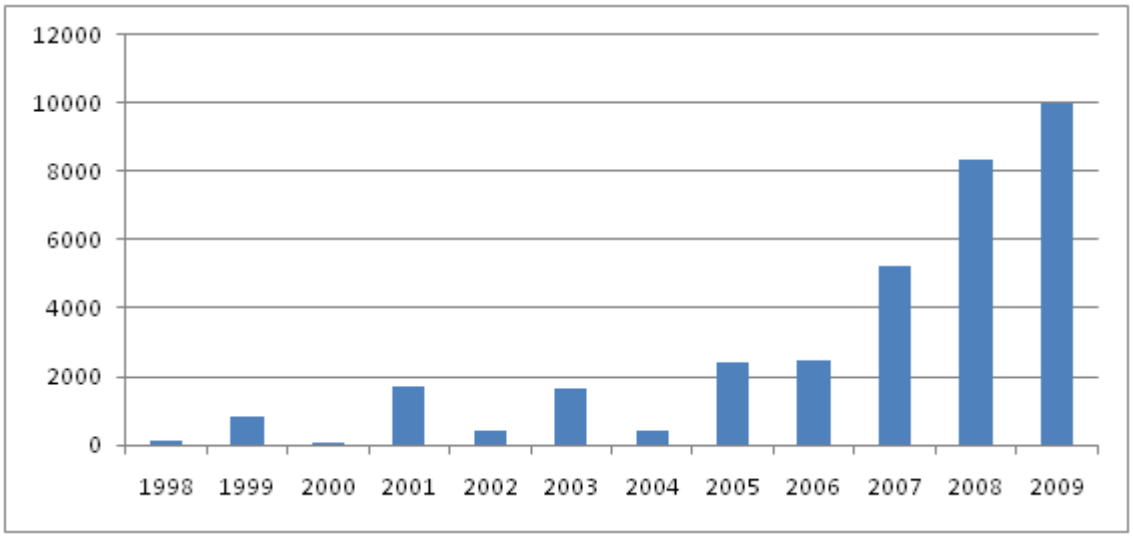

Figure 2.2 USA Total Installed Wind Capacity in MW over the years

Compared to the earlier designs, modern turbines are more reliable, efficient, cost-effective, and the turbine sound has been reduced. Although many improvements have been made, more research work is still needed to make wind power more competitive by reducing the manufacturing and installation cost, control strategies to maximize power extraction from the wind, development of new structurally efficient wind turbine blades, to make wind power generation a more reliable source of energy in the future.

2.3 Wind System Modeling

The wind energy system consists of a wind turbine connected to an electrical generator through a drive train, and the output of the generator is connected to the load through a power electronic interface. Figure 2.3 shows the wind energy system layout. As discussed in great detail in the next sections, there are several options for the type of wind turbine to be used, generator choice, selecting the appropriate power electronics interface

technology. The following sections describe the modeling of wind turbine and selection of the components of the wind system.

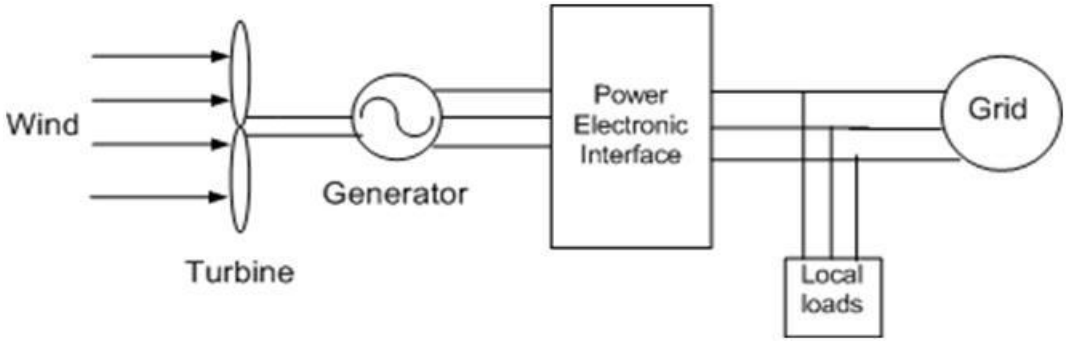

Figure 2.3 Wind Energy System

2.3.1 Wind Turbine Modeling

The wind turbine blades extract energy from moving air and convert it to rotational energy. Wind turbines can be broadly classified into horizontal axis and vertical axis types based on the axis of rotation, with the modern wind turbines mostly are of horizontal type. Figure 2.4 shows the vertical axis wind turbine and Figure 2.5 shows the horizontal axis wind turbine. In a horizontal-axis wind turbine the generator and gearbox are normally located in the nacelle. It has a high wind energy conversion efficiency, self-starting capability, and access to stronger winds due to its elevation from the tower. However, the disadvantages are high installation cost, need for a stronger tower to support the nacelle and rotor blade, and longer cables to connect the top of the tower to the ground [15].

In a vertical axis turbine the spin axis is perpendicular to the ground with the wind turbine vertically mounted, and the generator and gearbox located at the base [15]. Compared to horizontal-axis, the vertical axis turbines have reduced installation cost, and maintenance is easier. However the major drawback of the vertical wind turbine is that it

has low wind energy conversion efficiency, about half of the efficiency of horizontal axis wind turbines axis turbines and have high torque fluctuations with each revolution. Hence, horizontal wind turbines are mainly used, and are used in this dissertation.

Horizontal axis wind turbines can be further classified based on the rotor orientation (upwind or downwind of the tower), hub design, rotor control (pitch or stall), number of blades, and their yaw control system [16].

Figure 2.4 Vertical Axis Wind Turbine [5]

Figure 2.5 Horizontal Axis Wind Turbine [5]

Modern wind turbine designs allow the control of the rotor power and speed. The design allows for different rotor blade designs that optimize the converter and achieve higher efficiencies [16]. Figure 2.6 shows the main components of a horizontal axis modern wind turbine. The main components of a wind turbine are the rotor, the drive train, generator, nacelle and yaw system, tower and foundation, turbine control system and electrical connection system. The rotor is formed by the hub and blades of the wind turbine. The drive train consists of a low speed shaft, a gearbox, and high speed shaft on the generator side. The drive train also includes support bearings, couplings, and mechanical brakes. In some cases the generator is connected directly to the rotor, therefore no gearbox is used. The generator converts the mechanical power in the shaft to electrical power. The nacelle is the cover that protects the drive train and generator from the weather and the yaw system keeps the rotor shaft in alignment with the wind. This

system is controlled by an automatic control system that has a sensor that detects the direction of the wind and it then uses electric motors to rotate the nacelle to face the wind. Other electrical components are needed for the wind turbine connection to the electrical grid including cables, switchgear, transformers, power electronic converters, and in some cases power factor correction capacitors.

2.3.1.1 Power Extracted from Wind

From the kinetic energy relation of a moving object, the power in the air stream assuming a constant wind velocity is given as:

$$P_{\text{kinetic energy}} = \frac{1}{2} mv^2 \tag{1}$$

where m is the mass flow rate per second, v is the wind speed in m/sec.

When the air passes through the turbine of cross-sectional area A, the power in the air is given by:

$$P_{\text{wind}} = \frac{1}{2} \rho A v^3 \tag{2}$$

where ρ is the air density.

The mechanical energy which the wind turbine extracts from the airflow will be equal to the power difference of the air stream before and after the wind turbine [16]:

$$P_{\text{wind}} = \frac{1}{2} \rho A_1 v_1^3 - \frac{1}{2} \rho A_2 v_2^3 \tag{3}$$

where A_1 and A_2 are the cross-sectional areas before and after the turbine, and v_1 and v_2 are the wind speeds before and after the turbine.

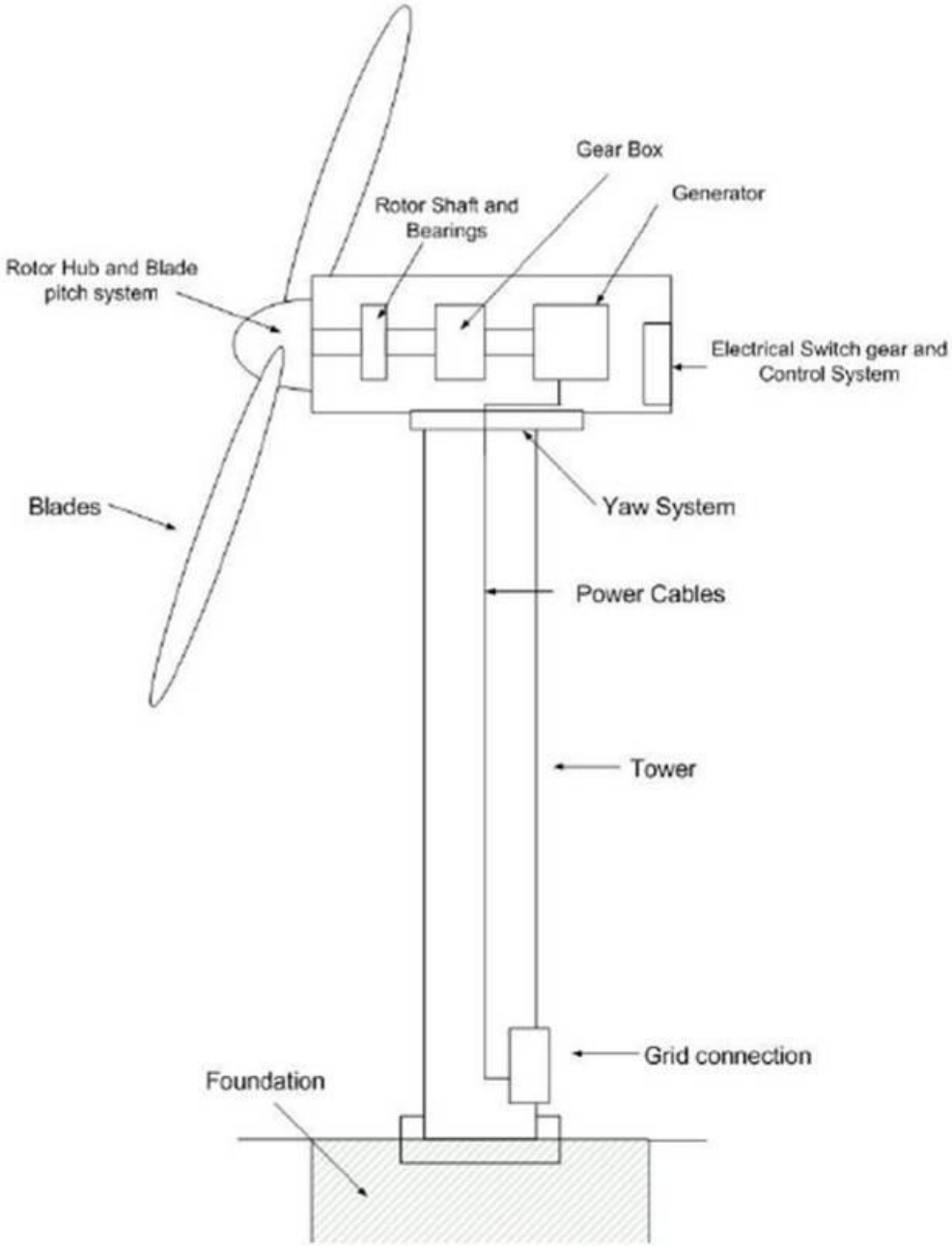

Figure 2.6 Horizontal Axis Wind Turbine Components [16]

Using the law of conservation of momentum, the force exerted by the wind on the turbine is given by [16]:

$$F = \dot{m}\,(v_1 - v_2) \tag{4}$$

and the extracted mechanical power is:

$$P_{mech} = F v' = \dot{m}\,(v_1 - v_2) \tag{5}$$

where v' is the air flow velocity.

By comparing the above two equations, the relationship for the flow velocity v' [16] is obtained as:

$$v' = \frac{1}{2}(v_1 - v_2) \tag{6}$$

and the mechanical power output of the wind turbine can then be expressed as:

$$P_{mech} = \frac{1}{4}\rho A(v_1^2 - v_2^2)(v_1 + v_2) \tag{7}$$

The ratio between the mechanical power extracted by the turbine P_{mech} given by (7) and the power contained in the air stream that passes through the same area P_{wind} given by (2) is called the *"power coefficient"* or "*performance coefficient*" Cp. From (7), a plot of the theoretical maximum performance coefficient also known as *Betz factor* is obtained and is as shown in Figure 2.7.

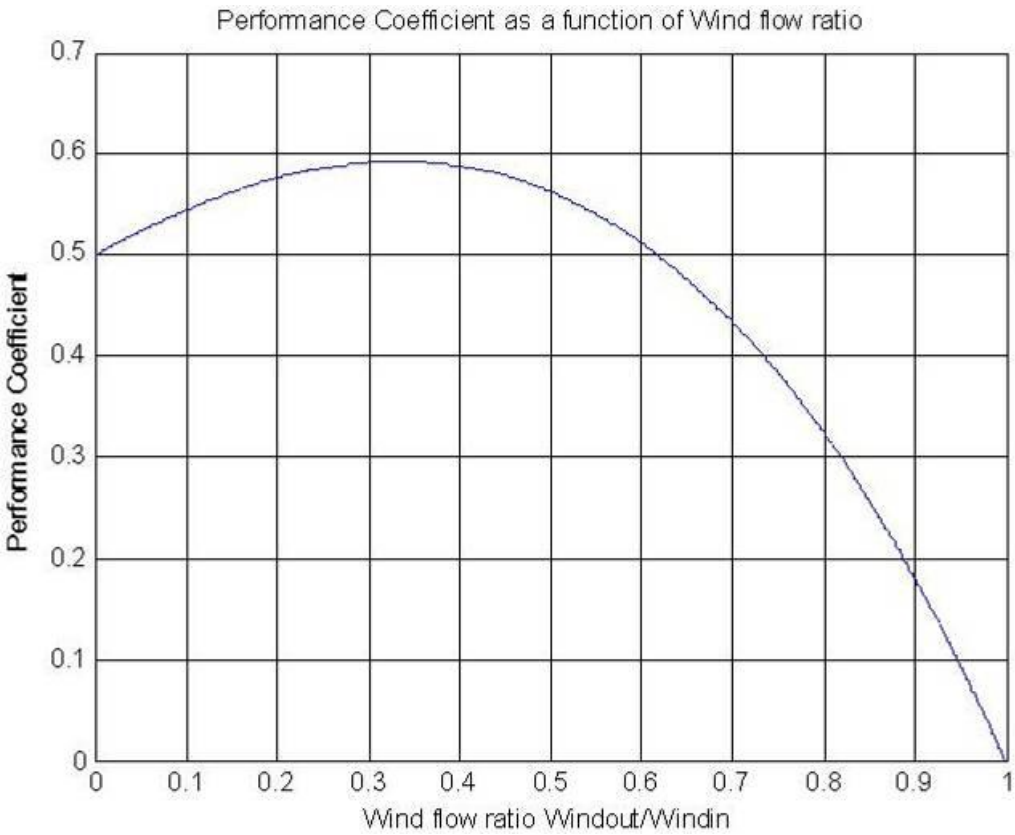

Figure 2.7 Performance Coefficient as function of Wind flow ratio

It can be seen from Figure 2.7 that the maximum theoretical performance coefficient is 0.593 i.e., around 59.3% of the wind power can only be converted into useful mechanical power. In real cases, the wind turbine will always have a smaller maximum power coefficient than the Betz factor [16]. This is due to many aerodynamic losses that depend on the rotor design and construction (number of blades, weight, stiffness, etc). The power coefficient is also dependent on the tip speed ratio λ and the blade pitch angle β of the turbine. The pitch angle is the angle between the plane of rotation and the blade cross-section chord [16]. The tip speed ratio of a wind turbine is defined as the ratio of linear speed of the turbine to the wind velocity and is given by:

$$\lambda = \frac{rw}{v} \tag{8}$$

where ω is the angular velocity of the rotor, r is the rotor radius in meters, and υ is the wind speed. Typically, the power coefficient can be obtained by manufacturer data or from look up tables and can be approximated using an analytical function given by [16]:

$$C_p = C_1 \left(\frac{C_2}{\Lambda} - C_3\beta - C_4 \right) e^{\frac{-C_5}{\Lambda}} + c_6\lambda \tag{9}$$

The coefficients c_1-c_6 and x vary from turbine to turbine and depend on the wind turbine rotor and blade design. The parameter $1/\Lambda$ is defined as:

$$\frac{1}{\Lambda} = \frac{1}{(\lambda+0.08\beta)} - \frac{0.035}{(1+\beta^3)} \tag{10}$$

From equations (9) and (10) we get the relation between the turbine power coefficient and tip speed ratio. Figure 2.8 shows the plot of variation of power coefficient with the turbine tip speed ratio, for the blade pitch angle of 0 degrees and the coefficients c_1-c_6 and x values are given in chapter 5. Figure 2.9 shows the plot for varying blade pitch angles. It can be seen that as the blade pitch angle is varied the power extracted from the wind is also changed accordingly.

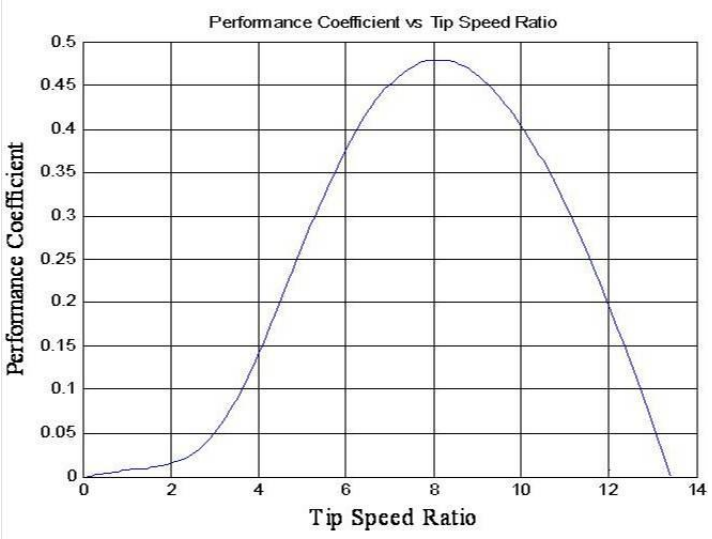

Figure 2.8 Variation of Power Coefficient with Tip Speed Ratio

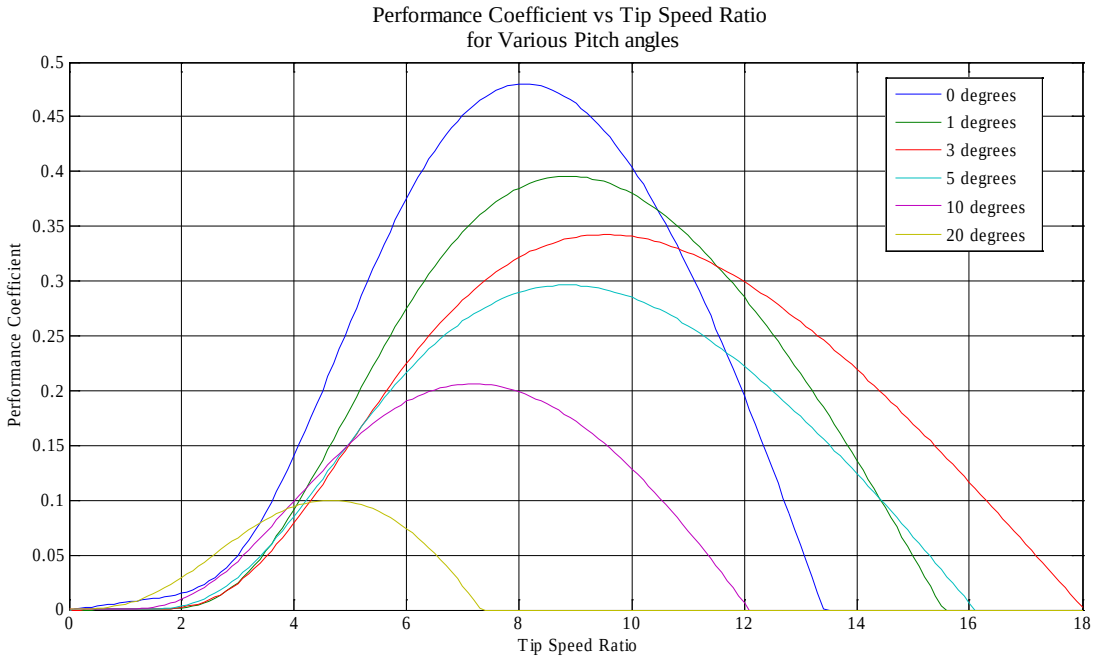

Figure 2.9 Variation of Power coefficient with Tip Speed Ratio

Finally, using the definition of power coefficient C_p as mentioned earlier, the mechanical power on the wind turbine rotor as a function of wind speed and turbine characteristics is given by:

$$P_{rotor} = \frac{1}{2}\rho A v^3 C_p \tag{11}$$

2.3.1.2 Wind Turbine Modeling

Based on the above described mathematical equations, the wind turbine model is developed in Simulink as shown in Figure 2.10. Figure 2.11 shows the obtained Power-Speed characteristics of a wind turbine for various wind speeds and a fixed pitch angle.It can be seen from Figure 2.11 that for each wind speed there exists a particular rotor speed (which is related to tip speed ratio given by (8)) at which the wind turbine output power is maximum. This is a very important characteristic feature of the wind turbine and is explained in great detail in Chapter 5.

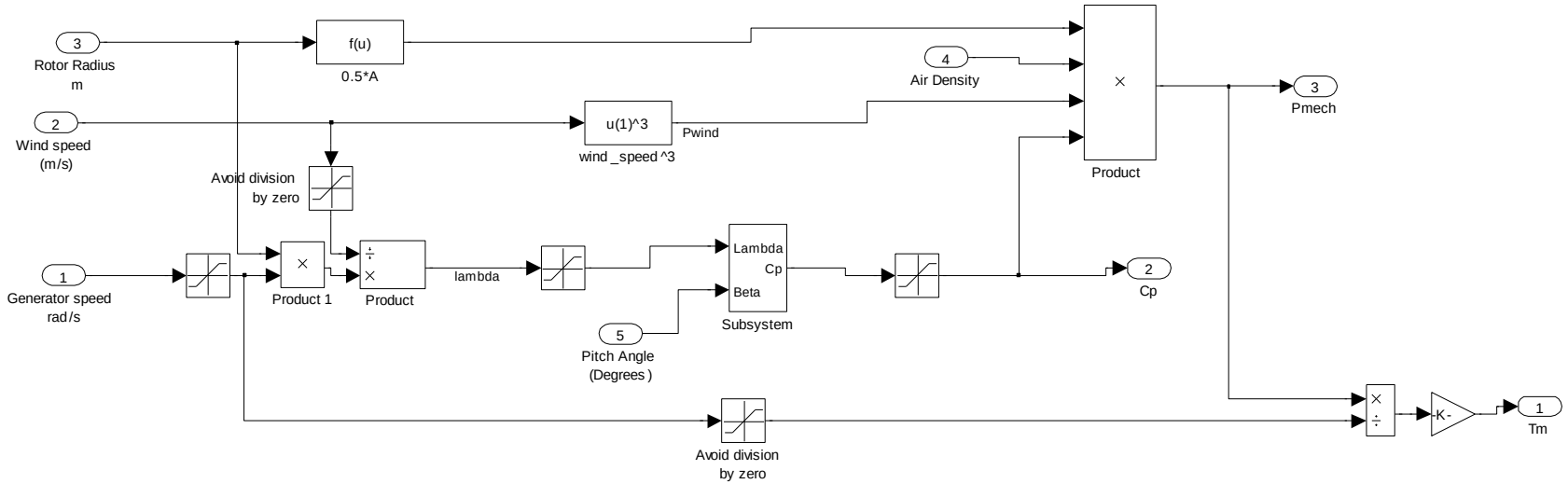

Figure 2.10 Wind Turbine Model

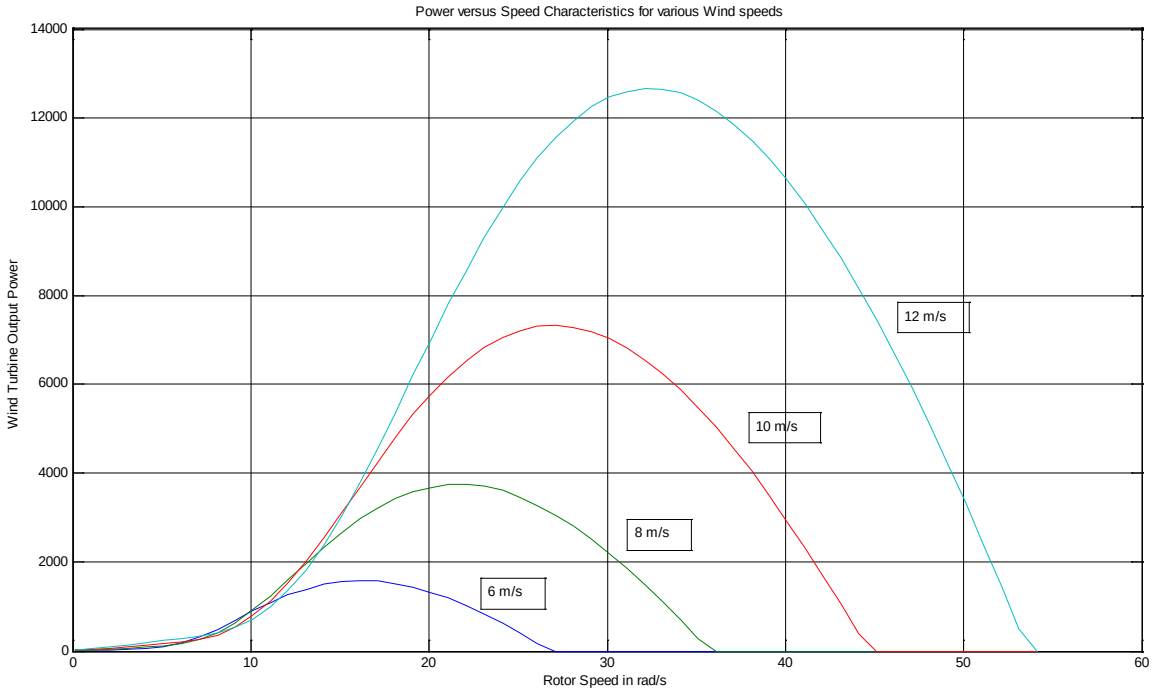

Figure 2.11 Wind Turbine Power Speed Characteristics

2.4 Selection of Generator

The generator provides a means of energy conversion between the mechanical energy contained in the wind turbine rotor, to electrical energy. The wind turbine is connected to the generator shaft either through a gearbox or directly (direct drive). The use of a gearbox allows matching of the generator speed to that of the turbine but the disadvantage of the gearbox is that it is subjected to wear and tear and in some cases has been relatively unreliable [5].

Based on the type of connection to the grid, the wind energy system can be categorized into constant speed and variable speed wind systems. In constant speed wind systems the generator is connected to a utility grid or local load directly. Since the generator is directly coupled, the wind turbine rotates at a constant speed governed by the frequency of the utility grid (60 Hz) and the number of poles of the generator. A major

disadvantage with constant speed operation for the small scale application is that as was seen earlier from the wind turbine characteristics, the power extracted is minimum due to turbine characteristics. Further, these machines are generally bigger in size. On the other hand, for a variable speed wind turbine, the generator is connected to the grid or load using power electronics interface converters. Wound rotor, double fed induction generator, permanent magnet synchronous generators are two popular generators in the variable speed wind turbine category. As mentioned in great detail in Chapter 5, it was shown [6] that variable speed wind generators produce 10-15% more power than constant speed turbines. Hence, the variable speed wind turbines have been used more often for wind systems now.

2.4.1 Review of Generator Types

While several generator types may be considered, historically the squirrel cage, wound rotor induction generator types and current excited synchronous generator are used more for wind farm applications [17]. Induction machines have the advantage that they have asynchronous operation, which allows some flexibility when the wind speed is fluctuating. The Squirrel Cage Induction Generator (SCIG) is a very popular machine for wind applications due to its mechanical simplicity and robust construction. The stator of the squirrel cage induction generator is connected to the grid through two back-to-back PWM converters with the stator side converter regulating the electromagnetic torque and supplying the necessary reactive power to magnetize the machine. The grid side converter controls the power quality of the power delivered to the grid. However, the requirement for reactive power and higher rating requirements of the converter to maintain the machine's magnetizing requirement, higher cost, bulky size are the major

disadvantages which makes it uneconomical for the system as the one that is under consideration in this dissertation.

While the advancements in wound rotor induction generator allow the generator output to be controlled using advanced methods like rotor slip energy recovery etc, the wound rotor is more expensive than a squirrel-cage rotor [17] and the windings on the rotor may be subject to stresses in addition to the requirement of excitation. The Wound Rotor Synchronous Generator is one of the earlier used machines for wind power generation. The large number of parts and windings make it an expensive solution when compared to induction machines. The wound rotor synchronous generator is generally used at constant speed, and is fixed to the grid frequency or in some cases used in variable speed operation using a full power inverter. However, as with the induction machines, it is necessary to excite the rotor winding, with DC, using slip rings and brushes, or a brush less exciter [17] making it not very attractive for low to medium power level wind energy systems.

An improvement compared to wound rotor induction generator is a Double Fed Induction Generator (DFIG) which has become popular for medium and large power applications wherein it has reduced the generator interface power electronic converter ratings and has high efficiency [6] [18]. The stator is connected directly to the utility grid to provide the necessary magnetization for the machine and the rotor, connected to the grid through two back-to-back PWM power converters regulates the electromagnetic torque and supplies reactive power. Compared to SCIG, the converter costs for the DFIG are reduced since their required rated capacity is only around 30% of the total system capacity. Further, lower losses, ability to achieve speed variation within +_ 30% of the synchronous speed which allows it to be used for a wide speed range enabling to extract

more power from the wind system are the main advantages of the DFIG. However, the requirement for periodic maintenance, high capital cost, requirement for gear box, increased control complexity; more number of electronic switches makes it a less favorable option for low power applications.

The Permanent Magnet Synchronous Generator (PMSG) differs from the Induction Generator in that the magnetization is provided by a permanent magnet pole system on the rotor, instead of taking excitation current from the armature winding terminals as is the case with induction generator. Permanent magnet machines are generally categorized into several categories, machines with surface mounted magnets, or with buried magnets, ones with damper windings etc. In a PMSG, the stator winding is connected to the load typically through a diode bridge rectifier or a PWM voltage source converter, and the rotor is provided with the permanent magnet pole system. Because of the relatively large air-gap, the leakage flux remains below an acceptable limit for PMSG with many poles and hence is generally of smaller size when compared to induction generators [17]. While the availability of permanent magnets is a bit difficult, the decrease in the cost of the magnets, higher power density, high torque capability, variable speed capability, lower maintenance costs and losses and the flexibility in design has made the PMSG a good option for wind applications, especially for low power wind systems, and as much many systems have been proposed with PMSG [9] [10].

The Switched Reluctance Generator is slowly gaining consideration for Wind Power applications because of its ability to continue operating at reduced output in the presence of faults on the generator and capability to operate without requiring gear box. However, the main problem with switched reluctance generator is that it is inherently unstable and requires the firing angles to be adjusted to suit the load exactly during both

normal and fault conditions [17]. Further, it is considered inferior to the PMSG, due to its lower power density, and the need for a sophisticated power converter [17].

Table 2.1 gives a comparison of the most common types of generators used for low to medium power wind applications as dealt in this dissertation. It can be seen that while there is a tradeoff between cost and efficiency, the lower costs, variable speed operation capability, and decreasing magnet costs made the PMSG a good option to choose for low to medium power applications. Hence, recently more PMSG based wind systems were being installed for low power applications by the industry and hence PMSG is chosen for this dissertation.

Table 2.1 Comparison of Generator Types for Wind Energy System

Generator Type	Advantages	Disadvantages
Permanent Magnet Synchronous Generator	• Flexibility in design • Lower maintenance and operating costs • Lower losses • No necessity of gearbox • High Torque capability • Does not require external excitation • Low cost converter topologies like diode bridge can be used 1.1 Variable speed operation	• Cost of magnets • Higher temperatures can demagnetize the magnets
Asynchronous Generator	• Lower capital cost for construction of generator • Rugged • Excellent damping of torque pulsations due to wind gusts	• Higher converter cost since converter must be rated for full power • Generator requires reactive power supply • Increased control complexity due to increased number of switches
Doubly Fed Induction Generator	• Reduced converter cost, typically 25% of total power • High efficiency • Ideal for high power • Variable speed operation	• Increased number of switches • Increased control complexity • High capital cost • Requires frequent maintenance • Typically requires gearbox

2.4.2 Permanent Magnet Synchronous Generator

Figure 2.12 shows a basic configuration of a four pole exterior mount PMSG [19]. The permanent magnets are mounted in the rotor, while the stator has sinusoid distributed windings. The electrical rotor speed and position are represented as given by:

$$\omega_r = \frac{P}{2}\omega_{rm} \text{ and } \theta_r = \frac{P}{2}\theta_{rm} \tag{12}$$

where: ω_{rm} is the rotor mechanical speed

θ_{rm} is the rotor mechanical position

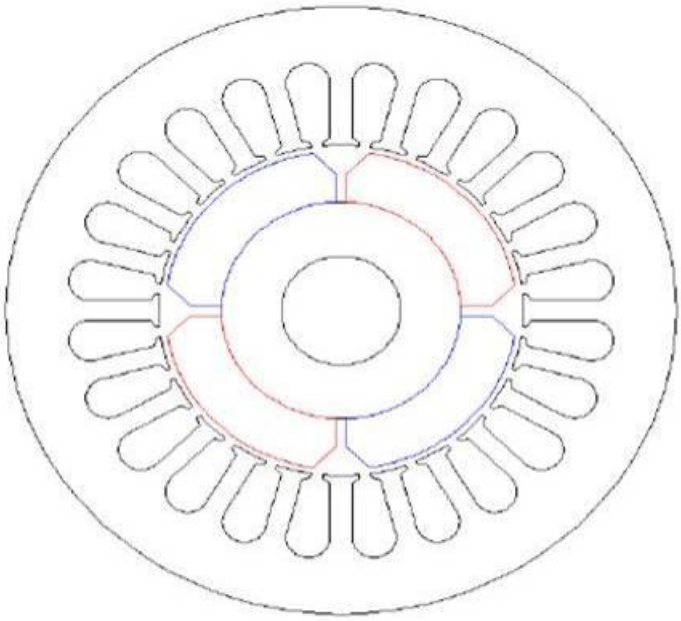

Figure 2.12 Permanent Magnet Synchronous Generator

The voltage equation in the abc stationary reference frame, as shown in Figure 2.13 [12], are given by:

$$V_a = R_a I_a + \frac{d}{dt}\lambda_a \tag{13}$$

$$V_b = R_b I_b + \frac{d}{dt}\lambda_b \tag{14}$$

$$V_c = R_c I_c + \frac{d}{dt}\lambda_c \tag{15}$$

The flux linkages of the PMSG are given by:

$$\lambda_{abc} = L_{siabc} + \lambda_m' \begin{bmatrix} \sin\theta_r \\ \sin(\theta_r - \frac{2\Pi}{3}) \\ \sin(\theta_r - \frac{4\Pi}{3}) \end{bmatrix} \tag{16}$$

where λ_m' is the amplitude of the flux linkages established by the permanent magnet

L_s is the stator self inductance matrix give by:

$$\begin{bmatrix} L_{ls} + L_A - L_B\cos 2\theta_r & -\frac{1}{2}L_A - L_B\cos 2(\theta_r - \frac{\pi}{3}) & -\frac{1}{2}L_A - L_B\cos 2(\theta_r + \frac{\pi}{3}) \\ -\frac{1}{2}L_A - L_B\cos 2(\theta_r - \frac{\pi}{2}) & L_{ls} + L_A - L_B\cos 2(\theta_r - \frac{2\pi}{3}) & -\frac{1}{2}L_A - L_B\cos 2(\theta_r + \pi) \\ -\frac{1}{2}L_A - L_B\cos 2(2\theta_r + \frac{\pi}{2}) & -\frac{1}{2}L_A - L_B\cos 2(2\theta_r + \pi) & L_{ls} + L_A - L_B\cos 2(\theta_r - \frac{4\pi}{3}) \end{bmatrix} \tag{17}$$

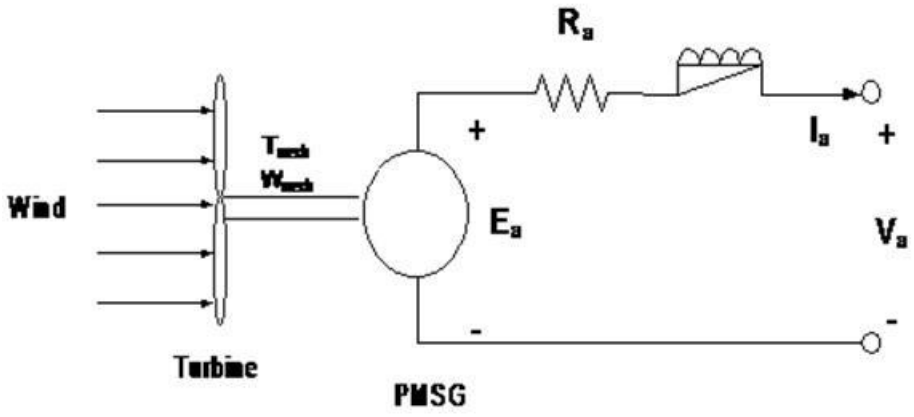

Figure 2.13 PMSG Circuit

The electromagnetic power of the PMSG is given by:

$$P_{em} = 3E_a I_a \cos\varphi \tag{18}$$

where: E_a is the generator EMF

I_a is the armature current

φ is the angle between phasors **E**a and **I**a

When the phase winding resistance in Figure 2.13 is ignored, the output electrical power is given by,

$$P_{em}=P_{out}=3V_aI_a\cos\varphi \tag{19}$$

2.5 Selection of Converter

Power electronics is a rapidly developing technology with high voltage and current carrying capable devices being developed. The electrical power generated from the wind energy system is connected to grid or to a local load using power electronics interface. With suitable control, the power electronics interface enables variable speed operation of the PMSG, allowing to extract more power from the wind system. The main task of power electronic systems is to process and control the flow of electrical energy efficiently. A power electronic unit usually consists of more than one power conversion stage, with different stages being decoupled on an instantaneous basis by means of energy storage elements such as capacitors and inductors. Each power conversion stage is called a converter, which is a basic module of power electronic systems. There are two ways the electrical power output of the PMSG can be connected to the grid or to a load as mentioned below.

2.5.1 Review of Converter Types

Broadly the power electronic interface of wind energy system to the grid can be classified into three topologies. They are:

1. AC – AC
2. AC – DC – AC
3. AC – DC – DC – AC

Of these methods, the first method comes under AC coupling category, and the other two methods come under DC coupling category. In the AC – AC coupling method, the electrical power generated is directly connected to the grid or load point through proper power electronic interfacing circuits to a power frequency AC bus. Typically, this topology is used for large single energy systems where generated power is generally constant, and is seldom used for low to medium power hybrid power system applications as considered in this dissertation. The dc coupling methods are the commonly employed methodologies for connecting the wind system to the grid. In these methods, the AC power generated from the wind turbine generator is converted to dc and connected to a dc bus and a DC-AC converter is used for connecting to the grid. Chapter 4 gives more details of the main problems associated with AC-AC coupling and the benefits of selecting a DC coupling methodology for the considered hybrid Wind – Photovoltaic system. Hence, this section deals only with the AC-DC converters typically employed for the wind energy system. It needs to be mentioned that the DC-AC conversion is a single stage and is the same for the entire hybrid system which is dealt in chapter 4.

Several variations exist in the AC- DC conversion topologies generally employed for wind energy systems with PMSG.

2.5.1.1 AC-DC- AC Topologies

The variable speed wind generator produces a voltage which varies in both magnitude and frequency, and a power electronic converter is required to convert it to a dc voltage. The diode rectifier as shown in Figure 2.14 is the most commonly used topology for wind energy applications due to its simplicity. A three phase diode rectifier consists of six diodes which are used to convert the three phase ac voltage to dc. The relation between the generator terminal voltage and the rectified diode voltage is given by [13]:

$$V_{dc} = \frac{3E_s\sqrt{6}}{\pi} \tag{20}$$

Where: Vdc is the rectified diode voltage and Es is the single phase RMS generator terminal voltage.

In this topology, the rectified dc voltage is connected to the dc bus and the DC-AC voltage source converter (VSC) is responsible for controlling the power flow to the grid. As was mentioned earlier, for extracting maximum power from the wind system, the rotor speed has to be maintained at the optimum level. In this topology, since the diode bridge is an uncontrollable rectifier, the VSC is controlled either to perform the maximum power extraction or is controlled to maintain a steady dc voltage and inject only the possible power without operating the optimal rotor speed. While this topology is very cheap and robust, it has several drawbacks like high harmonics, generator stresses, variation in dc bus voltage with wind speed, uncontrollable power flow etc.

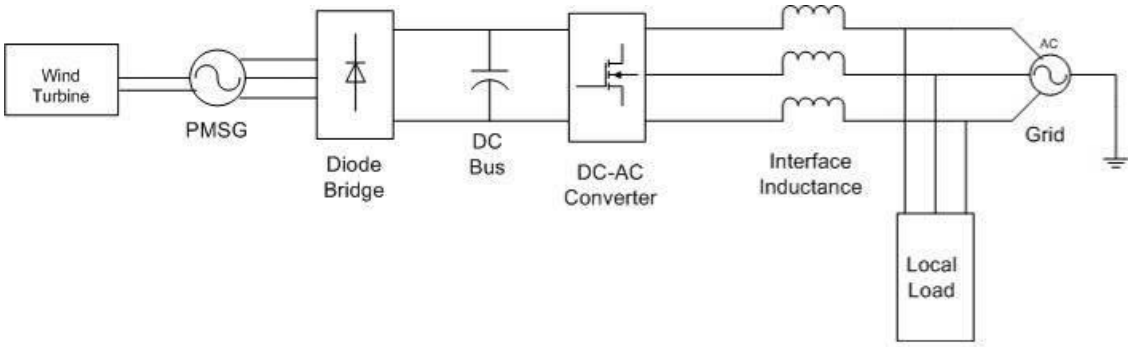

Figure 2.14 Diode Bridge Interface to DC Bus

Figure 2.15 shows another power electronic interface where instead of a diode, thyristors are used in the ac-dc conversion process. A thyristor is similar to a diode with the exception that it starts to conduct when it is not only forward biased but also its gate terminal receives a positive current pulse, and the thyristor continues to be conducting as long as it is still forward biased. In a thyristor controlled rectifier, the output DC voltage can be regulated by controlling the firing angles of thyristors, and hence they are called controlled rectifiers. The firing angle is the angular delay between the time when a thyristor is forward biased and the time when a positive current pulse is applied to its gate.

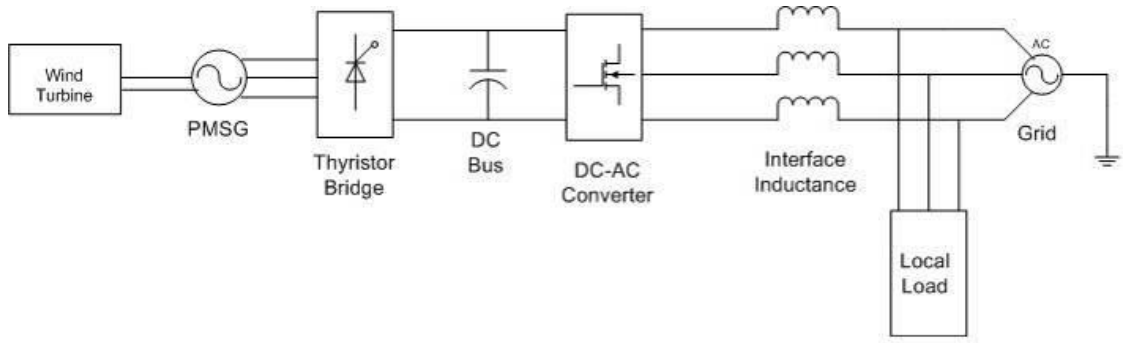

Figure 2.15 Thyristor Bridge Interface to DC Bus

The relation between the generator terminal voltage and the rectified voltage is given by [13]:

$$V_{dc} = \frac{3E_s\sqrt{6}}{\pi} cos\ (\propto) \tag{21}$$

where: V_{dc} is the rectified diode voltage,

E_s is the single phase RMS generator terminal voltage,

α is the gate firing angle.

The main problem with the thyristor rectifiers is that they generate higher harmonics and device stresses than the diode bridge rectifier and requires a firing pulse circuit which sometimes causes errors and hence is not used much for wind energy applications.

To overcome the above mentioned problems and to achieve full control, an IGBT rectifier is used. Figure 2.16 shows the wind energy system employing an IGBT rectifier with a pulse width modulated (PWM) grid connected voltage source converter (VSC) is used (back to back converter). The advantage with this topology is that by suitable control, the active and reactive power flow in the system can be fully controlled. By controlling the IGBT rectifier to operate with a high power factor, the generator stresses are reduced. Due to this reason, this topology is becoming popular for wind energy system applications for tens-hundreds of kWs power range. However, the disadvantage with this topology is that the system cost would be higher due to the increase in the number of sensors and switching elements, and the switching losses are higher. Due to these considerations, this topology is not considered for the hybrid system under consideration in this dissertation.

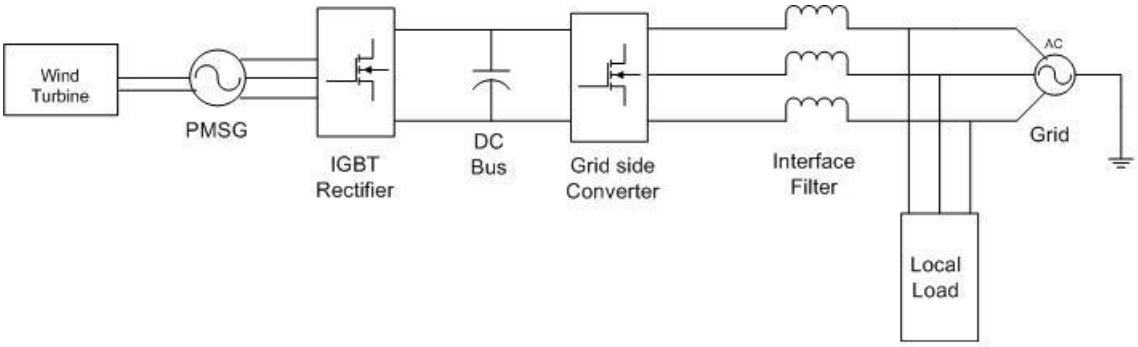

Figure 2.16 Back to Back PWM Voltage Source Converter

2.5.1.2 AC-DC-DC-AC topology

This is the most commonly used topology for wind energy system integration and is shown in Figure 2.17. As seen from the figure, the generator power is converted to dc either by a diode bridge or thyristor rectifier and an intermediate DC-DC converter is used for interfacing to the DC bus. As was mentioned earlier, due to the drawbacks of thyristor converter, much often a diode bridge rectifier is used as the front end generator interface converter. The diode bridge rectifier converts the generator AC power to DC, and the intermediate DC-DC converter is used to control the dc voltage from one voltage level to the other. As discussed earlier, the power extracted from wind system is maximum at certain optimal rotor speed, which changes with the wind speed. The intermediate dc-dc converter is used to indirectly control the loading of the wind turbine and generator speed, and operate at this optimal speed for extracting maximum power from the wind system. More details of this are given in Chapter 5. Even though an additional DC-DC converter adds to the additional cost of the system, this topology has several advantages like lower controllable switch count when compared to back to back converters, generator speed control, maintaining appropriate DC bus voltage, selective harmonic elimination, robust architecture, etc.

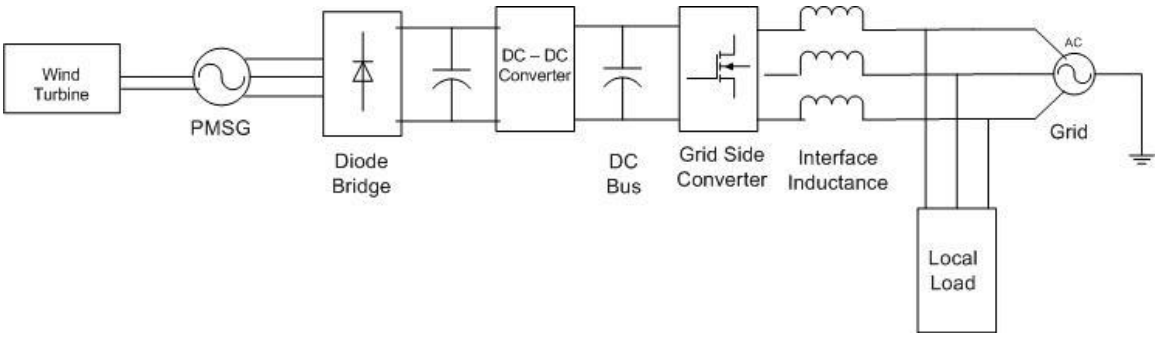

Figure 2.17 AC-DC-DC-AC Topology

The most popular DC-DC converters typically used are the Buck, Boost and Buck-Boost converter. In a buck converter the output dc voltage is less than the input voltage, and in a boost converter the output voltage is more than the input voltage. A bust-boost topology can either buck or boost the input voltage. For renewable energy applications like wind systems, the generator output voltage is typically less than the dc bus voltage, and hence a boost converter is generally used. Figure 2.18 shows the schematic of a boost converter. When the switch is closed, the input voltage is applied across the inductor causing the current through the inductor to increase and the energy is stored in the magnetic field of the inductor. When the switch is opened the inductor current flows through the diode and some of the energy stored in the inductor is transferred to the output filter capacitor and the output load. By controlling the duty ratio of the switch, the output dc voltage of the converter can be changed.

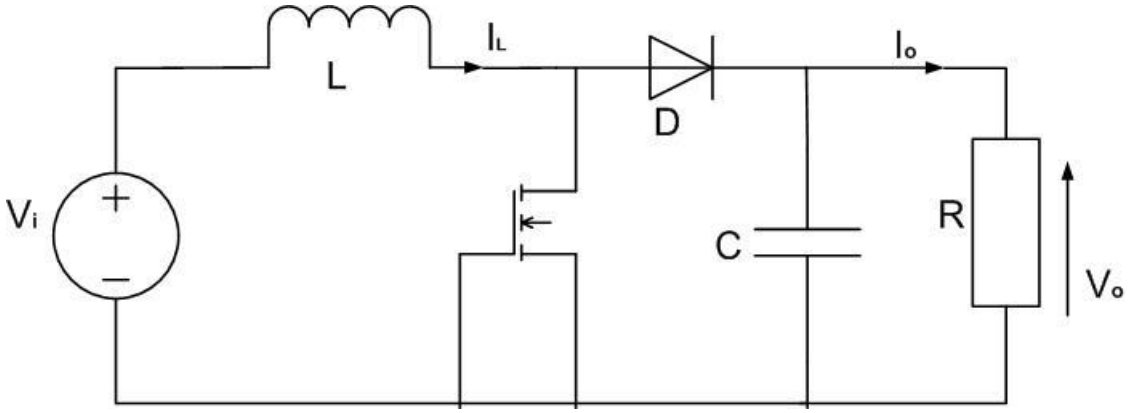

Figure 2.18 Boost Converter

For a boost converter, the relation between input and output dc voltages is given by:

$$V_o = \frac{V_{in}}{(1-D)} \tag{22}$$

Where: V_o is the output dc voltage of the converter

V_{in} is the input dc voltage

D is the duty ratio.

CHAPTER III

PHOTOVOLTAIC SYSTEM MODELING

3.1 Background

Solar energy basically is the ultimate source for all kinds of energy resources on the earth with only a few exceptions such as geothermal energy. Sunlight reaches the Earth's outer atmosphere at strength of 1367 watts per square meter, and atmospheric losses reduce the sun's power to about 1000 W/m2 when the sun is directly overhead on a cloudless day [22]. This gives the total solar power capacity to meet 10000 times the requirement for present day human electrical power consumption. This shows the tremendous potential of solar energy that is freely available in nature. This chapter gives a brief history of the photovoltaics and discusses the modeling and selection of photovoltaic energy subsystems.

3.2 History of Photovoltaics

There are normally two ways to generate electricity from sunlight: through photovoltaic (PV) and solar thermal systems. Solar thermal systems use the sun as a direct source of heat energy, and are most commonly used for applications like water heating etc. PV electricity, however, converts light from the sun directly into electricity, through a process known as photovoltaics. In this dissertation, only photovoltaic energy and system will be discussed. The earliest use of solar energy was noted in the 7th century BC, when a magnifying glass was used to concentrate the solar rays to light fire [13]. Since then, solar energy has found numerous applications. The scientific principle

behind solar electricity, the photovoltaic effect, was first noted over 150 years ago by the French physicist Becquerel. While experimenting with an electrolytic cell made of two different metal electrodes placed in an electrical conducting solution, he observed that electricity generation increased with exposure to light. This discovery was later clarified in 1905 when Albert Einstein revealed his theory of the photoelectric effect [13] and concluded that light was made up of discrete packets of energy called photons which are responsible for electrical power and/or heat generation.

Later in 1954, the first commercial silicon photovoltaic (PV) cell was invented at Bell Labs, USA. The earlier developed solar cells had an efficiency of only around 5-6%. The requirement for developing power sources for earth orbiting satellites pushed for more improvements in the solar cell technology with cell efficiency reaching to around 12% by the end of 1960s. In 1964 NASA launched the first Nimbus spacecraft – a satellite powered by a 470 W photovoltaic array [13]. Later in the 1980s solar power became a popular energy source for consumer electronics devices such as calculators, watches, radios and battery charges. During this time photovoltaic power generation also started to gain in popularity and some residential power applications have started like solar water heating etc. Currently, with the tremendous improvements in material fabrication and control technologies, solar power has become one of the most popular forms of renewable energy source for residential use.

Figure 3.1 [23] shows the worldwide installed photovoltaic (PV) power generation capacity over the last decade with the worldwide PV power generation increasing from a 700 MW in 2000 to around 22 GW by 2009 at an annual growth rate of around 20%. Figure 3.2 [2] shows the installed capacity growth in US. It can be seen that there has been a surge in the PV power generation in the last few years, and this is

expected to increase over the coming years as well. More recently, rooftop residential solar power applications with generation capacities capable of meeting average US household consumption have become a common trend.

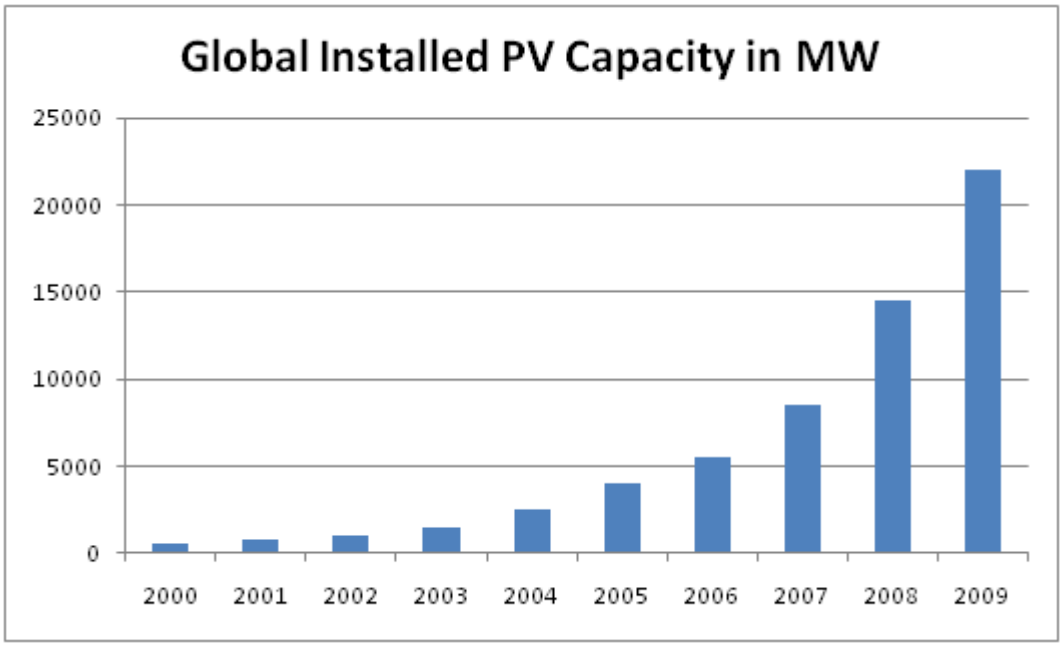

Figure 3.1 Global Installed PV Capacity in MegaWatts

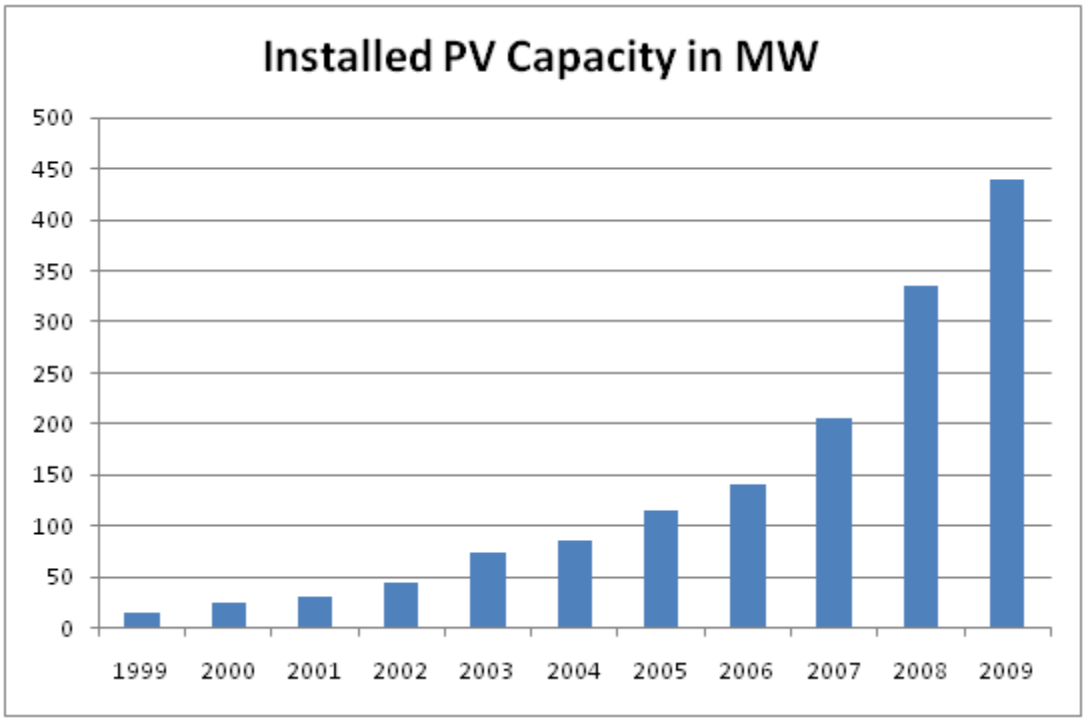

Figure 3.2 US Installed PV Capacity in Megawatts

Due to improvements in semiconductor materials, device designs production capacity, capital costs for PV panels have been decreasing significantly, from $50 per watt in the early 1980s [25] to about 4.5$ per watt in 2004 [25][26]. The cost of electricity produced by PV systems also continued to drop from $0.90/kWh in 1980 to about 0.20$/kWh in 2009 [25][26]. As seen from Figure 3.3, the module prices for PV electricity have been coming down significantly over the years [26].

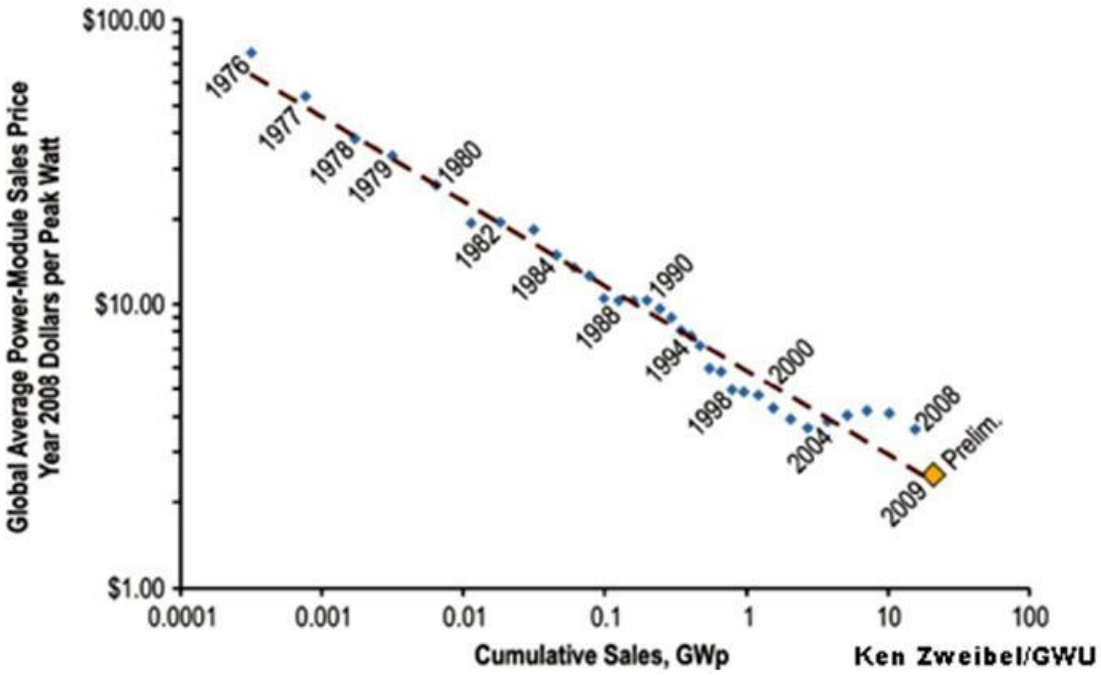

Figure 3.3 Global Average PV Module Price per Watt [26]

This could primarily be attributed to the growing governmental incentives, the decline in the solar cell production prices (which accounts for around 50% of the total PV system cost as shown in Figure 3.4), and increasing cell efficiencies. In 2010, the installed residential PV prices per kW are forecasted to be competitive with residential electricity prices after incentives and by 2013 the residential price per kW from PV is expected to reach the one with that from conventional utility grid [26]. With development and breakthrough in new cell materials and power electronics technologies solar power can prove to be an efficient, environmental friendly and safe means of power.

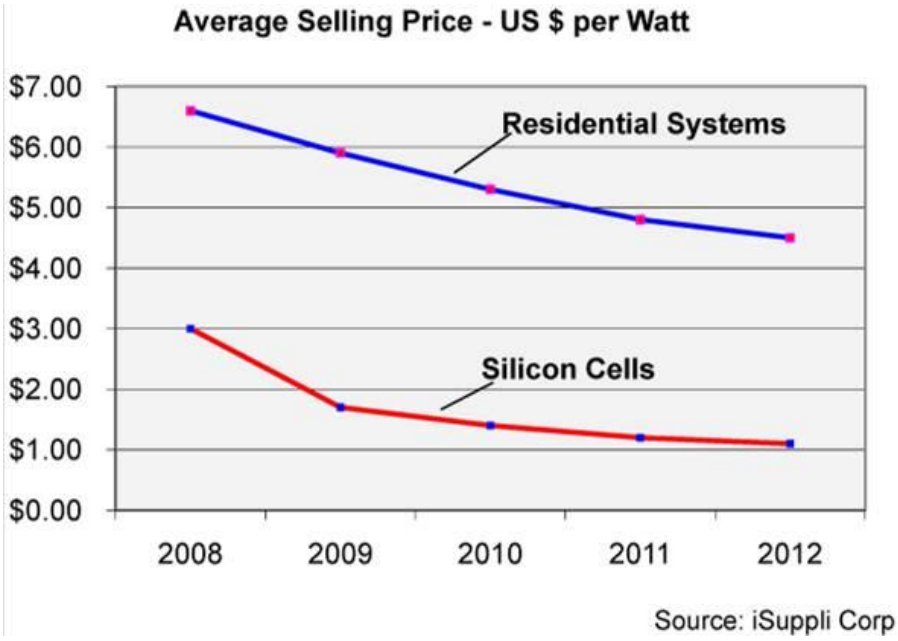

Figure 3.4 Average Selling Price of Cell per Watt - Present and Projected Future [26]

3.3 Modeling of Photovoltaics

3.3.1 Photovoltaic Cell

A photovoltaic (PV) cell, also known as solar cell is a semiconductor device that generates electricity when light falls on it. When sunlight strikes a PV cell, photons whose energy is more than the bandgap energy emit electrons from the atoms of the cell. The free electrons then move through the cell, creating holes in the cell, thus resulting in the generation of electricity. This process in which a PV cell converts sunlight into electricity is known as the photovoltaic effect. A single PV cell produces up to 2 watts of power [24], and depending on the application many PV cells are connected together to form modules, which are further assembled into larger units called arrays.

3.3.2 Types of PV Systems

Two major types of PV systems are available in the market, flat plate and concentrators [24]. Flat plate systems are the most prevalent type of PV systems, where the PV modules are built on a rigid and flat surface to capture sunlight. Concentrator systems use lenses to concentrate sunlight on the PV cells and increase the cell power output. Comparing the two systems, flat plate systems are typically less complicated but employ a larger number of cells while the concentrator systems use smaller areas of cells but require more sophisticated and expensive tracking systems. The concentrator type systems have the disadvantage that they do not work efficiently cloudy conditions. Due to these reasons, this dissertation focuses on the flat panel type of PV power, and Figure 3.5 shows a flat panel PV module in a residential rooftop example [27]. It can be seen from the figure that a series of panels are combined together to form a PV system for the particular application.

Figure 3.5 Rooftop Flat Panel Photovoltaic Array [27]

3.3.3 Types of PV cell materials

PV cells are made of semiconductor materials. The major types of materials that are used for PV cell are crystalline and thin films, which vary from each other in terms of light absorption efficiency, energy conversion efficiency, manufacturing technology and cost of production. The PV cell materials can be classified into crystalline type and thin film type, and following gives a brief overview of the most popular types that are being used in the industry today.

3.3.3.1 Crystalline Materials

3.3.3.1.1 Single-crystal silicon

Single-crystal silicon cells are the most common in the PV industry. A single-crystal silicon has a uniform molecular structure, and compared to non-crystalline materials, its high uniformity results in higher energy conversion efficiency which is around 15-20%. The single crystal silicon cells are not only energy efficient, but also are highly reliable for outdoor power applications. Hence they are most used in the PV industry [28].

3.3.3.1.2 Polycrystalline silicon

Consisting of small grains of single-crystal silicon, polycrystalline PV cells are less energy efficient than single-crystalline silicon PV cells, with energy conversion efficiency for a commercial module ranging between 10 to 14%. Compared to single-crystalline silicon, polycrystalline silicon material is stronger and can be cut into one-third the thickness of single-crystal material. It also has slightly lower wafer cost and less strict growth requirements. However, their lower manufacturing cost is offset by the lower cell efficiency [28].

3.3.3.1.3 Gallium Arsenide

Gallium Arsenide (GaAs) has a crystal structure similar to that of silicon. An advantage of GaAs is that it has high level of light absorptivity with a much higher energy conversion efficiency than crystal silicon, reaching about 25 to 30%. Its high resistance to heat makes it an ideal choice for concentrator systems in which cell temperatures are high. GaAs is also popular in space applications where strong resistance radiation damage and high cell efficiency are required. The biggest drawback of GaAs PV cells is the high cost of the single-crystal substrate that GaAs is grown on and hence is most often used in concentrator systems where only a small area of GaAs cells is needed [29].

3.3.3.2 Thin Film Materials

In a thin-film PV cell, a thin semiconductor layer of PV materials is deposited on low-cost supporting layer such as glass, metal or plastic foil. Since thin-film materials have higher light absortivity than crystalline materials, the deposited layer of PV materials is extremely thin. This makes the manufacturing process faster, uses lesser energy and is easier for mass production than the ingot-growth approach of crystalline silicon. However, thin film PV cells suffer from poor cell conversion efficiency due to non-single crystal structure, requiring larger array areas and increasing area-related costs such as mountings [28].

3.3.3.2.1 Amorphous Silicon (a-Si)

This is used mostly in consumer electronic products which require lower power output. A significant advantage of a-Si is its high light absorptivity, about 40 times higher than that of single-crystal silicon. Therefore only a thin layer of a-Si is sufficient for

making PV cells Also, a-Si can be deposited on various low-cost substrates, including steel, glass and plastic, and the manufacturing process requires lower temperatures and thus less energy is required. So the total material costs and manufacturing costs are lower per unit area as compared to those of crystalline silicon cells. However, a-Si still has two major problems. One is the low cell energy conversion efficiency, ranging between 5-9%, and the other is the outdoor reliability problem in which the efficiency degrades within a few months of exposure to sunlight, losing about 10 to 15% [29].

3.3.3.2.2 Cadmium Telluride (CdTe)

As a polycrystalline semiconductor compound, CdTe has a high light absorptivity level, and is relatively easy and cheap to manufacture when compared to other materials mentioned earlier. The low conversion efficiency for a CdTe module (about 7%), reliability problems, instability of cell, toxicity of cadmium are the major drawbacks of this type [29].

3.3.3.2.3 Summary

A review of the various materials has shown that crystalline silicon is the best available choice for rooftop electrical power generation application and has been the popular of the PV cells for the past two decades. However, recent progress in the thin-films technology has led to a growing interest in thin-films PV cells. While most PV cells in use today and in the near future are expected to be silicon-based, cells made of other semiconductor materials are expected to surpass silicon PV cells in performance, cost and become viable competitors in the PV market. Recently, breakthrough research has made it possible to develop solar cells with efficiencies more than 20%, and with superior performance.

3.4 Modeling of a Photovoltaic Cell

A photovoltaic cell consists of a p-n junction fabricated in a thin layer of semiconductor. When the incident radiation is low, the output I-V characteristics of a photovoltaic cell have an exponential characteristic similar to that of a diode [30]. However when the radiation is higher, photons with energy greater than the bandgap energy cross the p-n junction and a current proportional to the incident radiation is generated. When the cell is connected to an external load at the terminals, these current flows in the external circuit or else is shunted internally by an intrinsic p-n junction diode. Hence, it can be seen that the diode characteristics sets the open circuit voltage characteristics of a solar cell. A PV cell can thus be modeled as a current source in parallel with a diode with the output of the current source (current generated by the PV cell) proportional to incident sun radiation [30], and the temperature dependence, quality factor and resistance of the diode. Figure 3.6 shows the equivalent circuit of a PV cell.

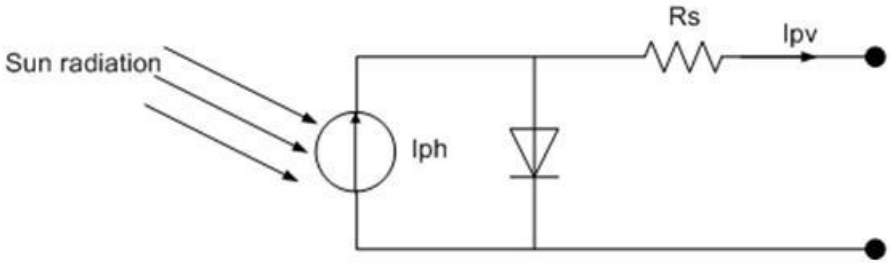

Figure 3.6 Photovoltaic Cell Equivalent Circuit

The equations which describe the characteristics of the PV cell are given by [30] and are given as follows:

$$I = I_L - I_O\left(e^{\frac{q(V+IR_S)}{\eta\kappa T}} - 1\right) \tag{23}$$

$$I_L = I_{LT1}\left((1 + \kappa_o(T - T_1)\right) \tag{24}$$

$$I_{LT} = \frac{G * I_{SCT1}}{G_{nom}} \tag{25}$$

$$K_O = \frac{1}{(T_2 - T_1)} \tag{26}$$

$$I_O = I_{OT1} \left(\frac{T}{T_1}\right)^{\frac{3}{\eta}} * e^{\left(\frac{-qV}{\eta\kappa\left(\frac{1}{T} - \frac{1}{T_1}\right)}\right)} \tag{27}$$

$$I_{OT1} = \frac{I_{SCT1}}{\left(e^{\frac{qV_{OCT1}}{(\eta\kappa T)}} - 1\right)} \tag{28}$$

$$R_S = \frac{-dV}{dI_{OC}} - \frac{1}{X_V} \tag{29}$$

$$X_V = I_{O(T_1)} \frac{q}{\eta} \kappa T_1 e^{\frac{qV_{OC(T_1)}}{(\eta\kappa T_1)}} \tag{30}$$

Where: I_L is the current generated due to sun radiation

I_O is the diode saturation current

η is the diode quality factor

R_S is the series resistance of the PV cell

q is the charge constant and is equal to 1.6×10^{-19}

κ is the Boltzmann's constant given by 1.38×10^{-23}

G is the sun radiation in W/m^2

T_1 is the nominal temperature in °C

G_{nom} is the nominal sun's radiation used for the modeling obtained from manufacturer's data

I_{SC} is the short circuit current through the PV diode

V_{OC} is the open circuit voltage of the panel, obtained from manufacturer's data

Based on the above equations, a model of a crystalline silicon PV cell is developed in Matlab/Simulink as shown in Figure 3.7.

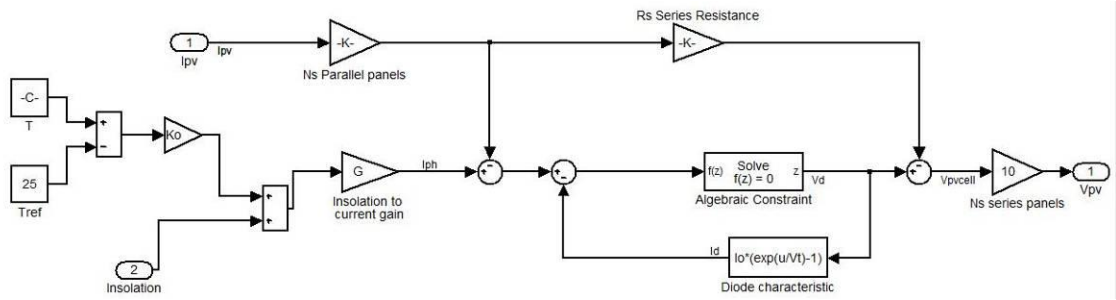

Figure 3.7 Photovoltaic Model

It can be seen that the developed model is moderately complex which takes into account the temperature dependence of the photocurrent I_L and the saturation current of the diode I_0. For validating the results of this model, the Solarex MSX60 [31] panel specifications are taken. Table 3.1 gives the specifications of Solarex MSX60 panel, and Table 3.2 gives the specifications for a 9 kW photovoltaic system used in this dissertation.

Table 3.1 Photovoltaic Module Specifications

Parameter	**Value**
Open Circuit Voltage/ module	21 V
Short Circuit Current/module	3.75 A
Voltage at Max. Power/module	17 V
Maximum Power/module	60 Watts

Table 3.2 Photovoltaic System Specifications

Parameter	Value
Open Circuit Voltage/ module	21 V
Short Circuit Current/module	3.75 A
Voltage at Max. Power/module	17 V
Maximum Power/module	60 Watts
Number of modules in Series	10
Number of modules in Parallel	15
Total Panel Power	9 kW

As given in Table 3.2, the selected PV system has 10 modules connected in series, with 15 such parallel modules, for a rated power of 9 kW. Figure 3.8 gives the current voltage characteristics of a PV cell. Figure 3.9 and Figure 3.10 gives the PV cell characteristics with varying sun radiation and temperature respectively. It can be seen from the figures that the generated PV current changes with the incident sun radiation and external temperature. Figure 3.12 shows the power generated from the PV system (10 series modules and 15 parallel modules combined) considered in this dissertation for a particular sun radiation. Figure 3.11 shows the variation of the system power as the incident sun radiation is changed when the external temperature is constant. It can be seen from the Figure 3.12 that for each sun radiation there is a particular PV terminal voltage at which the power from the PV system is maximum. This is an important characteristic feature of the PV system which is explained in more detail in Chapter 5.

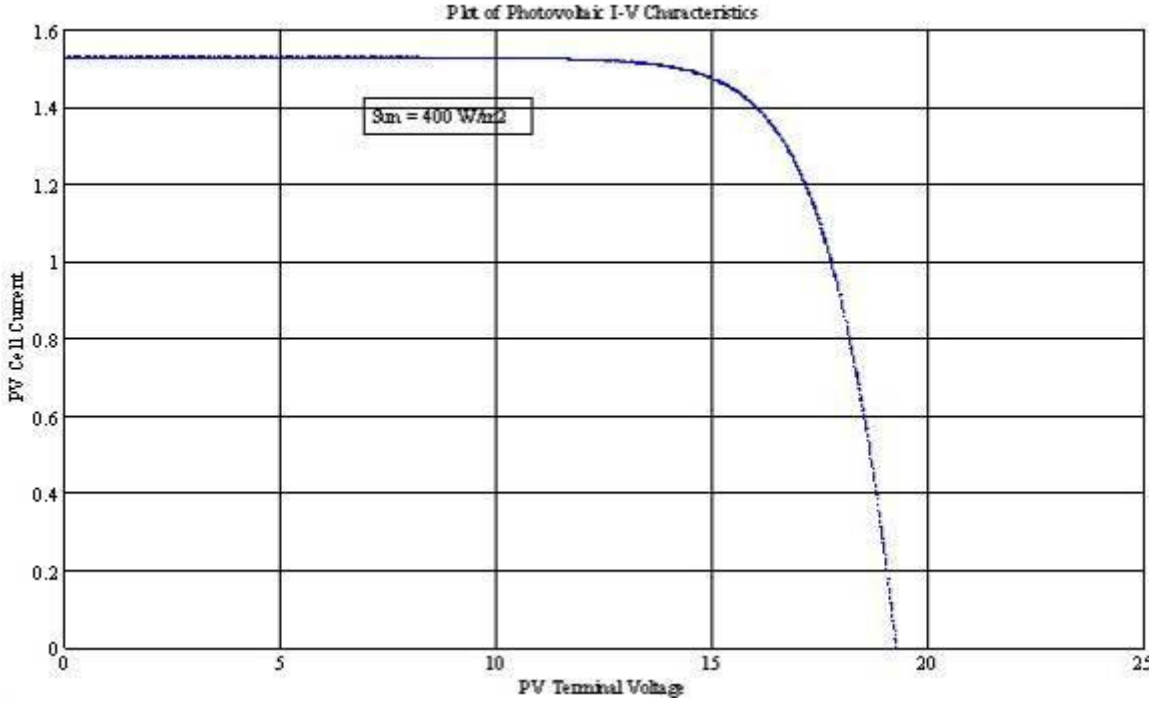

Figure 3.8 Photovoltaic Cell I-V characteristics

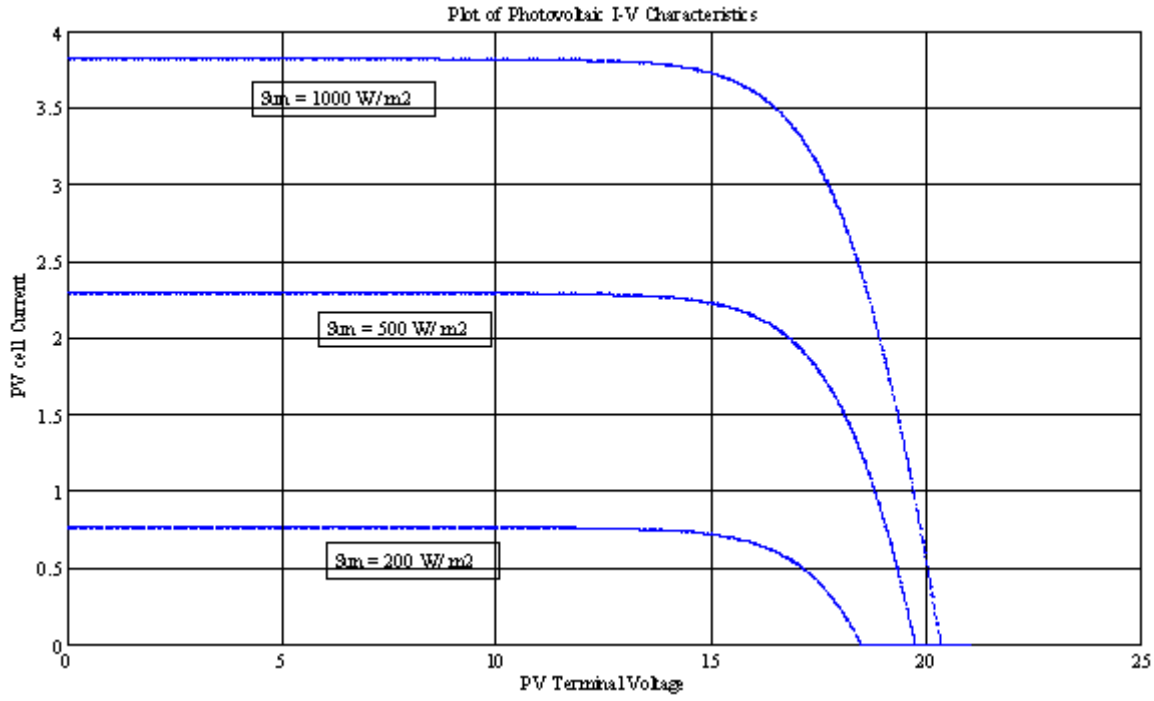

Figure 3.9 Photovoltaic Cell I-V Characteristics

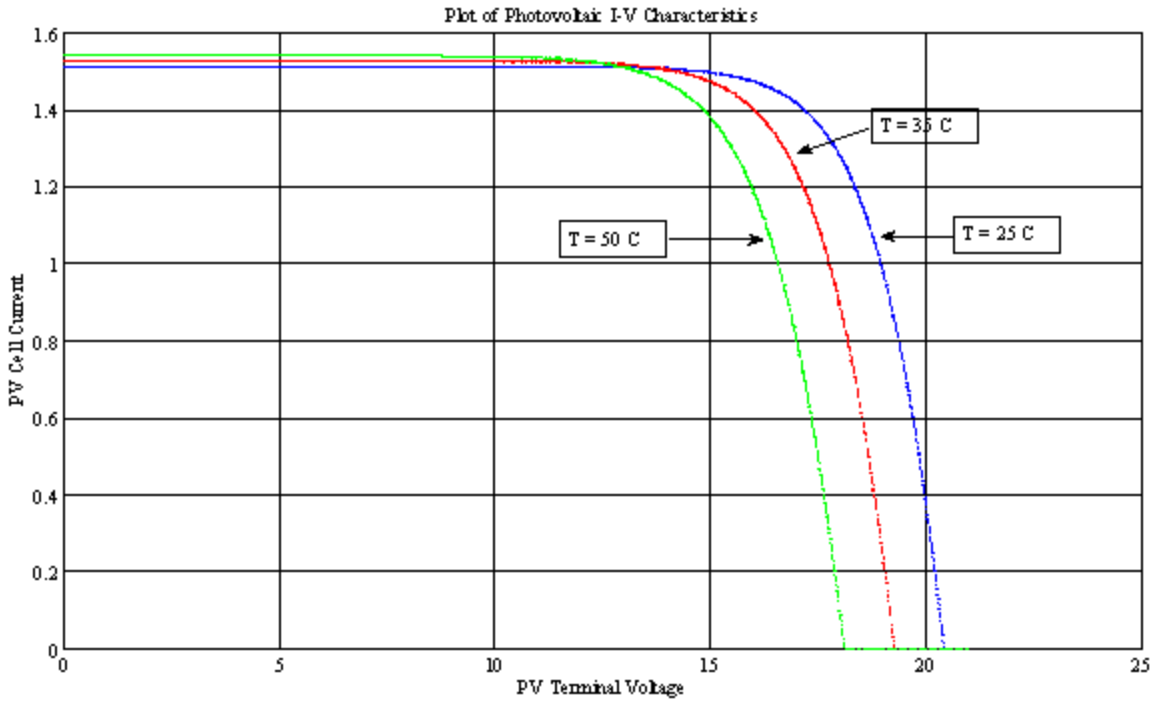

Figure 3.10 Photovoltaic I-V characteristics under Varying Temperature

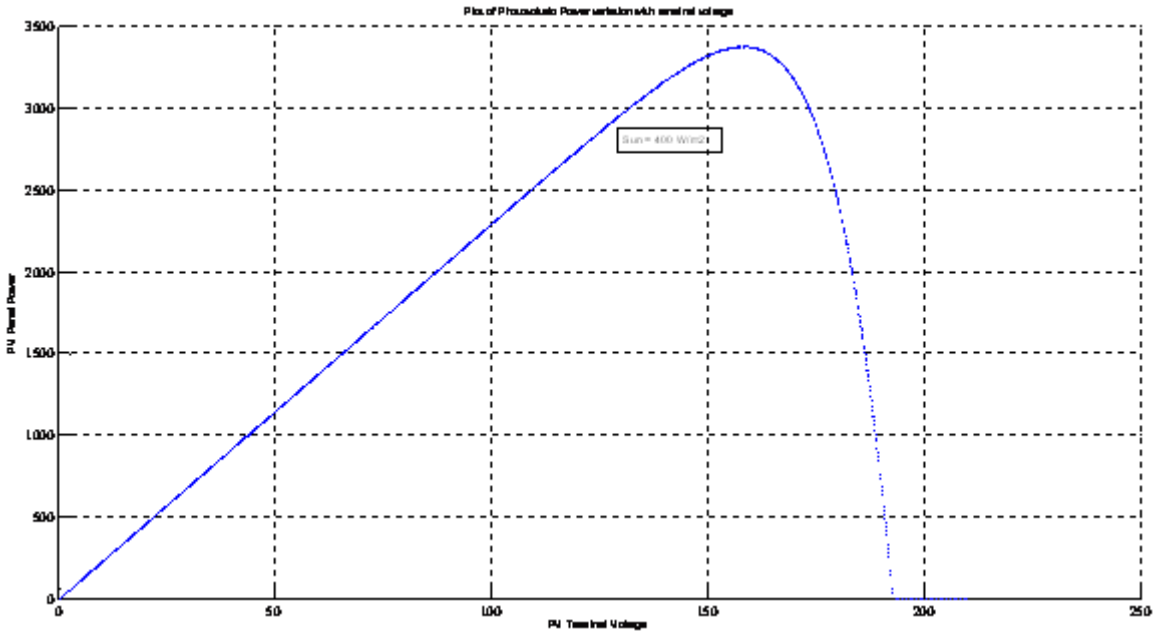

Figure 3.11 Photovoltaic System

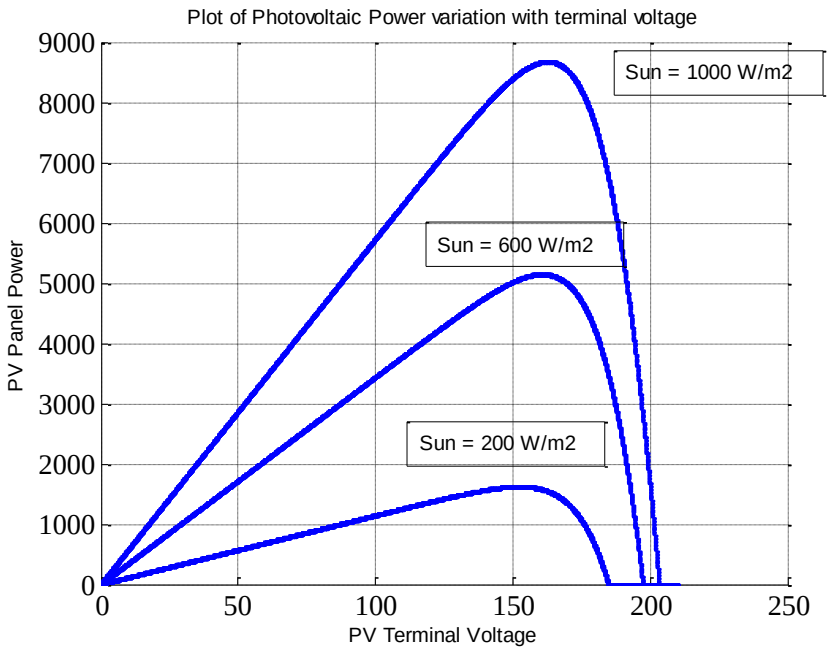

Figure 3.12 Photovoltaic System Power Variation with Sun Radiation

3.5 Photovoltaics System Architecture

The output dc voltage of the photovoltaic system is connected to the grid and local loads through power electronics converters. Broadly, there are two possible methodologies for interconnecting the PV system to the grid and local loads. They are:

- Direct DC – AC conversion
- DC-DC-AC conversion

3.5.1 Direct DC – AC conversion

In the first method, the output power of the PV system could be directly converted to the grid mains AC. The main problem with this option is that as seen from Figure 3.12, and explained in Chapter 5, the PV cell has high efficiency at certain optimal voltage points which change with various factors like sun radiation etc. Hence, it is necessary to control the PV system accordingly to operate the system at these high efficiency points,

thus deriving maximum benefit from the renewable system. Further, power electronics converters required for interconnecting the PV system to the grid need to boost the dc voltage to the level that is compatible with the grid voltage. Hence, an intermediate power conversion stage is always necessary, and accordingly the option of direct DC-AC conversion is never used for grid interface.

3.5.2 DC-DC-AC conversion

As was explained earlier, an intermediate power converter stage is required since the PV cell has high efficiency at certain optimal voltage points and also the intermediate stage helps in providing isolation between the power source and the grid. Even though the intermediate converter adds to the additional cost of the system, the above mentioned benefits outweighs the cost. Generally, transformers are preferred for voltage boosting and isolation purposes. However, the main issue with transformers is that they are generally bulky in size, and the cost of the system also increases. Hence, many transformer less varieties of isolated dc-dc converter topologies like the half bridge, full bridge, forward converter, fly back converter, push-pull converter, two inductor boost converter, cascaded isolated bridge converter followed by a non-isolated boost or buck converter, resonant converters etc [32] have been proposed for the PV system integration to the grid. While each topology has its own merits and demerits, for low power PV systems (~ 10 kW systems), isolation is not mandatory now as was in previous years [33]. Hence, in this dissertation isolation of the energy system was not considered. Hence, considering the cost and performance of the system, a non-isolated boost dc-dc converter is selected for PV system interconnection to the grid. The boost converter is an ideal choice for the PV system as the generated dc voltage is generally lower than the

required dc voltage for grid connection. Further, the control of the converter is also simple when compared to other types of converters.

Figure 3.13 shows the selected converter architecture for the photovoltaic considered. As was mentioned in Chapter 2, the selected architecture has many advantages, particularly when a hybrid renewable energy source system is considered. The following chapter 4 gives more details on the architecture of the grid side DC-AC converter selected for the hybrid system.

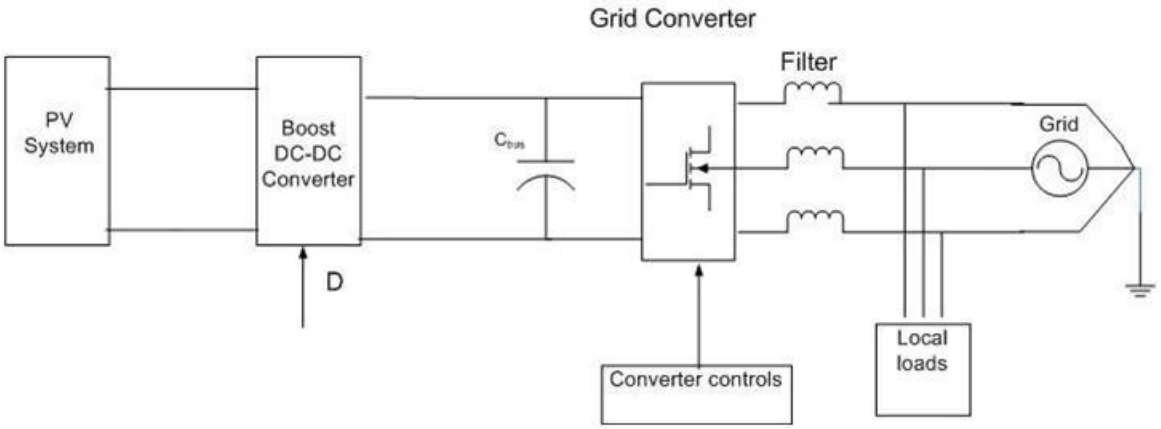

Figure 3.13 Photovoltaic System Architecture

CHAPTER IV

HYBRID WIND PHOTOVOLTAIC SYSTEM

4.1 Background

There are several ways to integrate different alternative energy sources to form a hybrid system. The configurations differ in the number and type of power electronic interface converters used, number of sensors required, switching losses etc. Broadly, the renewable energy integration can be divided into AC and DC Coupling, with the AC coupling classified further into power frequency AC (PFAC) coupling and high frequency AC (HFAC) coupling as shown in Figure 4.2 and Figure 4.3. In the DC coupling configuration, different alternative energy sources are connected to a common DC bus through appropriate power electronic interfacing circuits, and then the DC energy is converted into AC through a DC/AC converter. This scheme has the advantage of having simpler controls, and there are no synchronization issues as in AC coupling. In a PFAC coupling scheme, the different energy sources are integrated through power electronic converters to a power frequency AC bus, and in the HFAC scheme, the different energy sources are coupled to a HFAC bus, which is then converted into 60Hz AC power through an AC/AC converter. The HFAC configuration is mostly used in applications with HFAC (e.g., 400 Hz) loads, such as airplanes, vessels, submarines and space station applications [34]. Since it typically, requires more number of converter stages than the AC or DC coupling schemes, it is seldom used for renewable energy applications. While, the PFAC link scheme seems to be more modular than DC coupling

and is ready for grid connection, the synchronization issues, and control complexity are the main problems for being able to be used for hybrid energy source applications.

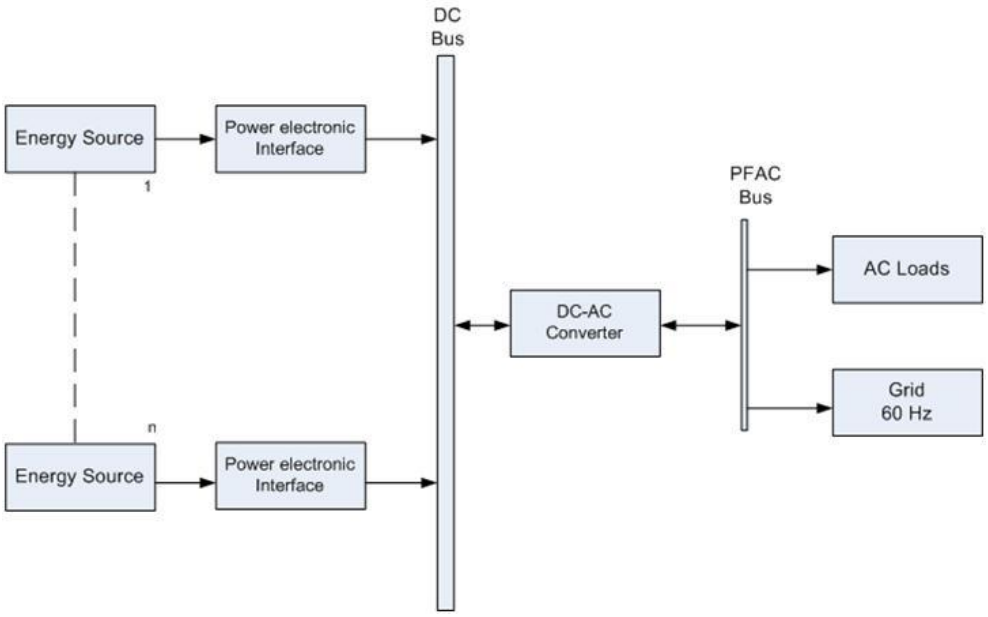

Figure 4.1 DC Bus Power Architecture

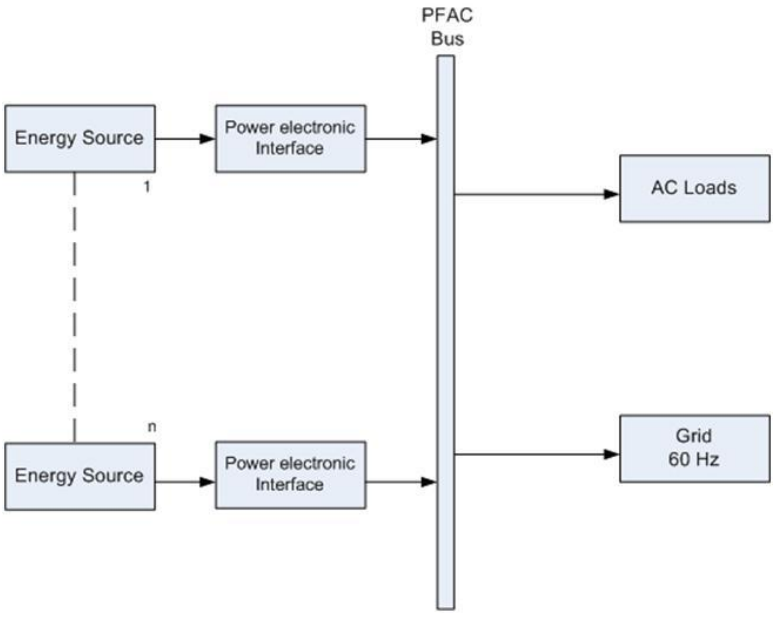

Figure 4.2 PFAC Architecture

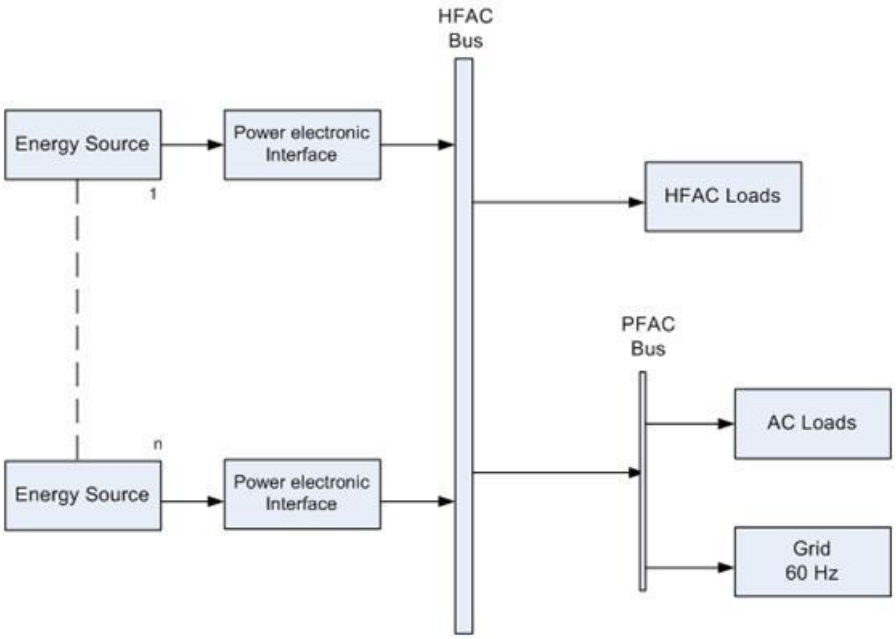

Figure 4.3 HFAC Power Architecture

Due to the above reasons, the DC coupling scheme is most used for hybrid energy source applications and is used in this dissertation. This chapter deals with the various configurations for the DC-AC power electronic converter (grid side converter) and the selected architecture for the considered hybrid renewable energy system.

4.2 DC-AC Converter Classification

As was mentioned earlier, there are several options for the grid side DC-AC converter, and they can be broadly classified into Voltage Source Converter (VSC), and Current Source Converter (CSC); Two-Level and Multi –Level Converters etc.

4.3 Voltage Source and Current Source Converters

Converters can be classified into voltage source converter (VSCs) or Current Source Converter (CSI) depending on the dc input source. The dc source in a VSC is a fixed voltage source and for a CSC the dc source is nearly a constant current source. In a

voltage VSC, the output ac voltage is a function of the converter operation, whereas the output current is given by the nature of the load. The DC link is parallel capacitors, which regulate the DC bus voltage ripple and store energy for the system. The inverter is composed of insulated gate bipolar transistor (IGBT) semiconductor switches. Due to the improvements in the power carrying capabilities of the IGBTs, they are being increasingly used for VSC. For a current source converter, the output current is a function of the converter operation, and the output voltage is determined by the nature of the load. The switches of a CSC generally need to have the reverse blocking capability, and hence typically diodes in series with switches are used when IGBTs are used as switches. [35]. Hence, typically, CSCs use SCR, GTO, SGCT devices for the converter applications. Figure 4.4 and Figure 4.5 shows the current source and voltage source converter architectures.

The main difference between a VSC and a CSC is that typically, the VSCs are fully integrated, while many CSCs are non-integrated devices hence requiring an external isolation which generally is a transformer or a harmonic filter/reactor [35]. Further, poor power factor and harmonics generated by the CSI input require very large K-rated transformers or reactor/filter banks. Also, for medium voltage applications CSCs still use SCR, GTO, SGCT devices for the converter applications, whereas the designs with IGBT based VSCs are being used in the recent years. It was seen that the IGBT based VSCs have the highest-efficiency design, and the SGCT based CSCs are efficient but come with slower switching speeds and higher on-state conduction [35].

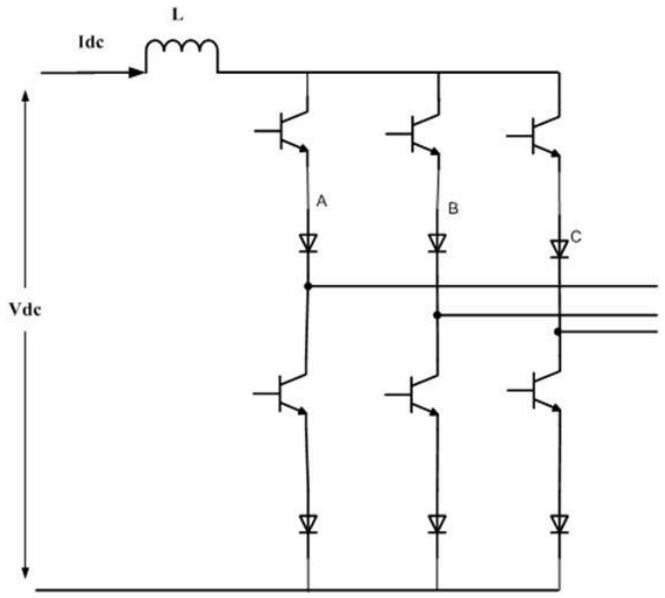

Figure 4.4 Current Source Converter

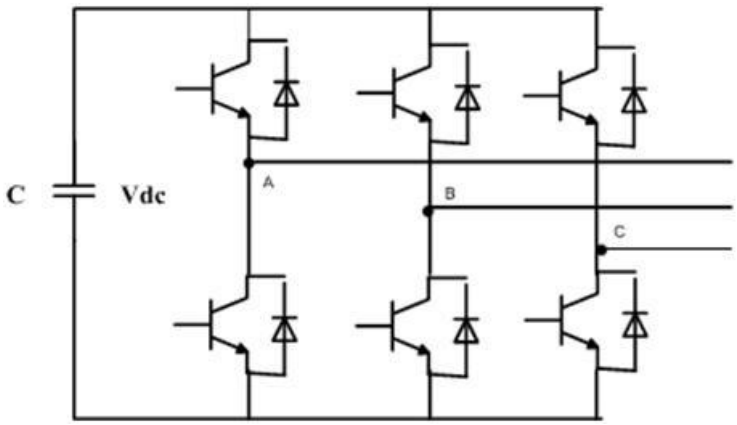

Figure 4.5 Voltage Source Converter

The CSCs typically incorporate two large DC inductors for current ripple minimization, energy storage and for fault current limiting. Since the time rate of change for current flow is proportional to the inductor size, the dynamic performance of the CSC decreases [35]. VSCs designs do not use DC inductors within the DC link but use capacitors. The capacitors provide the instantaneous current required for the dynamic systems, and therefore are better suited for high performance applications. It could be

seen that from size, efficiency, components, perspective, the VSCs are superior to CSCs and hence the VSC has been selected in this dissertation for the DC-AC converter. Table 4.1 gives the comparison of the Voltage Source and Current Source Converters.

Table 4.1 Comparison of Current Source and Voltage Source Converters

Comparison	**Current Source Converter**	**Voltage Source Converter**
Harmonics	High, requires isolation/filter	Low, meets IEEE 519 standards
Resonance Issue	Must tune input filter	No
Mean Time of Failure (MTTF)	~ 2 years	~11.5 years
Dynamic Response	Limited by DC choke, filter	Relatively faster
Efficiency	95.7%	97.7%
Size	Limited Integration, relatively high footprint	Small footprint

4.4 Two Level and Multi-Level Voltage Source Converters

The VSCs can be further classified into two level and multi level based on the number of dc voltage levels used to synthesize the output AC voltage. A two-level VSC uses two voltage levels (typically +Vdc, 0 or +Vdc, -Vdc) to synthesize the output AC voltage. The advantage of using only two voltage levels is that the converter control is simple, and even many advanced control techniques could be used. However, the disadvantage is that when compared to multi-level VSCs the harmonics are increased. Since the development of the neutral-point clamped three-level converter many multilevel converter topologies have been developed.

The different proposed multilevel converter topologies can be classified in the following five categories [17]:

- Multilevel configurations with diode clamps
- Multilevel configurations with bi-directional switch interconnection

- Multilevel configurations with flying capacitors
- Multilevel configurations with cascaded single phase H-bridge inverters

Figure 4.6 shows a brief overview of one phase leg of various multi level converters. A diode clamped multilevel converter is similar to a typical two level PWM-VSC, however, the main problem with this topology is that a voltage-balancing problem occurs for levels higher than three, but for a three level converter the problem do exist but is a minor problem [17]. The main problem with multi level configurations with bi-directional switch interconnection is that at least half of the total switches have to block the full DC-link voltage, which increases the losses. The topology of a multilevel configuration with flying capacitor multilevel converter is very similar to that of the diode clamped multilevel converter shown but without the voltage balancing problem. However, the main difference is that the two diodes per phase configuration may be substituted by one capacitor. The multilevel converter based on multiple H-bridge inverters is heavy, bulky and control is complex. Also, it is difficult to connect different DC-sources in a back-to-back configuration as it will lead to a short circuit when the two converters are not switching synchronously [17].

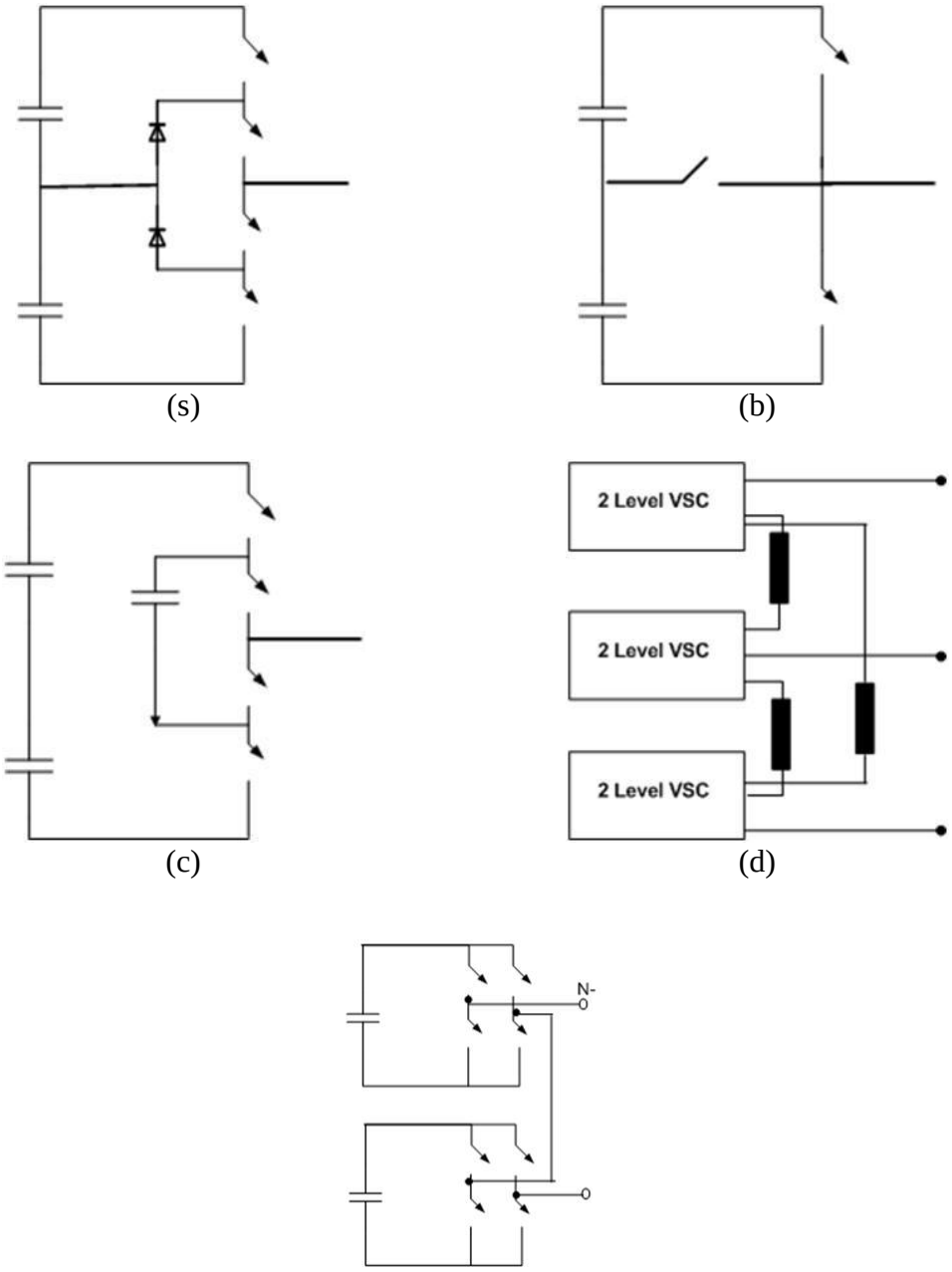

Figure 4.6 Multilevel Converter Configurations. a) Diode clamped multilevel converter , b) Multilevel converter with bidirectional switch interconnection, c) Flying capacitor multilevel converter, d) Multilevel converter consisting of three three-phase inverters

4.4.1 Advantages of Multilevel Converter

The main advantages of using multilevel converters are that the voltage capability of the converters is higher, voltage harmonics and EMI effects are reduced, thus requiring lower ratings for the filters. Also, for the same harmonic performance the switching frequency can be reduced to about 25% of the switching frequency of a two-level converter. Even though the conducting losses are higher for the multilevel converter, the overall efficiency for the diode clamped multilevel converter is higher than the efficiency for a comparable two-level converter [17].

4.4.2 Disadvantages of Multilevel Converter

The main disadvantage of the multi level (and mainly three level converters) converters with split DC-link is the voltage imbalance between the upper and the lower DC-link capacitor which is mainly caused by differences in the real capacitance of each capacitor, inaccuracies in the dead-time implementation or an unbalanced load [17]. Even though by a proper modulation control of the switches, the imbalance problem can be solved to a certain extent, it is necessary to measure the voltage across the various capacitors in the DC-link requiring more sensors. Also, many multi-level topologies have a higher component count which increases costs, control complexity and results in increase in losses. For example, an M level diode-clamped converter has (M-1) capacitors on the DC bus. In each phase leg, there are 2(M-1) switches, with each switching device required to block a voltage level of V_{dc}/(M-1) However, with the same rating, there will be (M-1)(M-2) clamping diodes required for each phase. Thus as M increases, there is a quadratic increase in number of clamping diodes which puts a practical limit on the number of levels. A flying capacitor topology requires (M-1)(M-2)3/2 +(M-1) number of capacitors. Another problem with many topologies (first three mentioned topologies) is

the unequal current stresses on the semiconductor switches. It was seen that the upper and lower switches in an inverter branch are derated compared to the switches in the middle, and it was suggested that for an appropriate design of the converter, different devices are required. And for some topologies, both the unequal current stress and the unequal voltage stress is a problem. Also, since the number of switching elements in the conducting path is higher than for the other converters resulting in increase in the conduction losses of the converter [17].

4.5 Hybrid Wind-Photovoltaic System Architecture

Based on the selection of the generator and converter topologies for the Wind and Photovoltaic systems as mentioned in the earlier chapter and the selected DC-AC grid side converter topology, Figure 4.7 shows the selected architecture for the hybrid Wind-PV renewable energy system used in this. It could be seen that the Wind and Photovoltaic systems use intermediate Boost DC-DC converters for extracting maximum power from the Wind and PV systems respectively as explained in the next Chapter. The grid side VSC converter is controlled in a way such that the interconnection standards as mentioned in the Appendix are met while supplying power to the local loads and to the grid. The selected architecture has the advantage that the Wind and PV system can be controlled independently, and there would not be a discontinuity in supply if either of these sources fail. Also, the cost of the system in less and has no synchronization issues since the multiple sources are connected to a common dc bus.

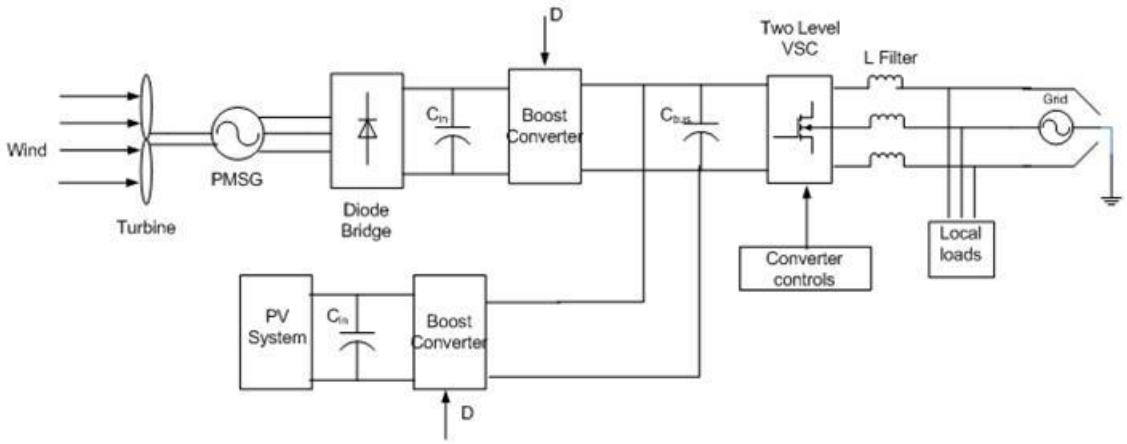

Figure 4.7 Hybrid System Architecture

CHAPTER V

MAXIMUM POWER EXTRACTION FROM HYBRID SYSTEM

5.1 Background

It was seen in Chapter 2 and Chapter 3 that for both Wind and Photovoltaic systems, the power extracted and system efficiency is high at certain optimal points which change with atmospheric conditions like wind speed, sun radiation etc. It was seen that by using advanced control methods more than 15% power can be extracted from both the wind and PV systems each [4][5]. Hence, it has become imperative to use these advanced control methodologies for extracting as much power as possible from these renewable energy sources, thereby reducing the cost to kW ratio which acts as an incentive in increasing the renewable energy penetration into the grid. This chapter gives a review of the various maximum power extraction algorithms proposed for the Wind and Photovoltaic systems and a modified algorithm is proposed for maximum power extraction for Wind energy system and based on the review the most optimum maximum power algorithm is chosen and developed for the photovoltaic system.

5.2 Wind Maximum Power Extraction Algorithms

5.2.1 Background

The advancements in the machine drive technologies and grid interconnection controls have increased the feasibility of more wind power penetration into the system. Although the wind energy systems have lower installation and maintenance costs when

compared to other renewable energy technologies, the overall system cost and hence the cost/ kW ratio can be further reduced by using high-efficiency power converters coupled to variable speed machines. It was clear from the discussion in Chapter 2 that compared to constant speed operation; variable speed wind turbines generate 10–15% higher power output. Recently, much effort has been placed on the use of a low speed direct-drive variable speed generator to eliminate the gearbox which results in lower mechanical stress and less power fluctuation. Hence, it is important to develop advanced control methods to extract maximum power output from wind turbines, and as such, many maximum power point tracking (MPPT) algorithms have been developed over the years.

5.2.2 Review of Wind Maximum Power Extraction Algorithms

5.2.2.1 Background

As was mentioned in the Chapter 2, the mechanical output power of a wind turbine at a given wind speed depends on the turbine's tip speed ratio (TSR), which is defined as the ratio of turbine rotor tip speed to the wind speed. The maximum turbine energy conversion efficiency occurs at a particular TSR for a particular wind speed and blade pitch angle. Hence, as wind speed changes, the turbine's rotor speed needs to be changed accordingly in order to extract maximum power. Figure 5.1 shows the turbine power variation for various wind speeds as a function of rotor speed. It can be seen that for each wind speed there exists a particular rotor speed at which the power available is maximum. The problem considered by the various MPPT methods is to determine the optimum rotor speed corresponding to the wind speed at which maximum energy capture could be achieved.

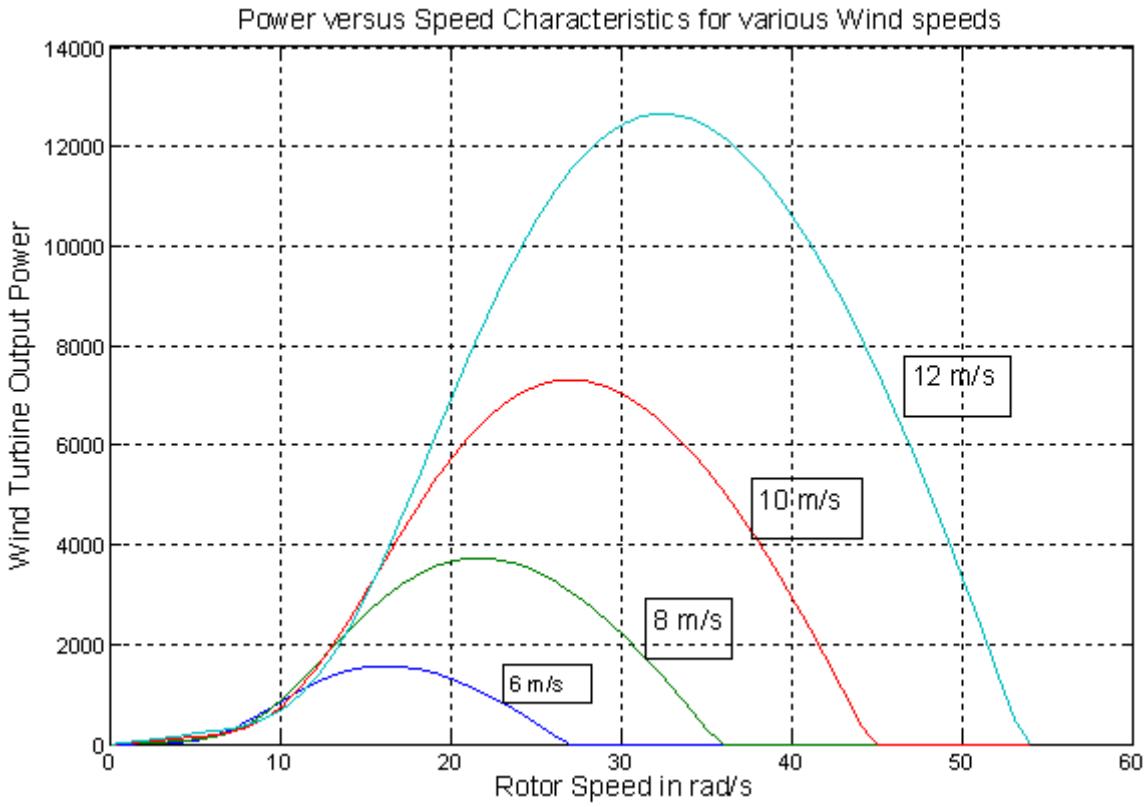

Figure 5.1 Wind Turbine Power- Speed Characteristics for Various Wind Speeds

Broadly, the MPPT algorithms are categorized into three types: Tip-Speed ratio control (TSR), Power-Signal feedback (PSF), Hill climb search (HCS) based. TSR control method regulates the wind turbine rotor speed to maintain an optimal TSR and requires measurement of both the wind speed and turbine speed. The optimal TSR for a given wind speed is obtained from the turbine-generator characteristics and varies from system to system. PSF control requires the knowledge of the wind turbine's maximum power curve obtained for a turbine speed via prior simulations or tests for individual wind turbines and the reference speed is obtained from the curve. It could be seen that both the TSR control and PSF control require extensive turbine knowledge and measurement of generator speed and/or wind speed thus increasing the number of sensors and the control complexity. This makes the practical implementation of the algorithm expensive and

difficult to implement. To overcome these difficulties, Hill climbs Search (HCS) based methods were proposed where the algorithm continuously searches for the turbine peak output power by varying the generator speed/torque and based on the change in power direction, determining the next variation. While each of these three methods has their own merits and demerits, a number of variations have been proposed over the last 30 years using different techniques that address these issues. Figure 5.2 shows the total number of MPPT papers published per year since the earliest known MPPT paper. It could be seen that the number of papers per year has increased considerably over the last decade, and much attention has been focused in the recent years. The developed methods vary in technique used, complexity, sensors required, convergence speed, memory requirement, range of effectiveness etc.

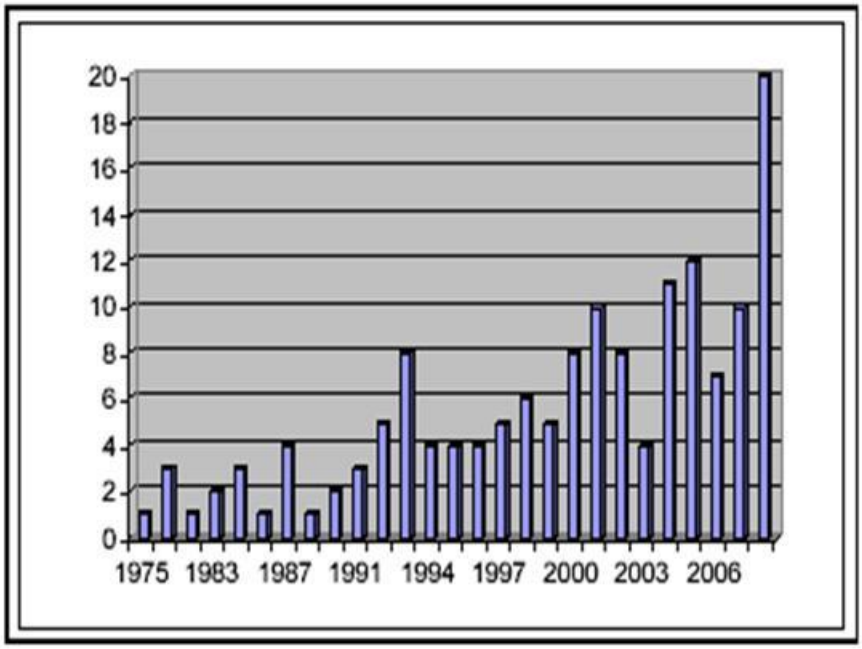

Figure 5.2 Number of Papers Proposed Over the Years

It is very important to adequately determine which method, newly proposed or existing, is appropriate for a given system. This discrepancy confuses a new researcher regarding the true status of MPPT techniques in wind systems. Given such large variations in MPPT algorithms, a survey of all the methods and variations proposed over the last 30 years would be very beneficial to researchers. Recent papers have generally had shorter literature reviews that largely summarize or repeat the literature reviews of only some quoted previous works. A comprehensive survey of all these variations result in the further classification of the proposed MPPT algorithms into eight types as shown in Figure 5.3. The above categorization was made based on the methodology employed in generating the reference signal (voltage/torque/speed) and the technique used.

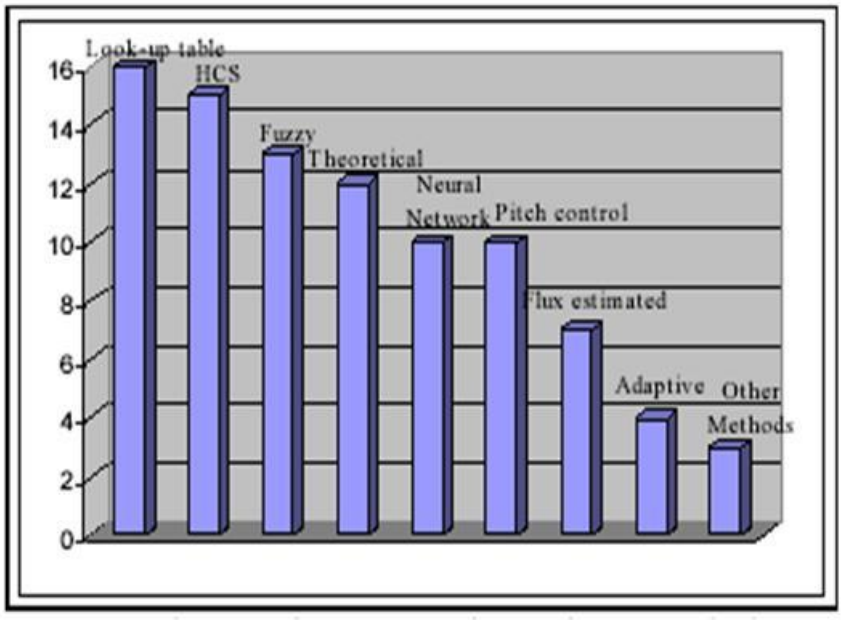

Figure 5.3 Categorization of Wind Maximum Power Extraction Algorithms

The difference between many of the proposed variations in the algorithms lies in the number of sensors required, type and method of generation of the reference signals,

the convergence speed, complexity, memory requirement, performance under varying wind speeds etc. It could also be seen that a number of papers have proposed methods that use a combination of techniques in achieving the maximum power tracking. Each of the above mentioned categories are mentioned briefly in the following sections.

5.2.2.2 Hill Climb Search

Hill Climb Search (HCS) [36]-[47] involves a perturbation in the reference signal, generally the generator rotor speed or the terminal voltage and observing the change in the power. Referring to Table 5.1, it can be seen that incrementing (decrementing) the generator speed (or terminal voltage) increases (decreases) the power when operating on the left of the maximum power point (MPP) and decreases (increases) the power when on the right. Therefore, if the power increases, the following perturbation step should be kept the same and if there is a decrease in power the perturbation should be reversed. This is repeated until the MPP is reached. While the algorithm implementation is simple and is independent of turbine characteristics, many issues exist like the selection of step size, inability to effectively track the true maximum power point when the system inertia is considered, oscillations around the maximum power point etc. The inertia of the system causes a time lag in response or inability to track the maximum point. Reducing the perturbation step size can minimize the oscillations around MPP. However, a smaller perturbation size slows down the MPPT process. A solution to this conflicting situation is to have a variable perturbation size that gets smaller towards the MPPT. Reference [36] proposes a modified HCS where the constant K_{opt} that describes the optimal power curve of a constant pitch wind turbine is determined during the normal hill climbing method by perturbing the generator speed. When the maximum is detected for a particular wind

speed, the K_{opt} value is determined by measuring the power, the rotational speed and the maximum point for other wind speed conditions could be determined by constructing the power curve from the K_{opt} value. The algorithm, however, doesn't take the inertia of the machine into account and suffers from the same drawbacks as the traditional HCS method in determining the K_{opt}. Reference [19] proposes a HCS method using the generator terminal voltage as a perturbation signal, but uses Newton Raphson method for determining the step length. In [47] the converter duty cycle is perturbed and the algorithm uses the steepest ascent method for determining the next step. A resistive dummy load is also used for protection of the system during high wind speed conditions. Reference [44] proposes a control strategy to reduce the overall system cost with reduced switch count using B-4 PWM converters instead of B-6 power converters. In [40] a modified HCS method using the generator speed as the perturbation signal is used, and specifies the sampling frequency and step length selection criteria for addressing the inertia problem of the HCS method. While the results are very promising, the determination of the constants required is very difficult.

5.2.2.3 Lookup Table

Several papers [48]-[58] were proposed that utilize prior knowledge of the wind generation system obtained either from simulations or field tests. The algorithm convergence speed and performance depends on the knowledge of system characteristics and its accuracy for various speeds. While some algorithms require the measurement of wind speed to generate a corresponding optimal rotor speed or terminal voltage reference, others are based on generating the optimal reference signals from the measured generator signals. Reference [42] is one of the earlier papers that proposed a control strategy using

the optimum values obtained from manufacturer data and compare the control policies. Reference [44] determines the optimal power reference from the wind speed estimated by calculating the tip speed ratio from a lookup table that uses the electric power and the rotor speed data at each sample interval. In [45] the tracking speed is varied according to the change in wind speed and in order to avoid inverter dead time effect, the algorithm is synchronized to generator rotation speed. The step length of the algorithm and the reference speed are pre-determined from experimental simulations. Both [47] [46] use the optimum shaft speed to wind speed data from manufacturer data and produces the reference power output. Reference [47] generates the reference duty cycle for the converter from the measured generator shaft frequency obtained through prior simulation. In [48] an optimum current reference is generated from a lookup table obtained via prior simulations.

5.2.2.4 Pitch Control

In large wind turbines pitch control is often used to regulate power flow especially when wind speed is above rated speed. In low to medium wind speeds, the pitch angle is controlled to allow the wind turbine to operate at its optimum condition and in the high wind speed region; the pitch angle is increased to shed some of the aerodynamic power which is limited by the pitch rate. The ability to control the rotor speed in the high wind speed region is dependent on the pitch-actuator response limit and the rating of the power converter. If the pitch actuator is too slow and the power converter size is too small, the controllability is poor [59]. Several papers [59]-[62] have been proposed over the last few decades that regulate the wind turbine power using pitch control. Many of the earlier strategies proposed use prior system knowledge of the pitch

angle to power or rotor speed characteristics obtained from prior simulations. More recently, with the advances in microcontroller and memory technologies, many intelligent techniques like neural network, fuzzy logic, adaptive based etc. pitch controllers are proposed obtaining the pitch angle. A fuzzy logic controller is used in [60] for selecting the required pitch based on the reference power. In [61] pitch control is used for maximum power extraction and for active stalling during high winds. The power reference to wind speed curve is used to generate the required pitch angle for control. In [62] an approach is proposed to realize the optimum control of pitch angle from momentum theory and blade angle analysis.

5.2.2.5 Fuzzy Logic Control

The advancements in the microcontroller technology and the capability to work with imprecise inputs and handle nonlinear systems has increased the fuzzy logic control (FLC) applications in wind maximum power control. Many control strategies [63]-[71] have been proposed that use the FLC for MPPT applications either independently or along with other methods. Fuzzy logic control generally consists of three stages: fuzzification, rule base table lookup, and defuzzification. In the fuzzification stage, input variables are converted into linguistic variables based on a membership function. The commonly used inputs to an FLC are error and change in error. Based on the input, a rule base lookup table obtained by prior knowledge of the system's response for various errors, the FLC generates output, which is typically a change in duty ratio or rotor speed. In the defuzzification stage, the FLC output is converted from a linguistic variable to a numerical variable using another membership function. While MPPT fuzzy logic controllers have been shown to perform well under varying atmospheric conditions, their

effectiveness depends a lot on the knowledge of the user in choosing the right error, levels of membership functions, and selection of rule base table. The memory requirement also poses limitations in its implementation.

Three FLCs are used in [63], with the first using HCS based method to vary generator speed and observe power output and tracking the generator speed for a particular wind velocity to extract the maximum power The second FLC is used when the maximum power point is reached by the first FLC to increase the machine-converter efficiency by reducing the rotor. The third FLC is used to provide robust speed control against wind gust and turbine oscillatory torque. Even though high efficiencies are observed in this paper, the constants used for scaling factors needs to be determined by prior experimentation. References [64], [65], [68], and [69] use the difference between the P_{max} and P_{out} and the derivative of this signal as inputs with standard triangular membership functions for both input and output. The variation of generator power and the variation of output torque command are used as inputs in [66] with triangular membership functions and seven level rule base table. A data driven design methodology able to generate a Takagi—Sugeno—Kang (TSK) fuzzy model for maximum energy extraction is proposed in [67]. The TSK model is generated by combining the fuzzy clustering methods for partitioning the input–output space with genetic algorithms, and recursive least-squares optimization for model parameter adaptation.

5.2.2.6 Neural Network

Similar to Fuzzy logic controllers, the neural networks (NN) have become popular and widespread with the advancements in microcontroller technology [72-78]. Neural Networks have three layers: input, hidden, and output layers and the number of nodes in

each layer vary and are user-dependent [72]. The input variables can be wind speed, pitch angle, rotor speed, output torque, terminal voltage etc. or any combination of these. The output is generally a reference signal like duty cycle, reference rotor speed, reference torque etc. that is used to drive the power converter close to the MPP. The closer the operating point gets to the MPP depends on the type of algorithm used by the hidden layer, the weights assigned to the layers and the training given to the neural network for a particular system for various input-output patterns. While the efficiency of the NN control strategies are generally good, since most mechanical parts have varying characteristics with aging and under different environmental conditions, the neural network has to be periodically trained to guarantee accurate MPPT, and also the selection of appropriate weights for the training is an important issue.

In [72][74] NN principles are applied for wind velocity estimation and generating the reference rotor speed from a lookup table based on the estimated wind velocity . The paper also proposes a method of generating pseudo-power curves to compensate the potential drift of wind turbine power. In [73] maximum power is tracked by changing the pitch angle of the wind turbine blades by the NN pitch controller and firing angles of the inverter switches. In [76] NN is used for determining the duty ratio of the first buck–boost converter to achieve maximum power tracking, and. the second buck–boost converter for output voltage regulation. A NN is used to determine the reference output power based on the wind speed average obtained from anemometer, the standard deviation and the past output power as input data in [76], and in [78] a three layer NN using Gaussian radial basis function network (GRBFN) is used to provide a nonlinear input-output mapping for the turbine aerodynamic characteristics. Based on this the wind speed is estimated from the measured generator electrical power while taking into

account the power loss. The optimal rotor speed is determined from the estimated wind speed by calculating the optimum tip speed ratio from the roots of the derivative of the polynomial describing the performance coefficient.

5.2.2.7 Theoretical

Several control strategies [79]- [83] have also been proposed that developed theoretical relationship between the control variables for achieving the maximum power from the system. For example, in [70] generator power and output dc voltage were expressed as a function of duty ratio of the boost chopper and generator rotational frequency and an optimum duty ratio for obtaining the maximum power was theoretically determined by differentiating the obtained expression with respect to duty ratio. In [71] the input current reference of boost converter for MPPT is calculated from a predetermined maximum output torque pattern according to the speed of generator. While no mention of the selection of pattern relationship was made, the simulation results seem to be satisfactory. In [72,73] and [57] a theoretical ideal relationship between dc-link voltage, electrical angular frequency and tip speed ratio obtained from manufacturer data. In [82] an optimum torque reference is calculated for an estimated generator speed by using the linear relation between these quantities at maximum power point. The corresponding optimum converter currents are generated from this optimum torque reference by obtaining a relation between them using the iron loss model of the machine. The paper also suggests a maximum torque control for increasing the efficiency of the system when the converter current reaches the limit by increasing the torque for the same current when the converter. While the simulation results appear very good, it could be

seen that the performance of the algorithm is very dependent on the constant parameters selection and the machine parameters.

5.2.2.8 Adaptive

As mentioned above the problem with varying system parameters and uncertain inputs could be overcome using fuzzy logic or neural network controllers. However, they do not guarantee an optimal response [84]. But, an adaptive controller could estimate the uncertain parameters, and could provide an optimal response. While not many strategies have been proposed over the years [84]-[90], provide an insight into the selection of the control laws. In [84] an adaptation law was chosen to provide an estimate of the turbine torque that varies with wind speed and a controller was then designed for the linearized system using linear control theory, with additional input that would result in a linear control law with the reference rotor speed. Reference [85] also proposes an adaptive feedback linearization to estimate the uncertain and changing plant parameters for a cage induction generator. The authors also develop a relationship between various parameters for ensuring the convergence of the system and hence the trade of between the desired dynamics and the size of the convergence region was taken into consideration in the design procedure. While detailed simulation results were not given, the algorithm requires the wind speed measurement and the knowledge of the system parameters to generate the speed reference from a lookup table. Also, the performance of the algorithm is highly dependent on the selection of the adaptive law for generating the necessary torque reference.

In [86] a modified hill climb search technique along with an adaptive feature realized by a programmable look up table and a programmable array that are trained by

updating for new wind speeds is used. The algorithm requires the measurement of wind speed, rotor speed, terminal voltage and current thus increasing the number of sensors required. Also, the drawbacks associated with HCS method apply, and the memory requirements for adaptive nature increases. In [89] an adaptive pitch controller is proposed to maximize the energy capture and to reduce the mechanical loads along with a fuzzy controller to improve the damping characteristics of the wind energy system over a wide range.

5.2.2.9 Other Methods

Apart from the above-mentioned methods, several other MPPT control strategies [91]-[94] have also been proposed recently. In [92] Hysteresis Maximum Power Tracking scheme is proposed that uses the differential of the voltage with time as the control parameter and has two control modes, one used to calculate the output power and the other used to decide the output power decrement. A hysteresis loop is defined for changing between the two modes. While the algorithm performance is satisfactory, it does not consider the change in load, inertia effect or the voltage ripples that might occur. Also the selection of the control parameters is difficult and might require prior knowledge of the system. A sensor-less control strategy that uses the electrical torque control for driving the system towards maximum power point is proposed in [91]. The reference torque component of the current is obtained by estimating the rotor speed using a model reference adaptive system (MRAS) observer. The authors propose using rotor slot harmonics determined with an algorithm for spectral analysis for rotor speed estimation of the speed and for tuning the observer and compensate for the parameter variation and uncertainties. A fuzzy controller is also used in the system for dc bus

voltage regulation. The performance of the algorithm is highly dependent on the selection of the constant parameters for generating the torque reference and in the accurate estimation of the rotor speed and requires knowledge of the system. In [93] a control system that regulates the wind system along with the photovoltaic generation, the load and battery is proposed using passivity and sliding mode techniques. The resultant control law does not require wind measurement and relies on rotational speed and current measurements. Based on the simulation results the algorithm performance seems to be satisfactory but is highly dependent on the selection of the control laws describing the system. In [94] a flywheel is used a power stabilizer to decrease the response time constant of high inertia wind systems. The simulation results show that the performance coefficient is high in systems using flywheel as power stabilizer when compared to normal systems.

5.2.2.10 Comparison of Methods

With so many strategies proposed over the years for wind maximum power extraction, it might not be obvious how to determine which one is best suited for an application. Table 5.1 gives the main aspects that could be considered for selecting a particular strategy. It can be seen that a majority of the methods proposed have either high memory requirements or prior knowledge of the system characterisitcs and more sensors. However, recently much emphasis has been placed on sensorless methods that do not impose such restrictions [34]. The hill climb search based algorithms are beneficial as they do not require more number of sensors, the control is simple and is independent of turbine characteristics. Many new modifications have been proposed to

this method to address some of the issues which the traditional HCS based algorithms have as in [34].

Table 5.1 Comparison of Various Wind MPPT Algorithms

Technique	Complexity	Convergence Speed	Prior Training/ Knowledge	Memory Requirement	Wind Speed Measurement	Performance under Varying Wind Conditions
Hill Climb Search	Simple	Depends	No	No/ Minimal	No	Moderate
Theoretical Based	Simple	Fast	No	No	No	Less
Lookup Table	Simple	Fast	Yes	High	Yes	High
Fuzzy Logic	High	Fast	Yes	High	Depends	High
Neural Network	High	Fast	Yes	High	Depends	High
Pitch Control	Medium	Slow	Yes	No	Yes	Less
Flux Estimated	High	Slow	No	Depends	No	Moderate
Adaptive Methods	High	Medium	Yes	High	Depends	High
Other Methods	Moderate	Medium	Depends on the method	Depends on the method	Typically, yes	Depends, typically Moderate

5.2.3 Proposed Wind Maximum Power Extraction Algorithm

As was mentioned earlier, the process of the general hill climb search for maximum power extraction is explained using Figure 5.4. Assume that a wind turbine generator is initially operating to the left of point A. The generator speed is increased and the corresponding generator output power is calculated. If the output power increases when compared to the earlier step, the search is in the correct direction and the generator speed is increased again. This process is continued until the powers slope becomes zero, signaling that the top of the hill (or the maximum power point) is reached, which in Figure 5.4 corresponds to the point at the right of point A. If however the output power decreases when compared to the earlier step, then the generator speed is decreased and the search is continued in the opposite direction. In case of a sudden change in the wind speed, as in the point A, where the wind speed is suddenly increased and the corresponding operating point is now B, the power-speed slope is technically very large

resembling a change in wind speed and depending on the slope sign the direction of search is continued. In Figure 5.4, the search is continued until point C is reached at which the maximum power point corresponding to the wind speed is attained. Now if there is a decrease in wind speed, and the operating point shifts from point C to D, the power-speed slope is negative and the generator speed is decreased and the slope is observed until it becomes zero. While the algorithm implementation is simple and is independent of turbine characteristics, many issues exist like the selection of step size, inability to effectively track the true maximum power point when the system inertia is considered, oscillations around the maximum power point etc. The inertia of the system causes a time lag in response or inability to track the maximum point. Reducing the perturbation step size can minimize the oscillations around MPP. However, a smaller perturbation size slows down the MPPT process.

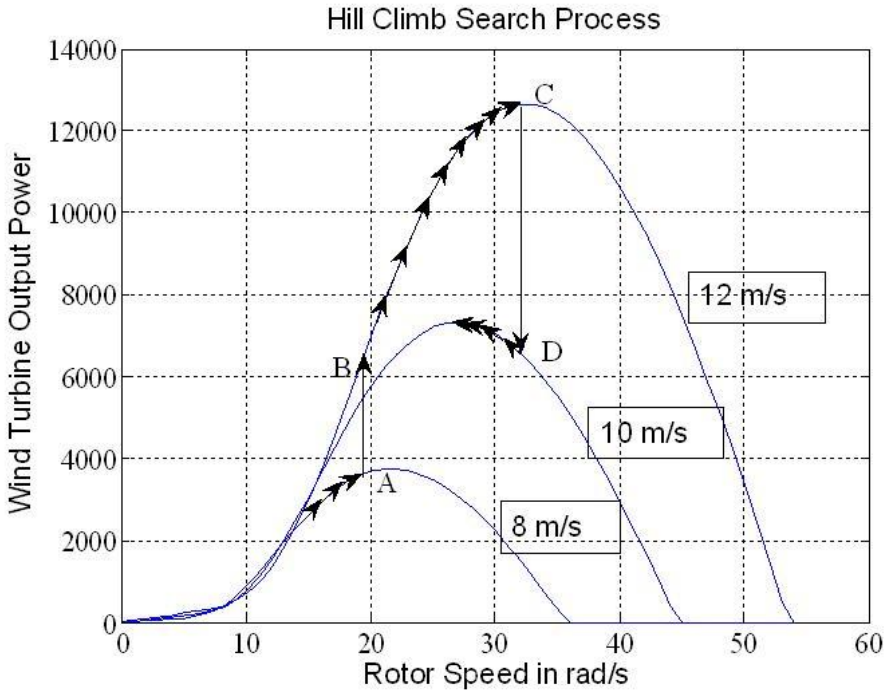

Figure 5.4 Hill Climb Search Process

As was mentioned in the earlier sections, the traditional hill climb search algorithm is not very efficient for small scale wind systems whose inertia is not negligible and at the same time is not as high as in the case of MW systems. When the system inertia is neglected, the turbine-generator system responds immediately to a change in wind speed or tracking process without any delay However, when the system inertia is considered, a sudden increase in the wind speed is not reflected in the generator speed as the inertia acts as an interlace. When the wind speed is suddenly increased, the rotational speed cannot change abruptly because of the inertia of the system. Therefore, the generator speed keeps operating at the same point, whereas the aerodynamic torque increases immediately. As a consequence of this positive torque unbalance, the rotor slowly accelerates reaching a steady state speed after a certain time lag. This causes a time lag in response and the generator speed takes time to reach steady state. This decreases the algorithms' ability to reach the maximum power at a faster rate.

Due to this time lag in response, the traditional hill climb search algorithm could not be used directly for wind energy systems when the inertia of the system is considered. Hence, a modification of the hill climb search algorithm is required for systems like the one under consideration with inertia.

5.2.3.1 PROPOSED ALGORITHM

For the purpose of explanation of the proposed algorithm, a variable speed wind turbine connected to a permanent magnet synchronous generator (PMSG) is considered. More details of the system considered are given in the next section.

The electrical output power from the PMSG is given by:

$$P_e = P_m - J\omega \frac{d\omega}{dt} \tag{31}$$

where: P_g is the generator output power,

P_m is the mechanical power input to generator,

$J\omega\, d\omega/dt$ is the power stored in the inertia of the machine.

Now, if the rate of change of generator speed $d\omega/dt$ in the above equation is kept constant equal to A, the above equation can be rewritten as:

$$P_g = P_m - J\omega A \tag{32}$$

The rate of change of generator output power is then given by:

$$\frac{dP_g}{dt} = \frac{dP_m}{dt} - JA^2 \tag{33}$$

Assuming the rate of change of mechanical power $dP_m/d\omega$ is also given by constant B, the above equation can be written as:

$$\frac{dP_g}{dt} = BA - JA^2 \tag{34}$$

It can be seen from Figure 5.5 that for each slope B, there exists a particular rate of generator speed increase $d\omega/dt$ at which the rate of generator output power increase is maximum. If the rotor speed increase rate $d\omega/dt$ is more than this optimal value, more energy is stored as a kinetic energy than that extracted from the system. If a lesser value is chosen, more time is taken for the algorithm to reach the maximum power point. It can be seen from the wind turbine Power – Speed characteristics in Figure 5.1 that the slope of the curve could be assumed to be varying linearly over a certain range i.e., the curve to the left of the maximum power point can be assumed to be composed of a set of lines, each with a different slope. By determining and fixing the slope value B until it changes to a predetermined value with respect to previous slope, say for example until it becomes 0.75B or so, the optimal rate of change of generator speed increase $d\omega/dt$ could be

determined for that slope B, and be kept constant. Once when the slope B decreases to the predetermined level when compared to the earlier value, the equation (4) is evaluated once again and the new optimal A i.e., the rate of generator speed increase is determined. This way, the inertia of the machine is taken into consideration when determining the optimal step length of the hill climb algorithm and hence the maximum power point is reached at a faster rate when compared to the traditional algorithm.

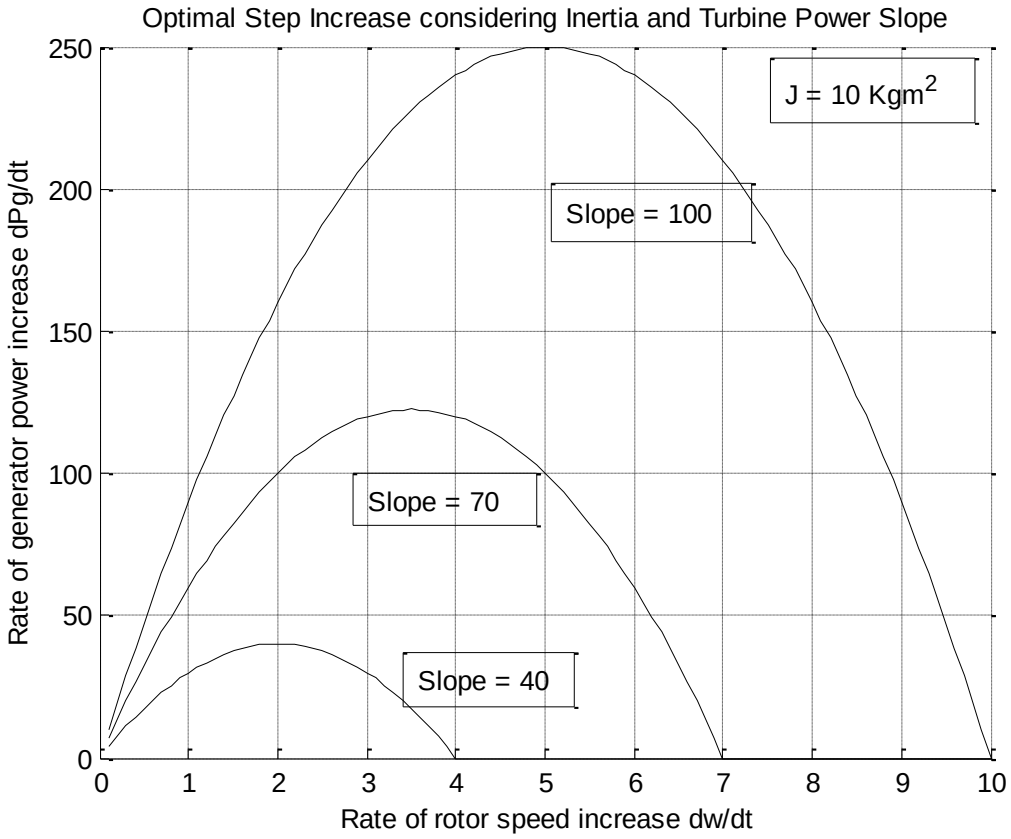

Figure 5.5 Rate of change of Generator Speed

When the wind speed changes, since the generator speed cannot change instantaneously due to inertia of the system, the generator torque (and hence the current) changes suddenly. This sudden change in the current is recognized by the algorithm as a

change in wind speed, and the prior optimal generator speed increase rate A is used for the next iteration. The equation (4) is then solved again, and the new optimal A is determined. Figure 5.6 shows the flow chart representation of the modified hill climb search algorithm. An optimum step length change C is determined based on the wind turbine power – speed slope, and the generator speed is changed in accordance to that. It should be noted that the rectified dc voltage of the generator is controlled rather than the actual generator speed in the above flowchart as is explained further in the next section. When the power-speed slope of the wind turbine is reduced to 70% of the initial value, the new optimum step length change is determined again and the process continues.

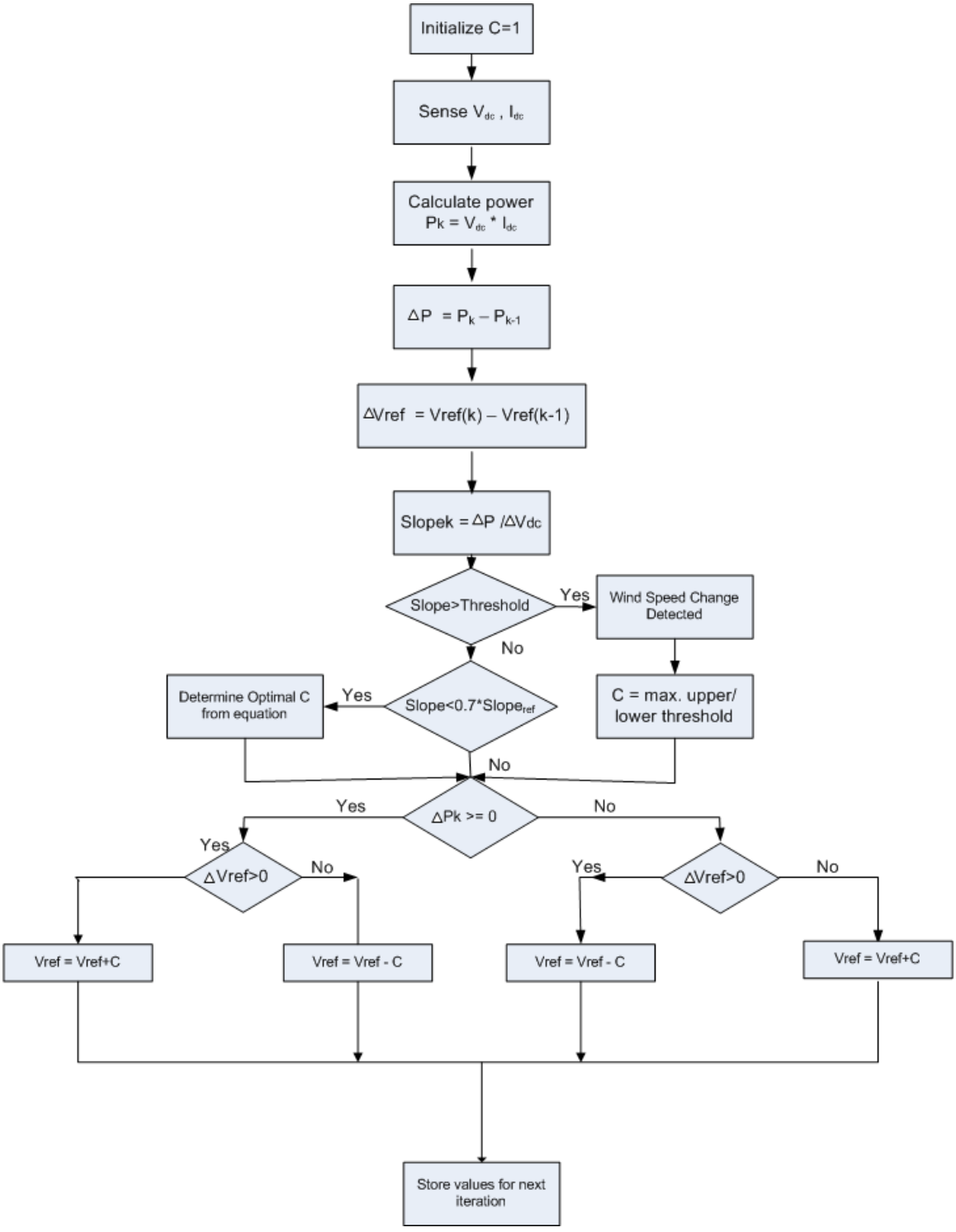

Figure 5.6 Modified Wind Maximum Power Extraction Algorithm

5.2.4 Wind energy system and simulation results

5.2.4.1 Wind Energy System

Based on the selection of appropriate generator and converter architecture mentioned in Chapter 2, the system under study consists of a variable speed wind generation system with the wind turbine connected to a permanent magnet synchronous generator. The generator speed is controlled by controlling the duty ratio of the DC-DC converter which connected through a diode bridge rectifier to the generator. Since the generator output voltage is analogous to the rotor speed as was mentioned in Chapter 2, the voltage at the output terminals of the diode bridge rectifier is controlled for the implementation of hill climb search algorithm, thus resulting in the minimum number of sensors. Figure 5.7 shows the developed wind energy system architecture under study in Simulink and with the turbine and generator parameters given in Table 5.2 and Table 5.3 respectively. The maximum power tracker controller commands a voltage reference that is compared to the actual value of V_{dc} and it is fed into a PI controller. The output of the PI controller is compared to a triangular waveform to determine the boost converter switching. As it was previously stated, wind turbines have an optimal speed that will yield maximum power for each wind speed. Therefore controlling the dc voltage (V_{dc}) allows the control of the current flow through the generator, which controls the speed of the turbine, to reach maximum power point.

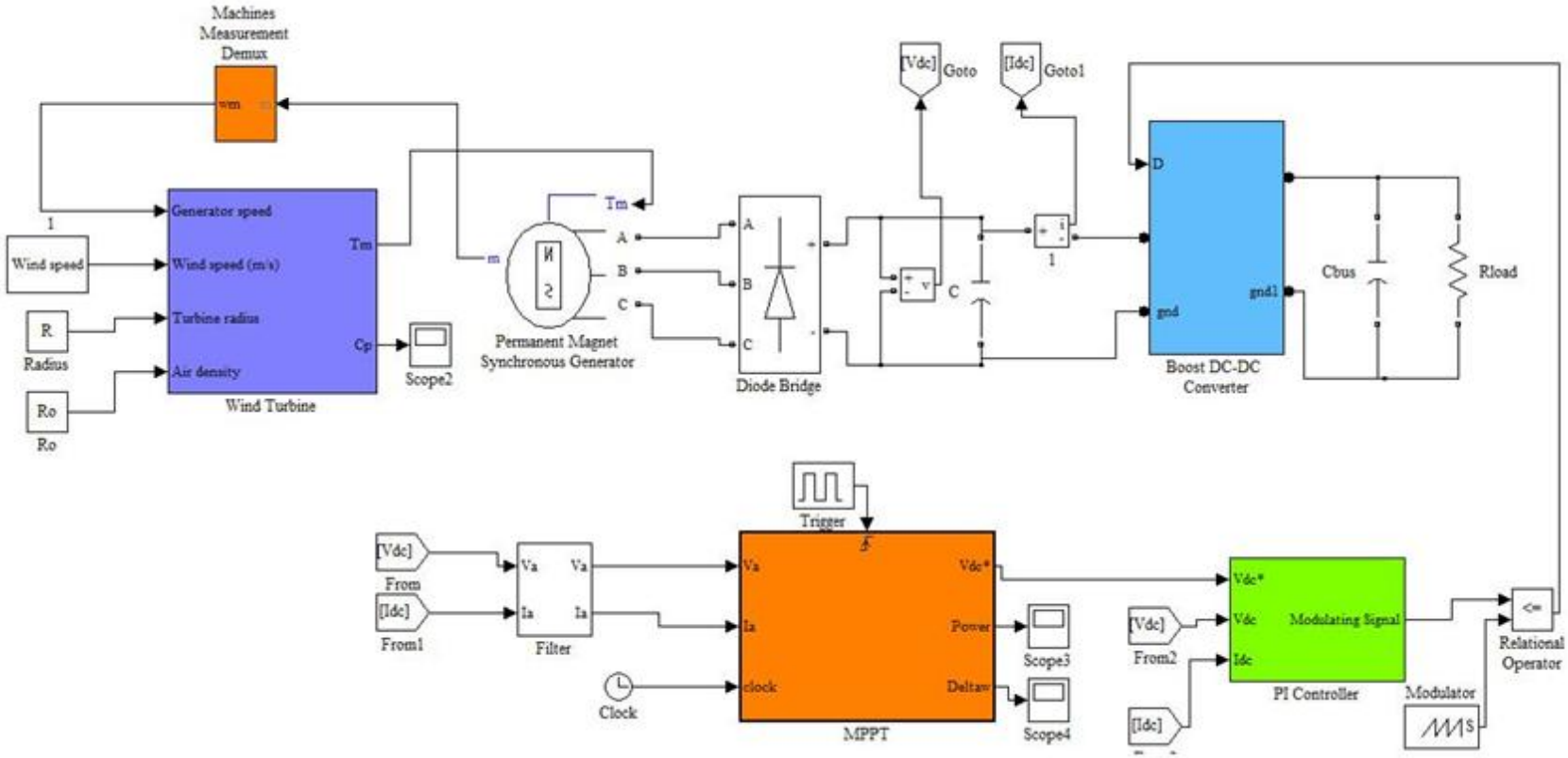

Figure 5.7 Wind Energy System Simulink Simulation

Table 5.2 Wind Turbine Parameters

Parameter	Value
Nominal power	12.5 kW
Cut-in wind speed	5 m/s
Maximum wind speed	14 m/s
Rotor radius	2.5 m
Pitch angle	0 deg

Table 5.3 Generator Parameters

Parameter	Value
Nominal power	14 kW
Poles	8
Stator resistance	0.5 ohms
Stator inductances (L_d, L_q)	0.5 mH
Moment of Inertia	10 kg.m^2

5.2.4.2 Simulation Results

Figures 5.8-5.11 show the simulation results of the proposed maximum power extraction algorithm for the system under study. For comparison, the traditional hill climb search algorithm results are also shown. In the Figure 5.8, the wind speed is changed at different time instants. It could be seen that the proposed algorithm extracts maximum power at a faster rate when compared to the traditional hill climb search algorithm, which is also evident from the higher performance coefficient for the proposed algorithm when compared to the traditional algorithm. Figure 5.11 also shows the variable step change of the proposed algorithm when compared to the fixed step size.

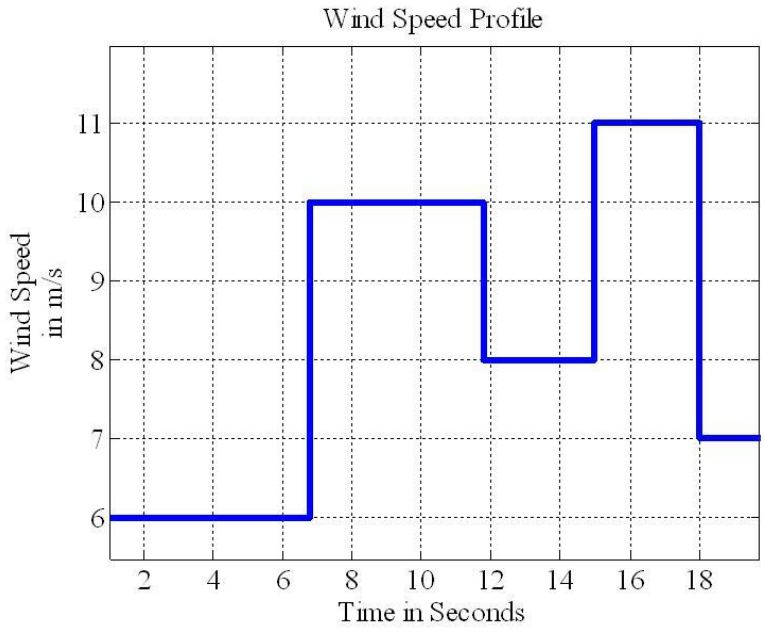

Figure 5.8 Wind Speed Profile

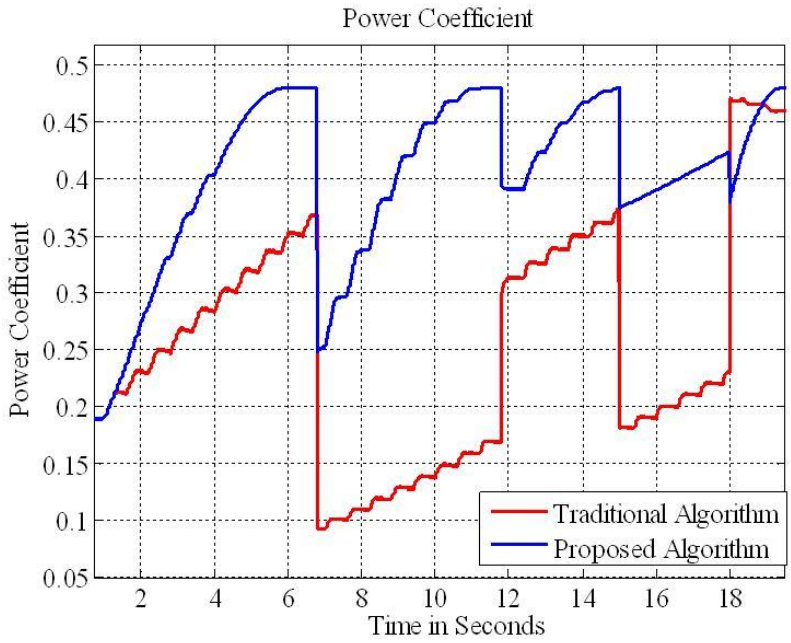

Figure 5.9 Power Coefficient

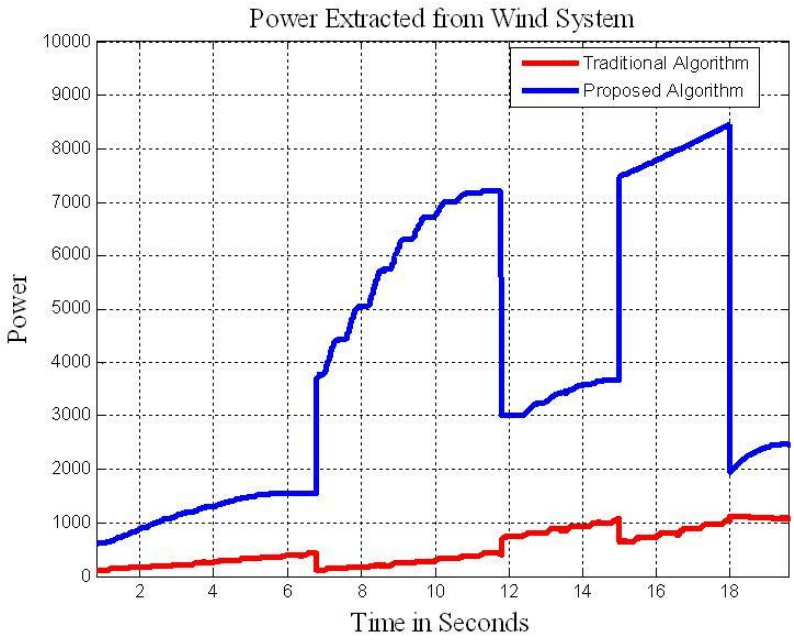

Figure 5.10 Electrical Power Output of Wind Energy System

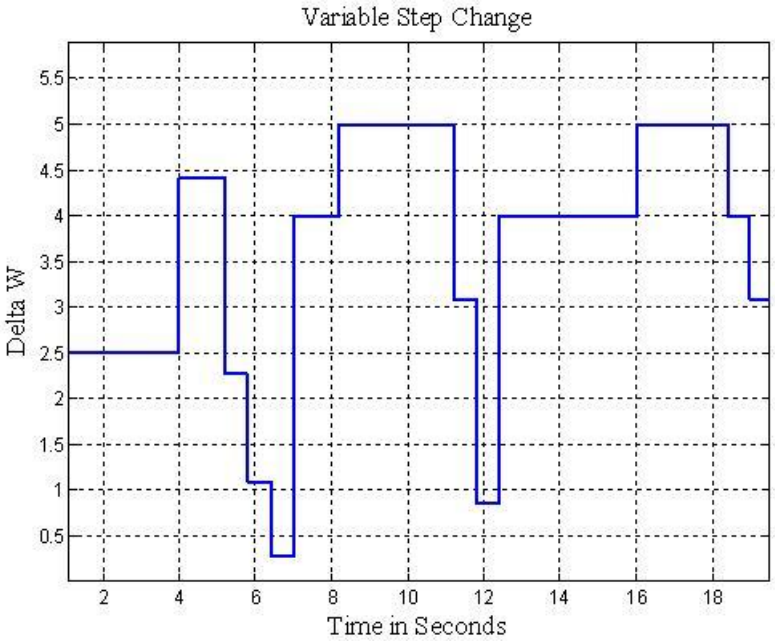

Figure 5.11 Variable Step change

5.3 Photovoltaic Maximum Power Extraction Algorithms

5.3.1 Background

As was mentioned in Chapter 3, it is clear from the Photovoltaic Power- Voltage Characteristics as shown in Figure 5.12 that there exists an optimum voltage for a given sun radiation and temperature at which maximum power can be extracted from the Photovoltaic cells. Hence, the problem considered by MPPT techniques is to determine this optimum voltage or current at which a PV array should operate for the particular sun radiation and temperature. Since it is not easy to have correct measurement of sun's radiation all the time, it is desirable to develop control techniques wherein the optimum V_{MPP} can be determined without having to measure it. Also, this would make the algorithm independent of any particular PV technology or characteristics.

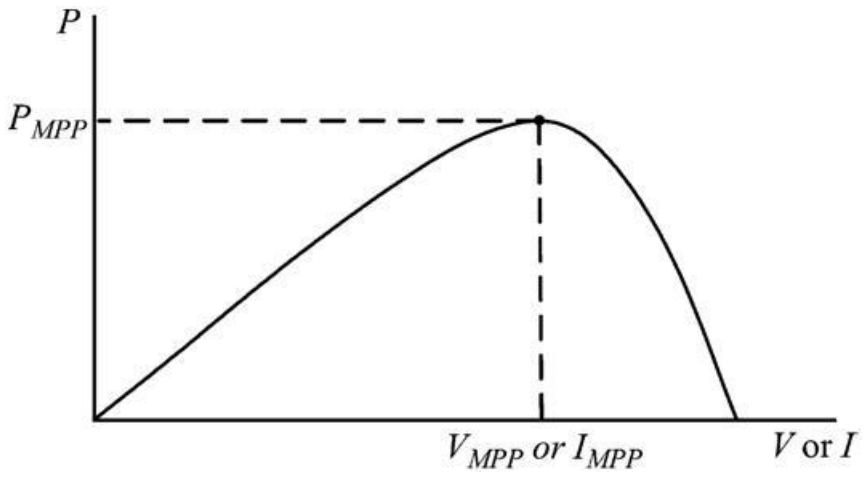

Figure 5.12 Photovoltaic Power- Voltage Characteristics

5.3.2 Review of Photovoltaic Maximum Power Extraction Algorithms

Similar to Wind energy systems, a number of MPPT algorithms for Photovoltaic systems have been proposed over the years as shown in Figure 5.13. As can be seen, there has been a growing interest in the developing new algorithms for maximum power

extraction. The algorithms vary in complexity, sensors required, convergence speed, cost, range of effectiveness, etc. While some of them are developed exclusively for a particular topology, some algorithms are not based on any particular topology.

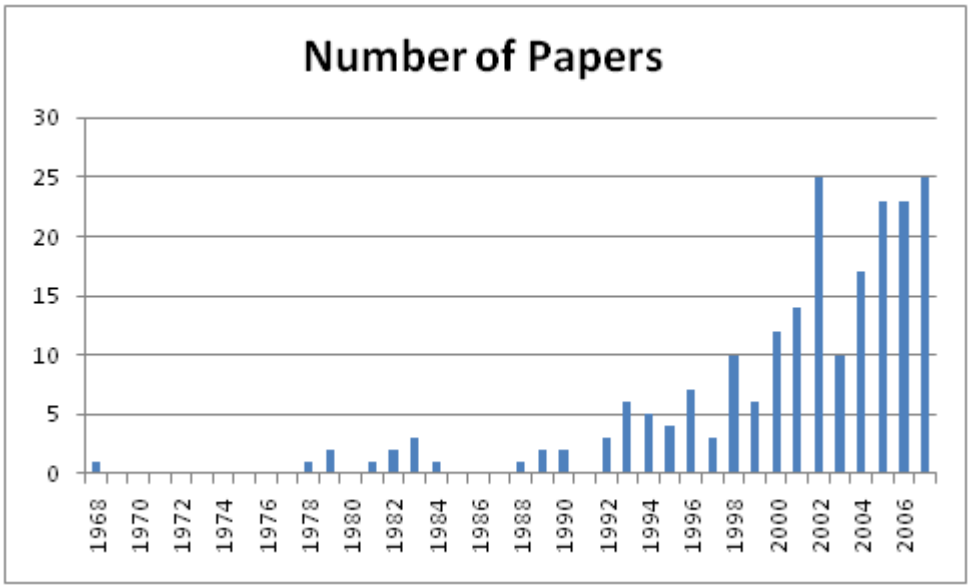

Figure 5.13 Papers Published over the Years

As is the case with the wind systems, many algorithms were proposed which were Hill Climb Search based, neural network based, Fuzzy logic based, advanced methods like sliding mode control, adaptive methods etc. These algorithms have the same pros and cons as was mentioned in the earlier sections, and hence is not elaborated here again. However, some of the algorithms proposed which were not mentioned earlier but most used in the PV literature are only briefly mentioned in this section. Table 5.4 gives the comparison of various PV MPPT algorithms.

5.3.2.1 Incremental Conductance Method

The incremental conductance [95]–[97] method is based on the fact that the slope of the PV array power curve is positive on the left of the MPP, and negative on the right, and at maximum power point slope is zero and the following relation can be obtained:

$$\frac{dI}{dV} = \frac{-I}{V} \tag{35}$$

where V and I are the array voltage and current respectively.

If the ratio dI/dV is more than (-I/V), then the system is operating to the left of MPP. If dI/dV is less than (-I/V), then the system is operating to the right of MPP. The method checks for these conditions and changes the switching accordingly. Though theoretically the system is supposed to reach MPP using this condition, it was seen that the MPP condition is seldom reached due to ripple and hence oscillations persist.

5.3.2.2 Ripple Correlation Control Method

The ripple correlation control (RCC) [98] method makes use of ripple present in the system to perform MPPT. RCC correlates the time derivative of the PV array power with the time derivative of the current or voltage, to drive the power gradient to zero, thus reaching the MPP. From the characteristics it could be seen that, if the array voltage or current is increasing i.e., $\dot{V} > 0$ or $\dot{I} > 0$ and the array power is increasing $\dot{P} > 0$, then the operating point is to the left of MPP and if the array voltage or current is decreasing i.e., $\dot{V} < 0$ or $\dot{I} < 0$ and the array power is increasing $\dot{P} < 0$, then the operating point is to the right of MPP. Combining these observations, it could be seen that $\dot{P}\dot{V}$ is positive to the left of the MPP, negative to right of the MPP, and zero at the MPP, and accordingly the duty ratio is given by [98]:

$$d(t) = -k_3 \int \dot{p}\,\dot{v} \tag{36}$$

Where k_3 is a positive constant and d is the instantaneous duty ratio of the dc-dc converter. While the method is found to have good and fast MPP convergence [99] when compared to other methods, it was found to have suboptimal performance at higher switching frequencies (> 2 kHz [87]), and the presence of PV array capacitance is found to cause problems in determining the true MPP. Also the RCC method is found not to have satisfactory performance when multiple PV arrays are connected in series – parallel connection [99].

5.3.2.3 Fractional Open Circuit Method

The near linear relationship [100]–[102] between the array voltage at maximum power point (V_{MPP}) and array open circuit voltage (V_{OC}) under varying irradiance and temperature levels could be used to determine the optimal voltage for maximum power given by:

$$V_{MPP} \approx k_1 V_{OC} \tag{37}$$

where k_1 is a constant which depends on the characteristics of the PV array being used, and is computed prior by empirically determining V_{MPP} and V_{OC} for the specific PV array at different irradiance and temperature levels using manufacturer data. Upon determining k_1 the V_{MPP} can be computed using above equation with V_{OC} being measured periodically by momentarily shutting down the power converter. While this method is very simple, it has many disadvantages like it requires temporary disconnect of the source floss leading to power loss and synchronization issues and that k_1 changes with the presence of partial shading.

Table 5.4 gives a comparison of the various PV MPPT algorithms proposed. It could be seen that the hill climb search method has a faster convergence speed, simple

implementation, and is independent of the array characteristics. Hence, the hill climb search algorithm is selected for this dissertation considering the cost, performance and simplicity.

Table 5.4 Comparison of Photovoltaic Maximum Power Tracking Algorithms

MPPT Method	Implementation Complexity	Convergence Speed	Knowledge of Characteristics	Memory Requirement	Periodic Tuning
Hill Climb	Simple	Varies	No	Minimal	No
IncCond	Moderate	Varies	No	Minimal	No
Fractional Voc or Isc	Simple	Fast	Yes	Minimal	Yes
Ripple correlation control	Moderate	Fast	No	Minimal	No
Current Sweep	High	Moderate	Yes	Minimal	Yes
Theoretical Relationship	Simple	Fast	Yes	Moderate	Yes
Slide mode control	Moderate	Moderate	Yes	Minimal	No
Neural Network	High	Fast	Yes	High	Yes
Fuzzy Logic	High	Fast	Yes	High	Yes
State based MPPT	High	Moderate	Yes	Moderate	Yes

5.3.3 Hill Climb Algorithm Used

As was explained before for the wind energy systems, the hill climb search algorithm for the Photovoltaics perturbs the reference current VPV at the panel terminals, checks for the power- current slope and determine the next step direction based on the sign of the slope. The step length could be fixed or could be varied dynamically. For the

fixed step length, the determination of the step length is problematic, since a bigger step length increases the oscillations around MPP, while a smaller step length increases the time taken to reach the MPP. Hence, a commonly used approach is to determine variable step lengths based on Newton-Raphson or Steepest descent methods. The Newton Raphson method converges much faster than the Steepest descent method and hence is used in this dissertation for Photovoltaic systems [102]. Using this variable step will allow the maximum power tracker to converge faster to the maximum power point and will decrease power oscillations due to large values of ΔV_{PVref} when maximum power is achieved. For protection purposes the value of ΔV_{PVref} is often limited. The complete flow chart of the algorithm is given in Figure 5.14.

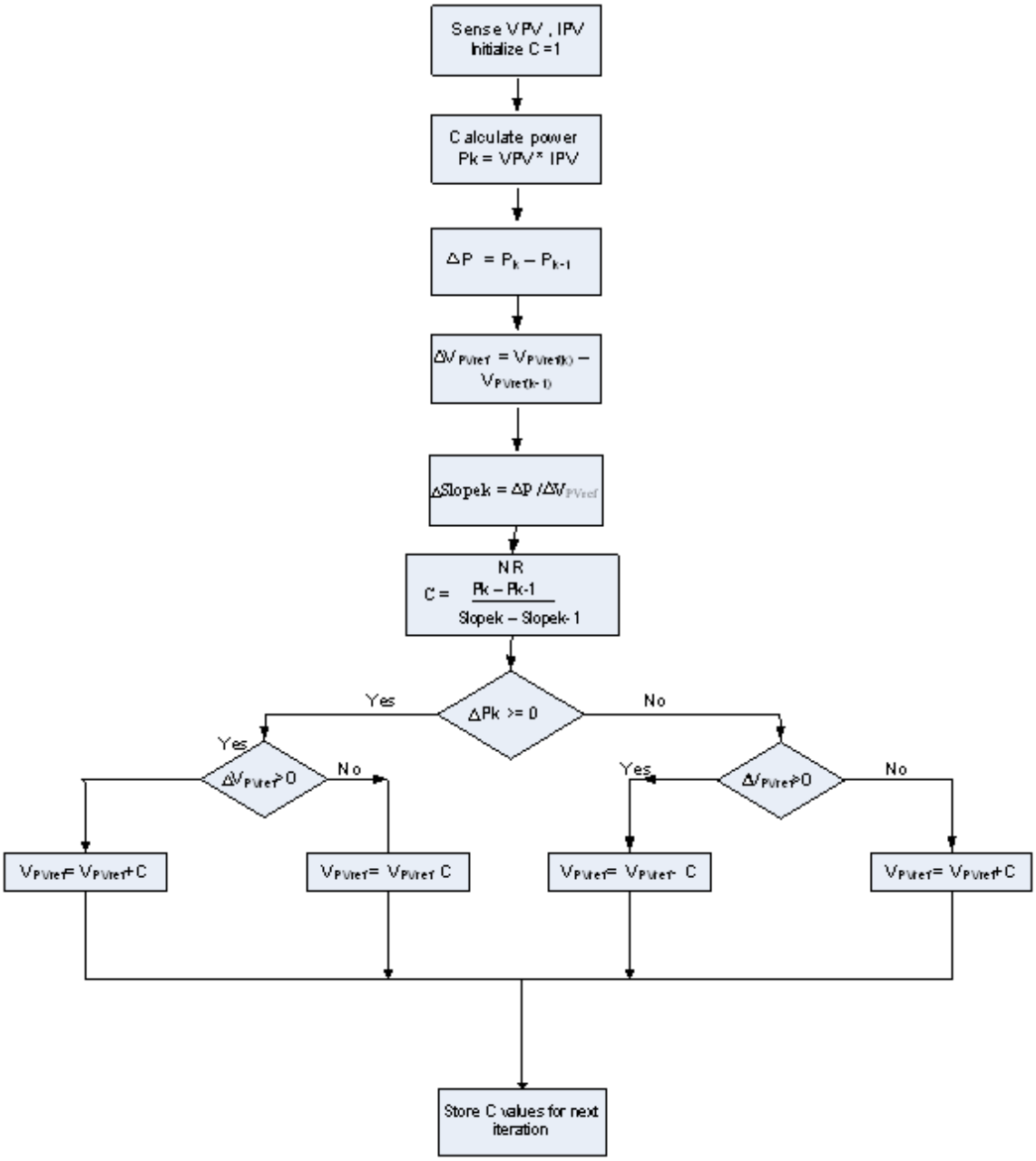

Figure 5.14 Flowchart of Photovoltaic Maximum Power Point Tracking Algorithm

5.3.4 Simulation Results

Table 5.5 gives the considered PV system characteristic values. The system consists of 60 watt modules of 10 series and 15 parallel panels amounting to a 9 kW photovoltaic system. Figure 5.15 shows the developed simulation circuit in Simulink and

Figure 5.16 shows the Simulink representation of 10 series connected modules and 15 such modules are connected in parallel. Figure 5.17 to Figure 5.19 shows the results of the case where the sun radiation is changed 1000 W/m^2 with T = 35°C at time t = 0.05 sec. Figure 5.17 shows the step change in voltage of the MPPT algorithm simulation, Figure 5.19 shows the PV array voltage and Figure 5.18 shows PV array power. It could be seen from the results that the algorithm is able to track the maximum power effectively by dynamically changing the step length. The effectiveness of the maximum power point tracking is verified by the PV array voltage at the corresponding sun radiation which is about 165 V and is closer to the manufacturer provided PV specification of 170 V for the considered PV system. It could also be seen from Figure 5.19 that the algorithm continues to oscillate around MPP since it keeps checking for any change in the radiation, however as seen from the PV power figure the change in power is very small and could be controlled by restricting the search when the MPP is reached.

Table 5.5 Photovoltaic System Specifications

Parameter	Value
Open Circuit Voltage/ module	21 V
Short Circuit Current/module	3.75 A
Voltage at Max. Power/module (for 25 °C)	17.0 V
Maximum Power/module	60 Watts
Number of modules in Series	10
Number of modules in Parallel	15
Total Panel Power	9 kW

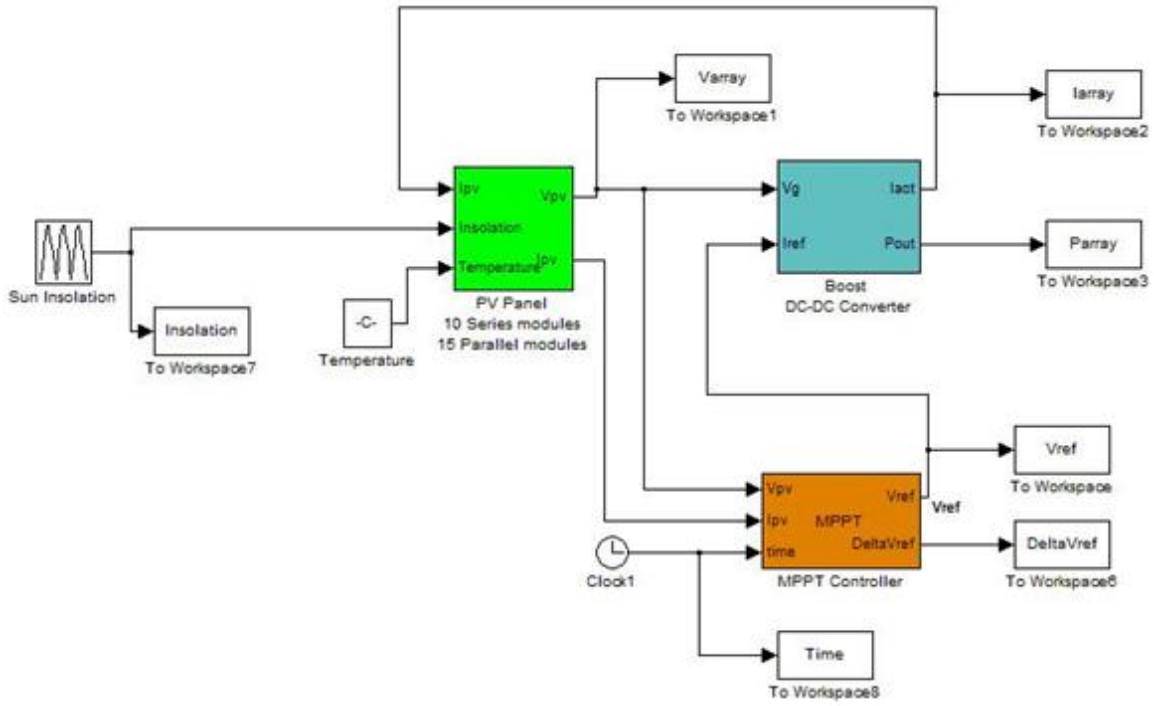

Figure 5.15 Photovoltaic Simulation Circuit in Simulink

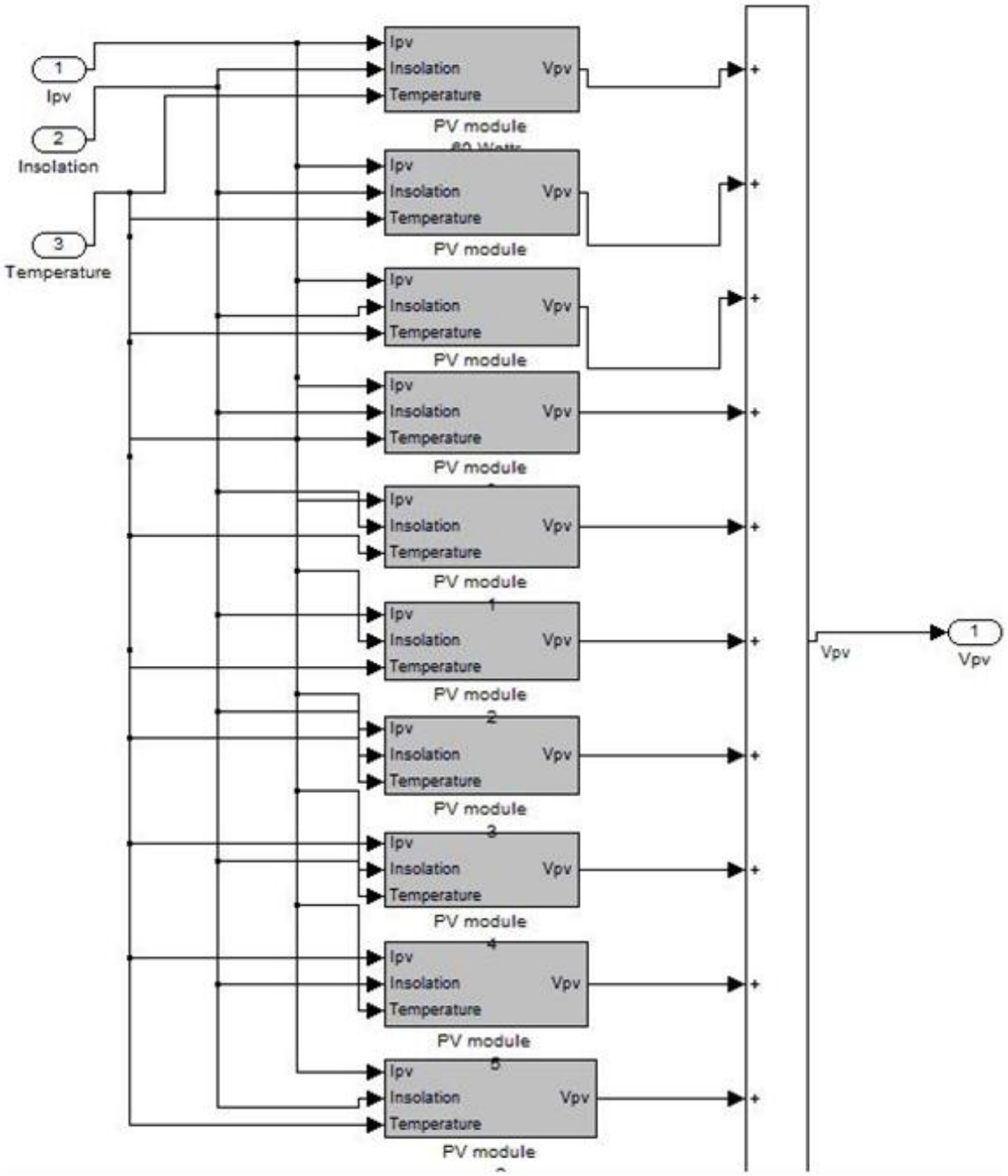

Figure 5.16 Series Connected Photovoltaic Modules

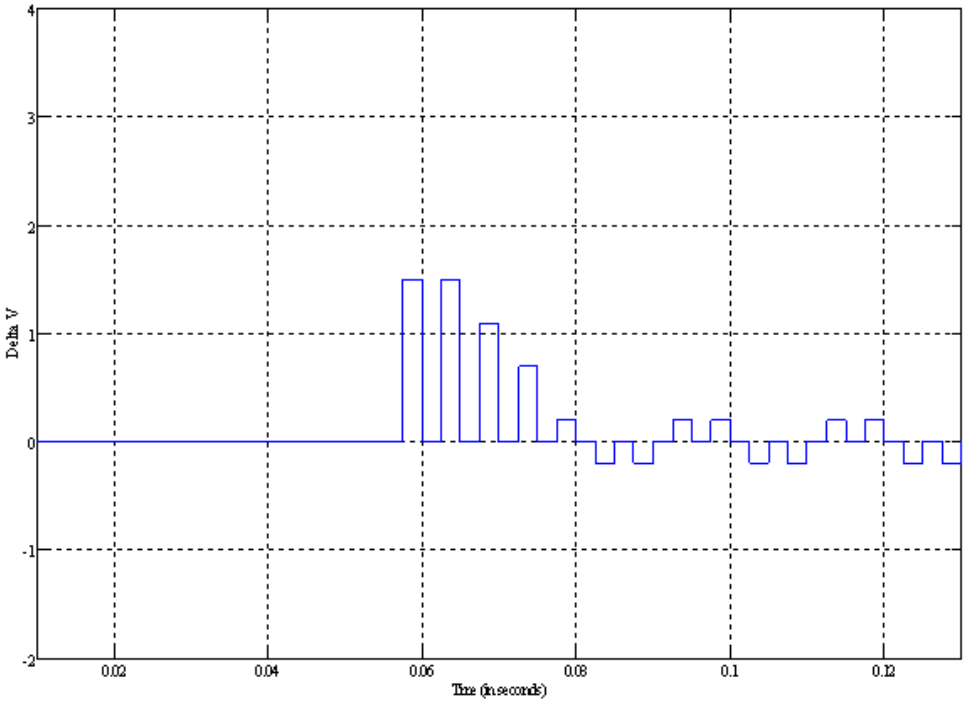

Figure 5.17 DeltaV for Sun = 1000 W/m2 case

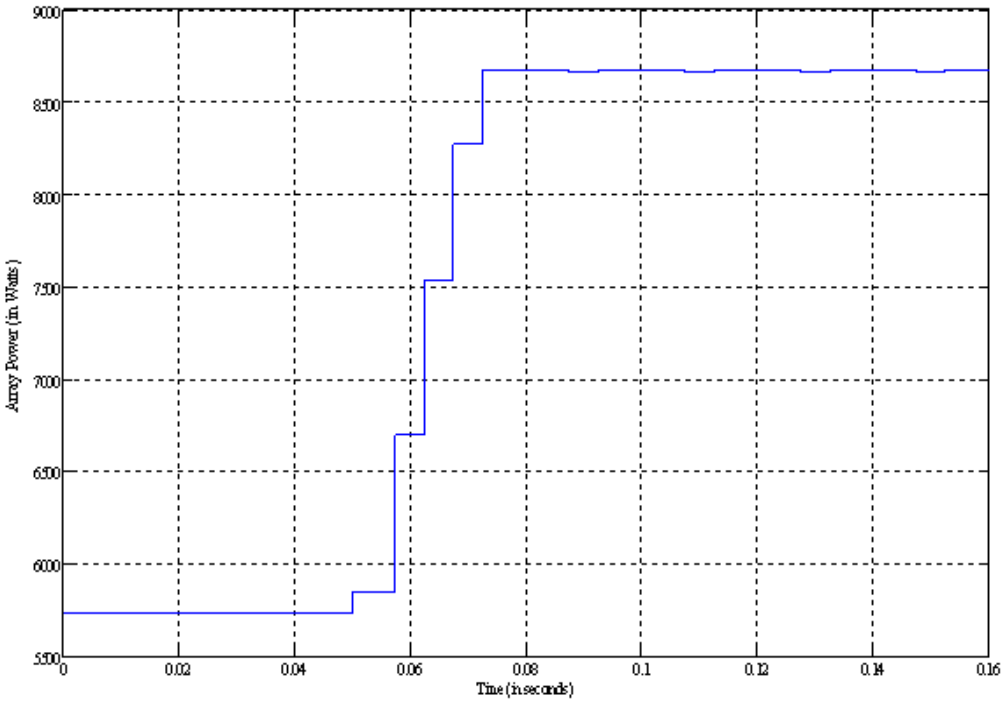

Figure 5.18 PV Array Power

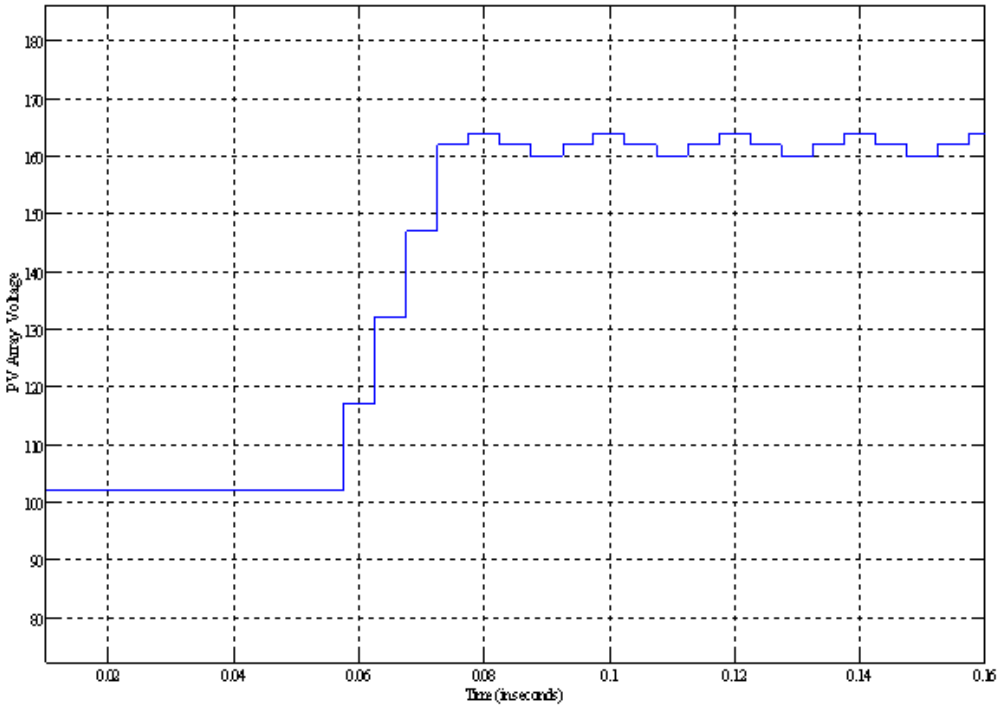

Figure 5.19 Photovoltaic Array Voltage

As was mentioned in the Chapter 3, the PV array power and voltage at MPP changes with both solar radiation and temperature. It was seen from the PV characteristics that as the temperature increases, the PV array reaches the MPP at a lesser array voltage. Figure 5.20 and Figure 5.21 shows the simulation results for the case when the sun radiation changes from 500 to 800 W/m^2 and the temperature increases from 35 to 55 °C at time t=0.2 sec. It was seen that the PV reaches the maximum power point in this case as well (array voltage of about 148V) which is verified from the corresponding maximum power array voltage (which is about 150 V) obtained from the PV characteristics results given in Figure 5.22.

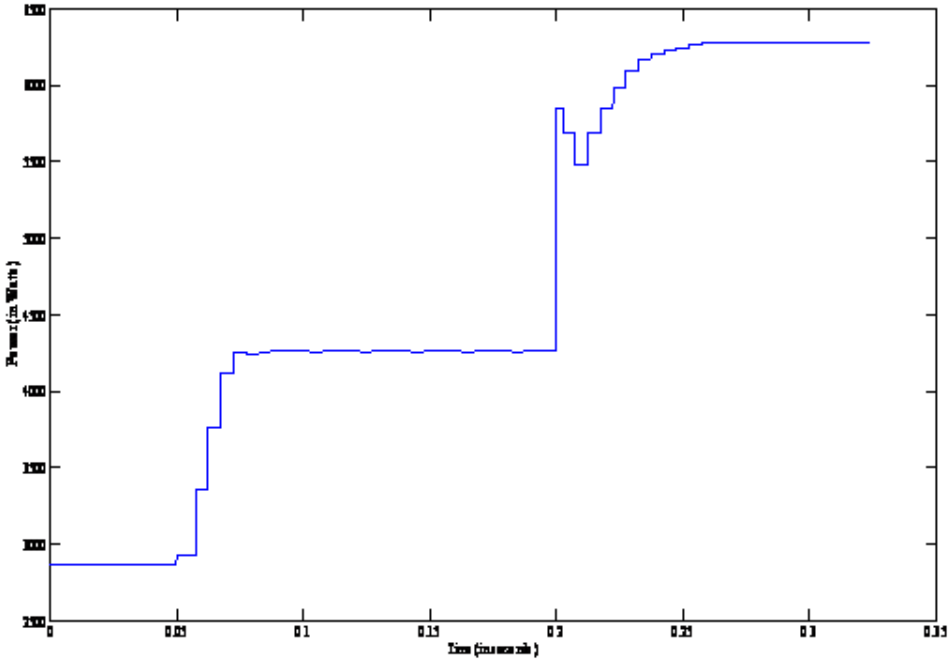

Figure 5.20 Photovoltaic Array Power for the case when radiation changes from 500 to 800 W/m^2 and Temperature increases from 35 to 55 °C

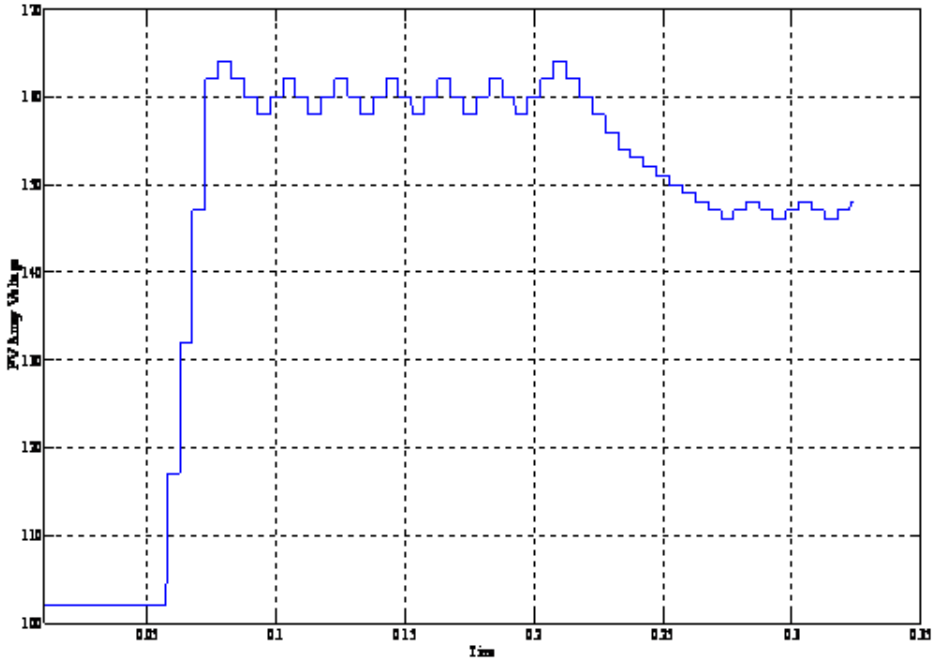

Figure 5.21 Photovoltaic Array Voltage for the case when radiation changes from 500 to 800 W/m^2 and Temperature increases from 35 to 55 °C

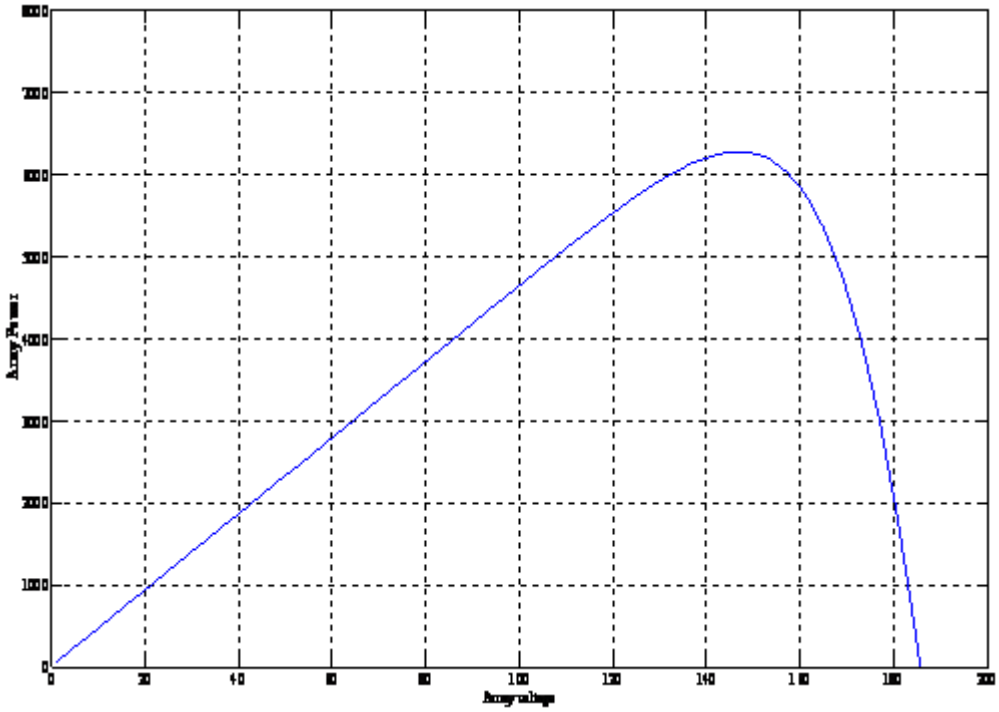

Figure 5.22 PV characteristics curve for Corresponding 800 W/m^2 Radiation and 55 °C Temperature obtained from PV Characteristics

CHAPTER VI

REDUCTION OF DC BUS VOLTAGE RIPPLE SENSITIVITY

6.1 Background

A three-phase voltage source converter (VSC) is a main component in the majority of grid connected power electronic application and is being increasingly used for in motor drive and in renewable energy interface to grid applications. Figure 6.1 shows a very commonly used two level VSC for grid interface application. It employs three IGBT bridges with two switches per bridge connected to a common dc-link bus. When used as a grid side converter, the VSCs transform the input dc power from the renewable energy sources to an AC output at grid frequency (60 Hz in this case) by modulating the switches.

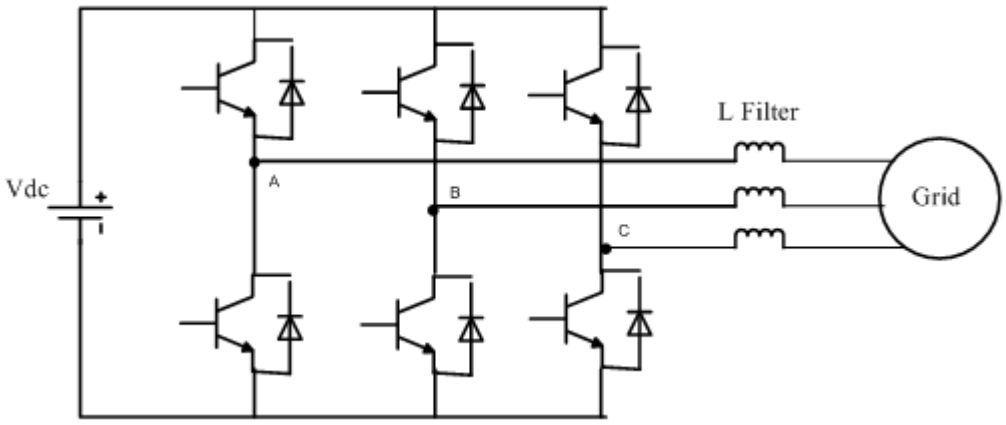

Figure 6.1 Three Phase Voltage Source Converter

The IGBT-based converter shown in the figure has several advantages such as high efficiency, controllable reactive power, fast response, etc when compared to

thyristor based switches, and hence are being increasingly used for renewable energy applications. VSCs have advantages that include better dynamic performance, bidirectional power flow, and almost perfectly sinusoidal supply current. In order to simplify the control of VSC when dealing with three phase quantities, Clarke and Park transformations are generally employed. Considering for a balanced system, the three phase voltages are given by:

$$Va\,(t) = V\cos(\omega t) \tag{38}$$

$$Vb\,(t) = V\cos\left(\omega t - \frac{2\pi}{3}\right) \tag{39}$$

$$Vc\,(t) = V\cos\left(\omega t + \frac{2\pi}{3}\right) \tag{40}$$

The Clark transforms maps the three-phase a, b, c components into a two phase system represented by two orthogonal components α and β, which is called a space vector as shown in Figure 6.2. The space vector consists of a real (α) and imaginary (β) part which represents two sinusoids shifted by 90° in time. Assuming the real axis (α) coincides with phase A of the AC system, the Equation 4 gives the matrix of transformation from ABC to α β coordinates, and equation 5 gives the transformation from α β to ABC coordinates.

$$\begin{bmatrix} V\alpha \\ V\beta \end{bmatrix} = \sqrt{\frac{2}{3}} \begin{bmatrix} 1 & \frac{-1}{2} & \frac{-1}{2} \\ 0 & \frac{\sqrt{3}}{2} & \frac{-\sqrt{3}}{2} \end{bmatrix} \begin{bmatrix} Va \\ Vb \\ Vc \end{bmatrix} \tag{41}$$

$$\begin{bmatrix} Va \\ Vb \\ Vc \end{bmatrix} = \begin{bmatrix} 1 & 0 & 1 \\ \frac{-1}{2} & \frac{\sqrt{3}}{3} & 1 \\ \frac{-1}{2} & \frac{-\sqrt{3}}{3} & 1 \end{bmatrix} \begin{bmatrix} \alpha \\ \beta \\ o \end{bmatrix} \tag{42}$$

Where: $V_a = V_b = V_c = V$ is the RMS phase voltage.

The stationary frame two coordinate system variables are then transformed to a two coordinate rotating frame dq variables using park transformation given by the following equation 6:

$$\begin{bmatrix} Vd \\ Vq \end{bmatrix} = \begin{bmatrix} \cos\theta & \sin\theta \\ -\sin\theta & \cos\theta \end{bmatrix} \begin{bmatrix} V\alpha \\ V\beta \end{bmatrix} \tag{43}$$

and equation 7 gives the inverse park transform from dq to ABC frame.

$$\begin{bmatrix} V\alpha \\ V\beta \end{bmatrix} = \begin{bmatrix} \cos\theta & -\sin\theta \\ \sin\theta & \cos\theta \end{bmatrix} \begin{bmatrix} Vd \\ Vq \end{bmatrix} \tag{44}$$

Where θ is the angle between the (α) axis and d axis.

The advantage of transforming the stationary frame abc coordinates to a rotating frame dq coordinates is that the ac quantities appear as dc values in the rotating frame, and hence the control becomes simple. Figure 6.3 shows the vector diagram of the Clarke and Park transformations. From the figure, the transformation of the abc coordinates to dq frame can be directly obtained from the equation 8.

$$\begin{bmatrix} Vd \\ Vq \\ Vo \end{bmatrix} = \sqrt{\frac{2}{3}} \begin{bmatrix} \cos\theta & \cos\left(\theta - \frac{2\pi}{3}\right) & \cos\left(\theta + \frac{2\pi}{3}\right) \\ \sin\theta & \sin\left(\theta - \frac{2\pi}{3}\right) & \sin\left(\theta + \frac{2\pi}{3}\right) \\ \frac{1}{\sqrt{2}} & \frac{1}{\sqrt{2}} & \frac{1}{\sqrt{2}} \end{bmatrix} \begin{bmatrix} Va \\ Vb \\ Vc \end{bmatrix} \tag{45}$$

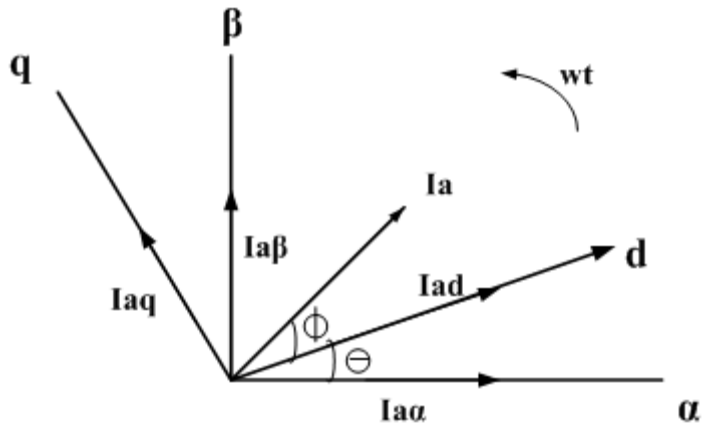

Figure 6.2 Coordinate Transformations

The Space Vector Pulse Width Modulation (SVPWM) [103] is the most commonly used PWM strategy for controlling the VSC switches where a set of voltage vectors are used to generate the revolving voltage vector. In addition to high utilization of the DC bus voltage, the SVPWM has the advantages of having lower harmonic distortion of produced current and voltage waveforms when compared to sinusoidal or other PWM strategies. The current controllers combined with the SVPWM modulator produce the current on the output of the VSC in such a way that it matches the output of the reference signal generator.

Figure 6.3 shows the overall control architecture of a voltage source converter. Various control strategies can be employed in VSCs. Most commonly a two control loop structure is used where the outer loop sets the desired voltage across the DC bus terminals of the VSC and generates an appropriate current reference to control the power flow between the input and output of the VSC, and the inner loop follows the set current reference from the voltage loop. Typically, the outer dc voltage loop is chosen to have a low bandwidth when compared to the inner current control loop in order to avoid the interference of the outer loop with the inner loop.

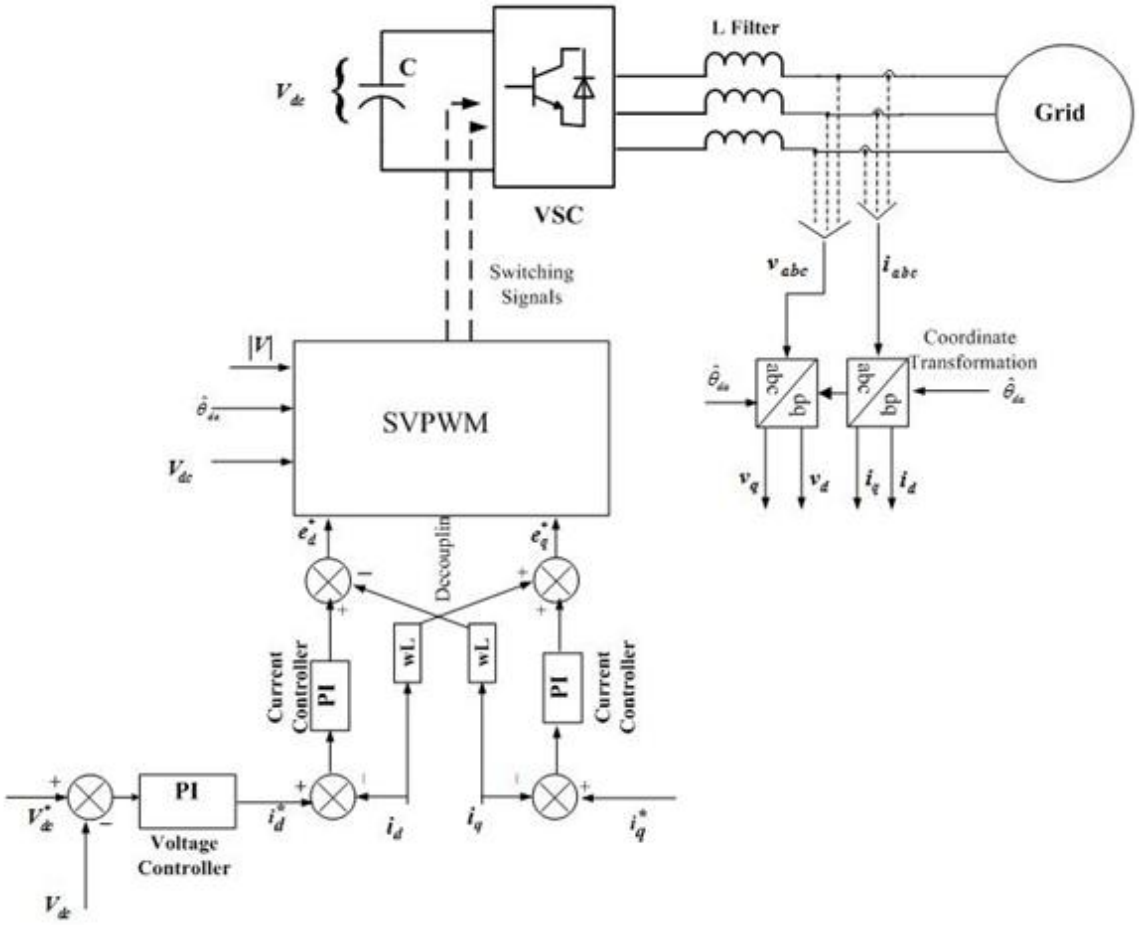

Figure 6.3 Overall Control Architecture of the VSC

6.2 Grid Interface Filter

6.2.1 L Filter

Typically, an L filter is used as an interface between the voltage source converter and the grid. The selection of the filter value depends on the allowable current ripple and is generally given by [104][105]:

$$L = \frac{V_{dc}}{4\sqrt{3} f_{sw} \Delta I_{ripple}} \tag{46}$$

Based on the system specifications mentioned in Appendix, the grid filter inductance value is calculated to be 3 mH.

6.2.2 LCL Filter

Typically, an L filter is used as an interface between the voltage source converter and the grid. However, a high value of inductance is required to reduce the current harmonics around the switching frequency. In high power applications like renewable energy, it becomes quite expensive to realize larger harmonic reactors. Moreover, the dynamic response of the system becomes poor. In contrast, the LCL filters result in the reduction of harmonics with smaller inductance values when compared to the L-filter. Hence, more research has been done lately on the application of LCL filter for renewable energy applications. However, the addition of an LCL filter results in the resonance oscillation of the system due to the frequency response characteristics of the filter. In order to reduce the oscillations several methods have been proposed over the years to damp the system. As discussed in the APPENDIX, some methods (called "passive damping") use resistor in series with the LCL filter elements, some methods damp the system by changing the control structure ("active damping") of the system using some extra sensors. Figure 6.4 shows the LCL filter connected to a VSC. The LCL filter parameters are chosen such that the following conditions are satisfied [106] [107]:

- The grid side inductance is generally chosen as a fraction of the converter side inductance, since the converter side inductance is responsible for the attenuation of most of the switching ripple. It should however be noted that a too high value of converter side inductance results in losses in the system [106], and typically an acceptable ratio of 3-7 is selected.
- The capacitance value is selected such that the decrease in power factor is generally limited to around 0.95 at rated power.

- The resonance frequency of the filter is generally chosen to be in the range between ten times the fundamental frequency and one half the switching frequency inorder to avoid resonance problems in the lower and upper parts of the harmonic spectrum. If the resonant criterion is not met then the inductance ratio has to be changed until this criterion is met. Figure 6.5 gives the plot of change in filter resonance frequency with the converter to grid side filter ratio.

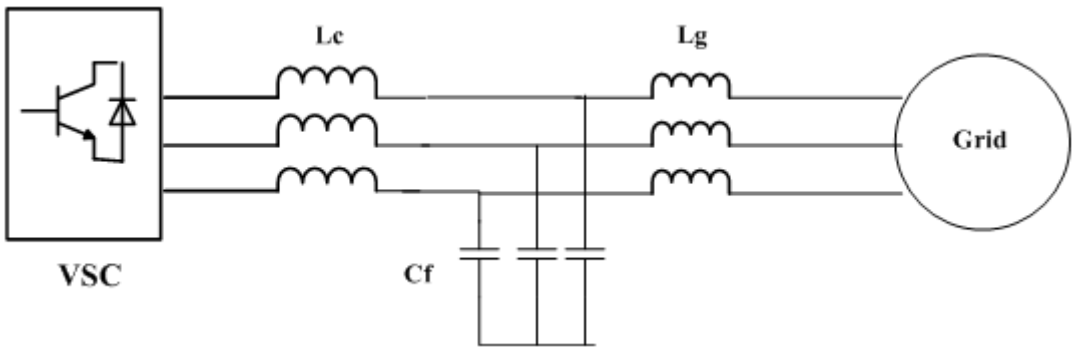

Figure 6.4 LCL Filter

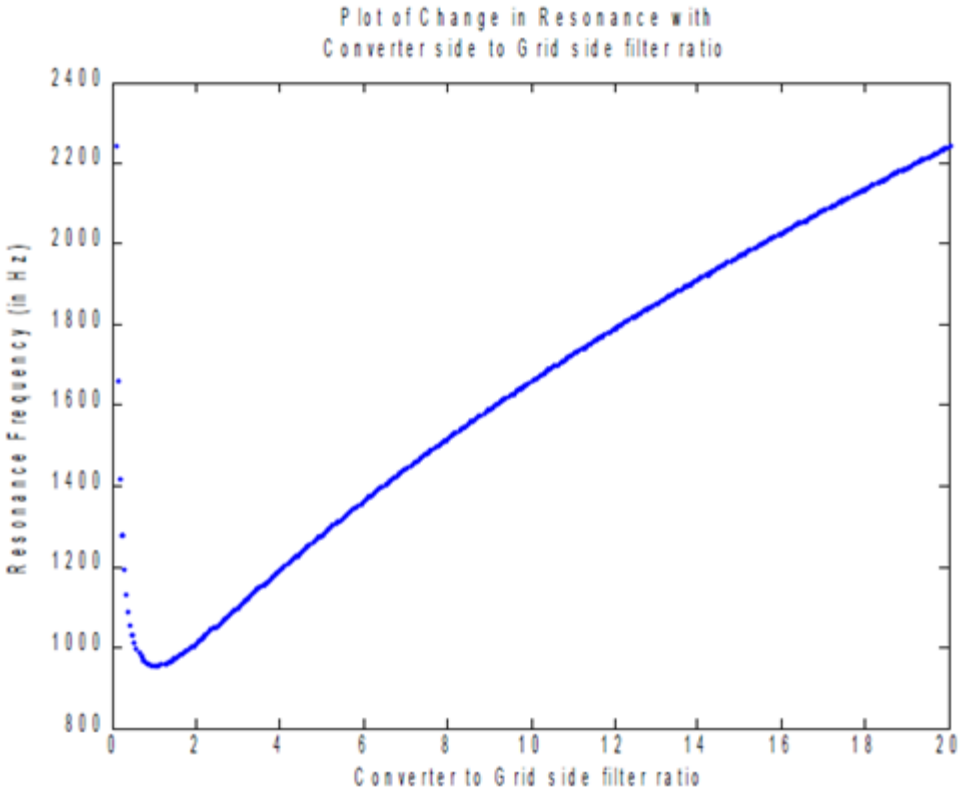

Figure 6.5 LCL Filter Resonance Change with Filter Ratio

Based on the above mentioned procedure, the calculated parameters values for the system under consideration are: L_{total} = 3 mH, Converter side filter L_c = 2.2 m H, Grid side filter L_g = 0.8 m H, C_f = 31 uF, w_{res} = 1.05 kHz. The matlab code for filter calculation and damping mechanisms are given in the Appendix.

6.3 DC Bus Capacitor Selection

The dc bus capacitors are generally designed considering the allowable dc bus voltage ripple. However in practicality, the electrolytic capacitors are generally selected 2-3 times the designed values as their ripple current handling capability is low and is a big constraint. The electrolytic capacitor also is big in size and suffers from frequent maintenance, higher life expectancy etc. Hence, in recent years focus has been shifting

slowly towards using thin film capacitors for electric vehicle and renewable energy applications as they have greater ripple current handling capability and hence have lower rating. The dc bus capacitor is selection is given by the following equation:

$$C = \frac{2\Delta P \Delta t}{(\Delta V_{dc}^2 + 2V_{dc}\Delta V_{dc})} \tag{47}$$

Based on the above equations, a 400 uF dc bus capacitor is selected for the system allowing a 10% voltage ripple. For comparison, of the results, a 3000uF dc bus capacitance value used in the references [13][19][39] is taken.

6.4 Reduction of DC Bus Voltage Ripple Sensitivity

6.4.1 Background

Generally, the grid side converter controls (esp. SVPWM) are designed assuming the input dc voltage to the converter as constant or having a relatively small perturbation that could be controlled. This assumption however is not true for systems like renewable energy interface applications where the dc bus voltage undergoes variations due to changes in the environmental conditions. The problem becomes much worse for hybrid renewable energy systems like Wind- Photovoltaic systems. The dc bus voltage variation for a hybrid Wind- PV system can be attributed to the following reasons:

1. A sudden change in wind speed or solar radiation causes a sudden change in the dc bus voltage.
2. The MPPT tracking process of wind and PV systems.
3. Changes in the local load connected to the grid side converter.

Typically, this problem is addressed by using a high rated dc bus capacitor or an energy storage device connected to the dc bus. Many hybrid renewable energy system

methodologies are proposed which typically use a large electrolytic dc bus capacitor. Reference [19] uses a 3000uF dc bus capacitor for a 10 kW wind system and reference [19] uses uses a 2300 uF capacitor for a 2.3 kW system. Further, the problem is increased by using large electrolytic capacitors which are expensive, bulky, have a short life span and require frequent maintenance [39]. This poses a big restriction especially for renewable energy applications in tens of kWs range. Hence, recently emphasis has been increasing on using lower dc bus capacitance like thin film capacitors for renewable energy and hybrid electric vehicle which are relatively cheap and small in size.

6.4.2 State of art Control Methodology

As was mentioned earlier, Figure 6.6 shows the commonly employed control methodology for a grid connected voltage source converter. By controlling the dc bus voltage, the input power from the energy sources is sent to the grid.

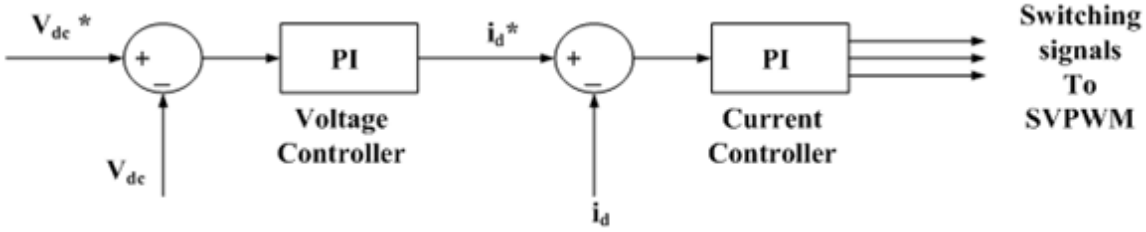

Figure 6.6 Conventional Control Architecture

The main problem with this control method is that since the dc voltage is controlled to a constant value, the ripples in the voltage would be reflected into the grid current. To reduce this, a high rated dc bus capacitor has to be selected resulting in the selection of a low bandwidth for the voltage controller. This reduces the dynamic performance of the system, and also increases the cost of system due to high rated

capacitance. Figure 6.7 and Figure 6.8 shows the performance of the system with a 3000uF capacitor which was used in references [13][19]. It could be seen that when a high rated dc bus capacitor is selected the output grid current has low harmonic distortion. However, this increases the cost and reduced the dynamic performance.

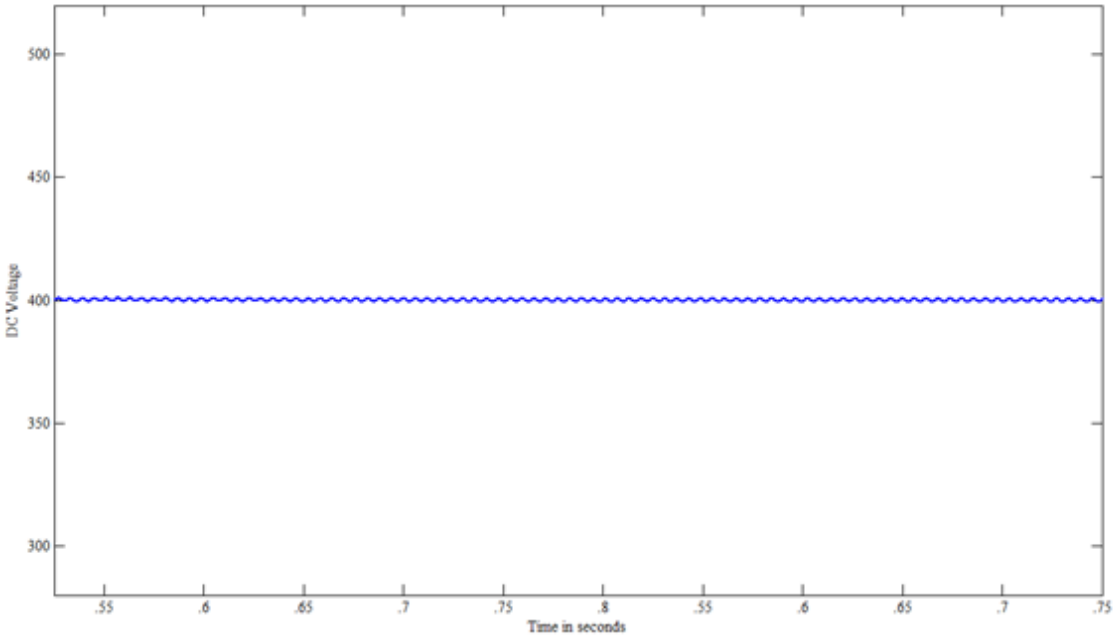

Figure 6.7 DC Bus Voltage with 3000 uF Capacitor

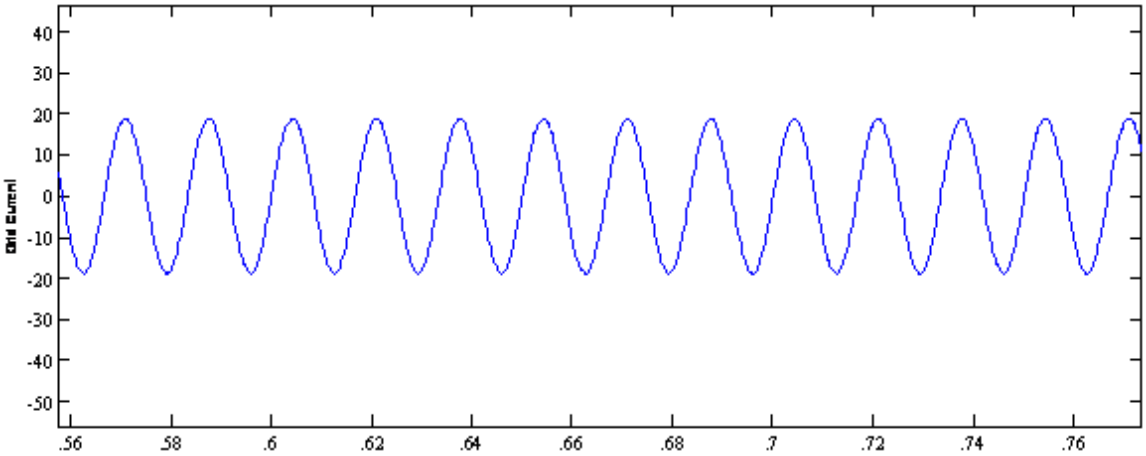

Figure 6.8 Grid Current with 3000 uF Capacitor

As was mentioned earlier, in order to improve the dynamic performance, cost and size of the system it would be better if a small capacitor could be used. Accordingly, a reduced capacitance value of 400 uF has been designed as was mentioned in the earlier section. Figure 6.9 and Figure 6.10 gives the performance of the system with the reduced capacitance using the conventional control architecture. It could be seen that with the conventional architecture considerable ripple is generated in the grid current since the ripple in the bus voltage passes through the controller into the current reference. It was seen that the current THD is around 7.6% which is higher than the IEEE specified limit of 5% as given in the Appendix A.

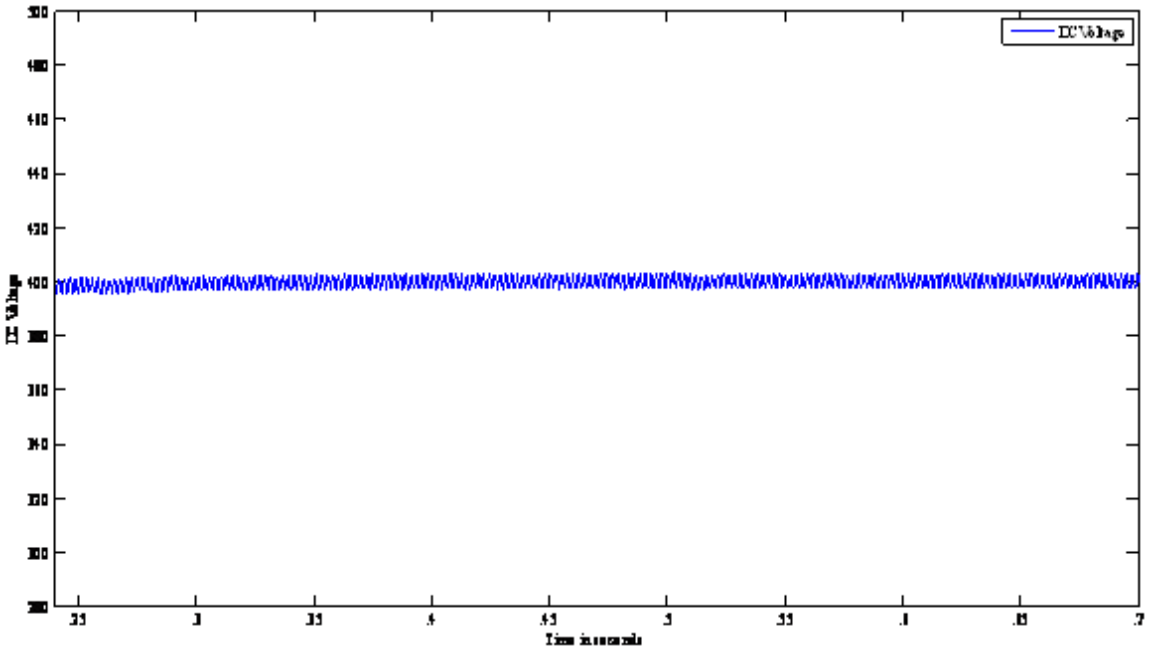

Figure 6.9 DC Bus Voltage With Conventional Architecture and Reduced Capacitance

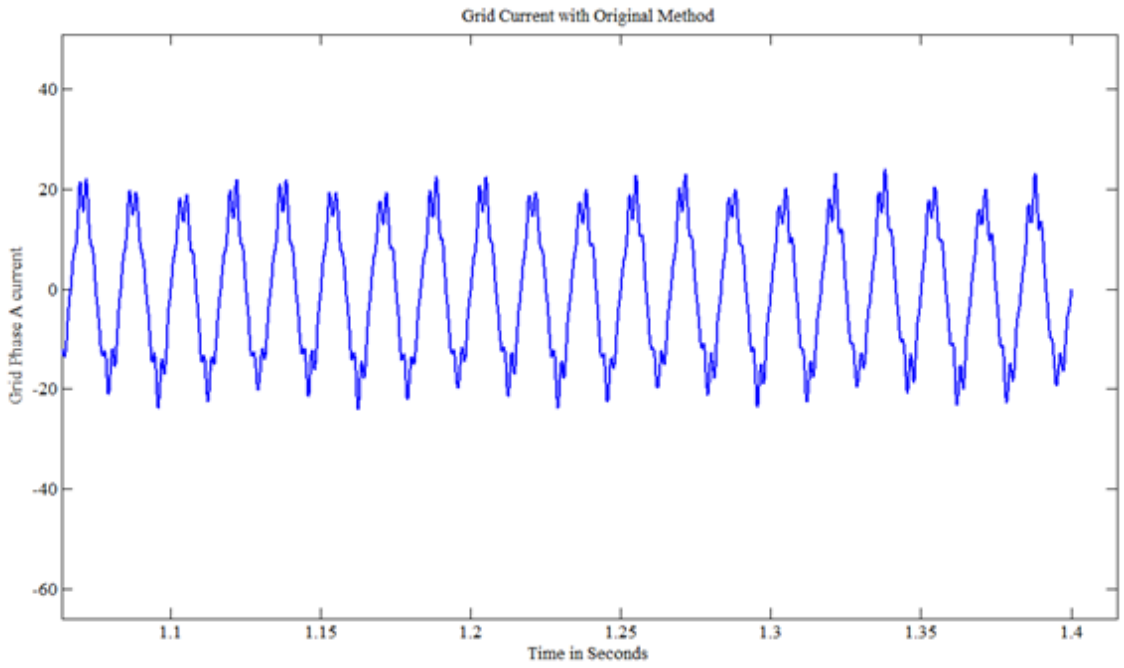

Figure 6.10 Grid Current with Conventional Architecture and Reduced Capacitance

6.4.3 Proposed Dual Band Voltage Control Methodology

As was mentioned earlier, the power into the grid side converter is typically controlled by controlling the dc bus voltage. Since the output voltage of a voltage source converter depends on the dc link voltage, the dc bus voltage is typically controlled to a constant value to keep the converter output voltage constant. While this is important for applications that are not connected to the grid (like stand-alone operation etc.), for grid connected applications since the grid acts as an infinite source the grid side converter output voltage is dictated by the grid and can be considered to be constant. Hence, it is not required to keep the dc bus voltage constant.

Considering this, the power quality of the grid connected system can be improved by allowing the dc bus voltage to vary within a certain range, and preventing the ripple from the voltage control loop to reach current controller. This sensitivity to the dc bus voltage ripple can be reduced by either keeping the current controller reference i_{dref}

constant or by varying with a low bandwidth like (2-3Hz) as long as the dc voltage is within a certain range. When the dc bus voltage changes beyond this range due to input power increase, a high bandwidth controller is used to quickly get the voltage within the band in order to prevent damage to the capacitor, and then is controlled to vary within the range. This approach has the advantage of reducing the current harmonic distortion and helps in improving the power quality while improving the dynamic performance of the system. Further, the dynamic performance of the system can be improved by employing filtered feed-forward signals from the Wind and PV systems which are used for the maximum power point tracking algorithms. Figure 6.11 shows the proposed control architecture.

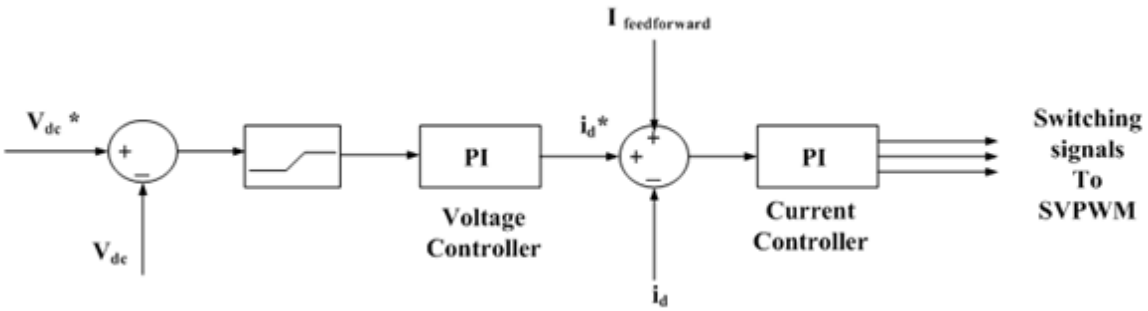

Figure 6.11 Proposed Control Architecture

Typically, the capacitors are designed to handle to around 10-15% of voltage ripple, and hence, for the present system, a 10% voltage ripple handling capable thin film capacitor is selected and accordingly the voltage band is selected to be 40V (for a 400 V dc bus). Further, for the simulations, as long as the dc voltage is within the band (380-420V), the reference to the current control loop has been kept constant. This helps in smoothing the output power injected into the grid while maintaining the power quality. When the dc voltage is increased beyond the selected range due to an input power

increase, the voltage is quickly brought into the range with a high bandwidth controller. In this regard, an analytical equation relating the minimum ΔI_d required to maintain the dc bus voltage within the given range is derived by considering the energy change in capacitor at step k as follows [41]:

$$\Delta E_c\,(k-1) = \frac{1}{2} C(V_{dc}^2(k) - V_{dc}^2(k-1)) \tag{48}$$

$$\Delta E_c\,(k) = \frac{1}{2} C(V_{dc}^2(k+1) - V_{dc}^2(k)) \tag{49}$$

The change in energy exchanged in the capacitor is given by the difference of the above two equations. This change is energy exchange which is injected into the grid is given by the following equation, where f is the grid frequency, ΔI_d is the change in the grid current d component.

$$\Delta E_c\,(k) - \Delta E_c\,(k-1) = \frac{-3}{(2f)} E_d \Delta I_d \tag{50}$$

By comparing (13) with the difference of (11) - (12), a relation for ΔI_d is obtained as follows

$$\Delta I_d = C\left[2(V_{dc}^2(k) - (V_{dc}^2(k+1) - V_{dc}^2(k-1)\right] \frac{f}{[3E_d]} \tag{51}$$

From the above equation, if the dc bus voltage in the next step (k+1) exceeds V_{dchigh} or V_{dclow}, then the dc bus voltage can be quickly brought into the range by changing the i_{dref} as given in the above equation with a high bandwidth controller. Figure 6.12 and Figure 6.13 shows the performance of the system with the proposed approach.

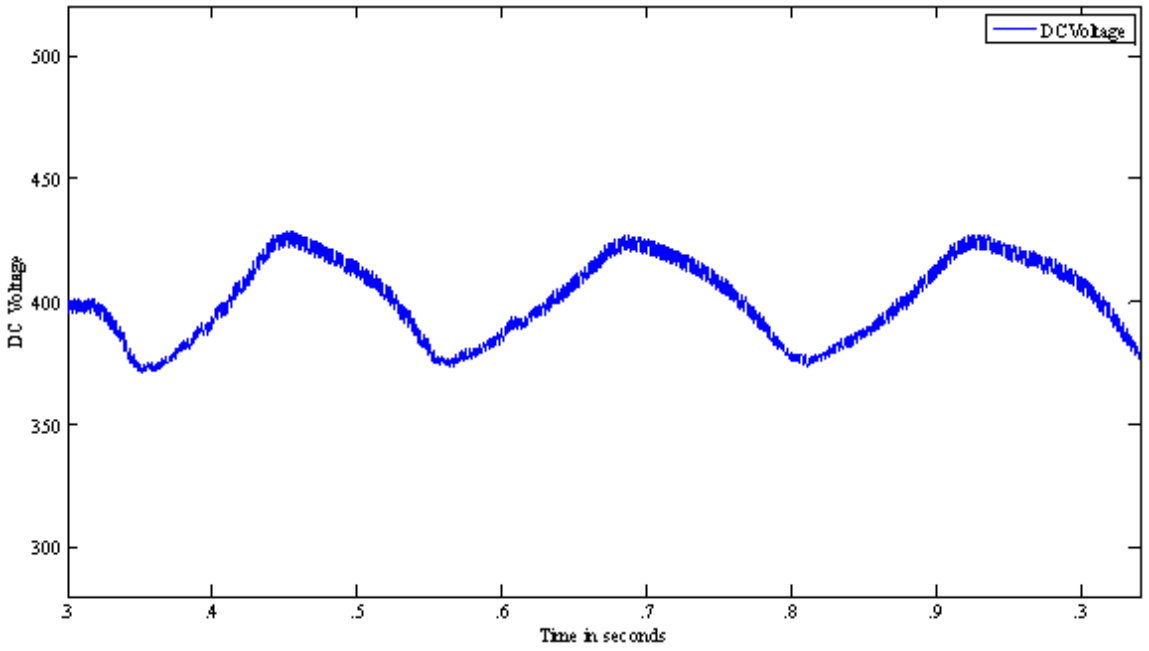

Figure 6.12 DC Bus Voltage with Proposed Method

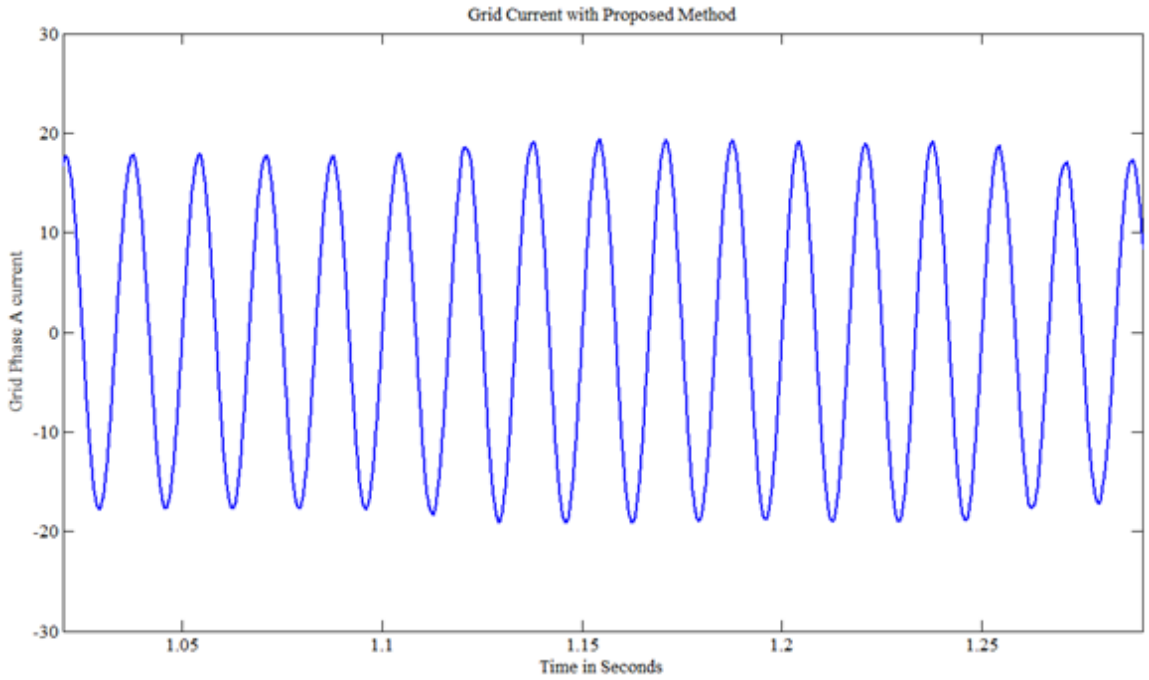

Figure 6.13 Grid Current with Proposed Method

It can be seen from the figures that when compared to the conventional control method, the proposed method has significantly lower current ripples and the current THD was found to be around 2.5% which is well within the IEEE specified limits.

6.4.4 Hybrid Wind- Photovoltaic System Simulation With Proposed Control Architecture

The proposed control architecture is employed for the hybrid Wind Photovoltaic system developed. Figure 6.14 shows the developed simulation model developed in MATLAB/SIMULINK. In the first case simulation, the local load is not connected and the wind is assumed to be blowing at 12 m/s and the solar radiation is assumed to be at 500 W/m^2 at 45 °C with the MPPT algorithms switched on at time 0.6 sec. At time 1.25 seconds, the solar radiation is increased to 1000 W/m^2. Figure 6.15 shows the MPPT tracking process and Figure 6.16 shows the power increase. As explained earlier, the dc bus voltage is allowed to vary within the band between 380-420 V. It could be seen that at the instant when the input power is increased, the dc bus voltage has an overshoot, but the voltage is quickly brought into the selected voltage range using the proposed control method and by employing feed forward signal. Figure 6.18 - 6.20 show the grid current with the proposed control method. It could be seen that with the proposed method the grid current ripple is considerable decreased. Figure 6.21 shows the grid voltage. In the second case, a local load of 3.6 kW and 1 kVAR is applied at time 0.7 sec. It could be seen from the simulation that the controller works good even when the load is applied and the load demand is met. Figure 6.23 shows the actual load current, and it can be seen that the current quality is good with low harmonic distortion.

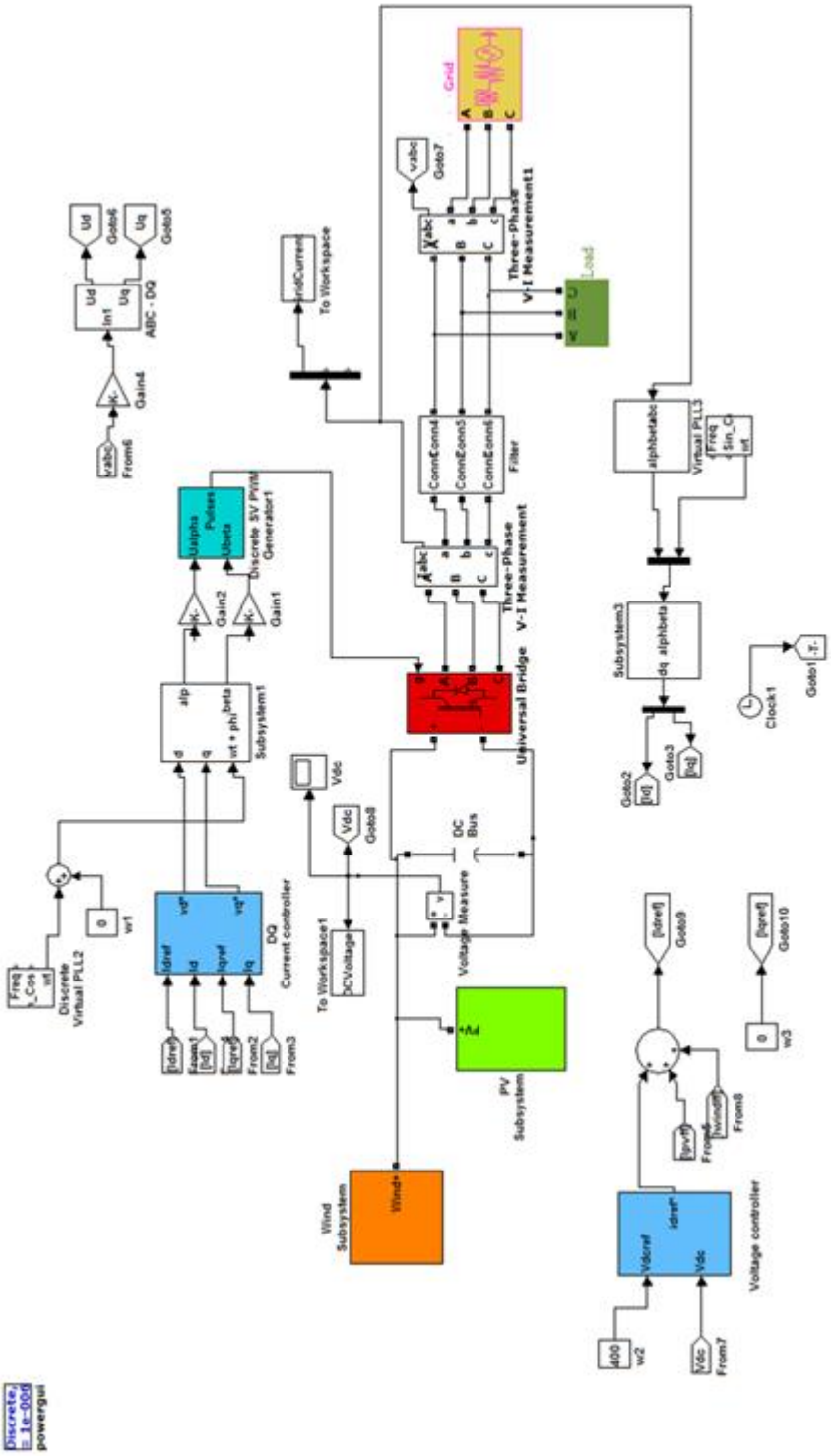

Figure 6.14 Hybrid Wind Photovoltaic Simulation

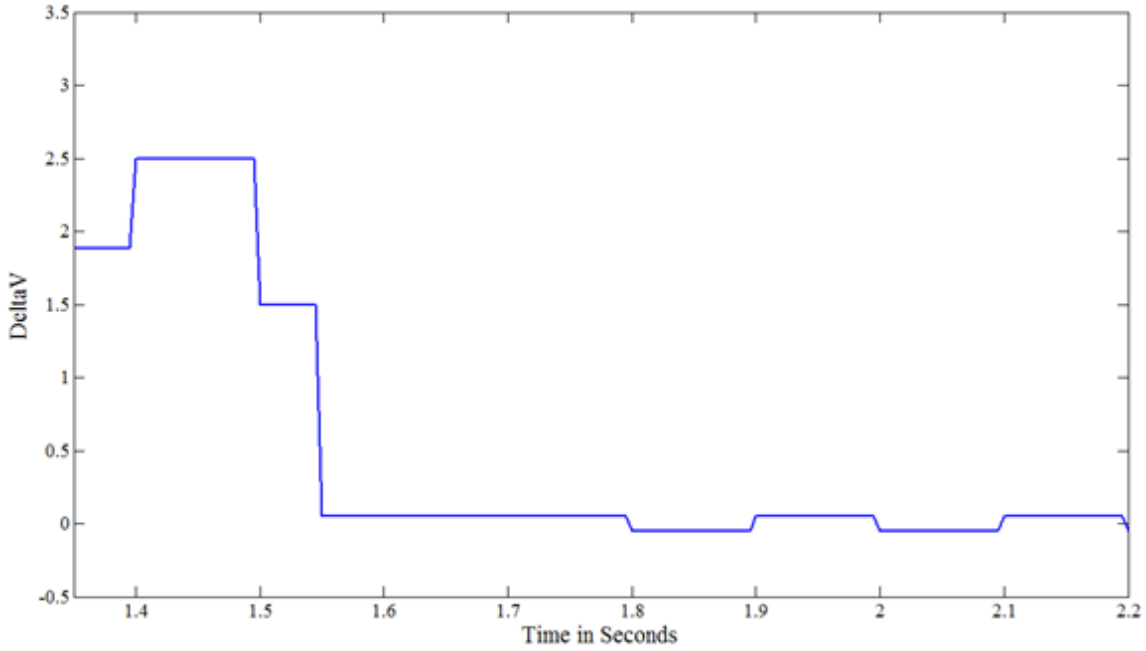

Figure 6.15 DeltaV for PV MPPT Tracking

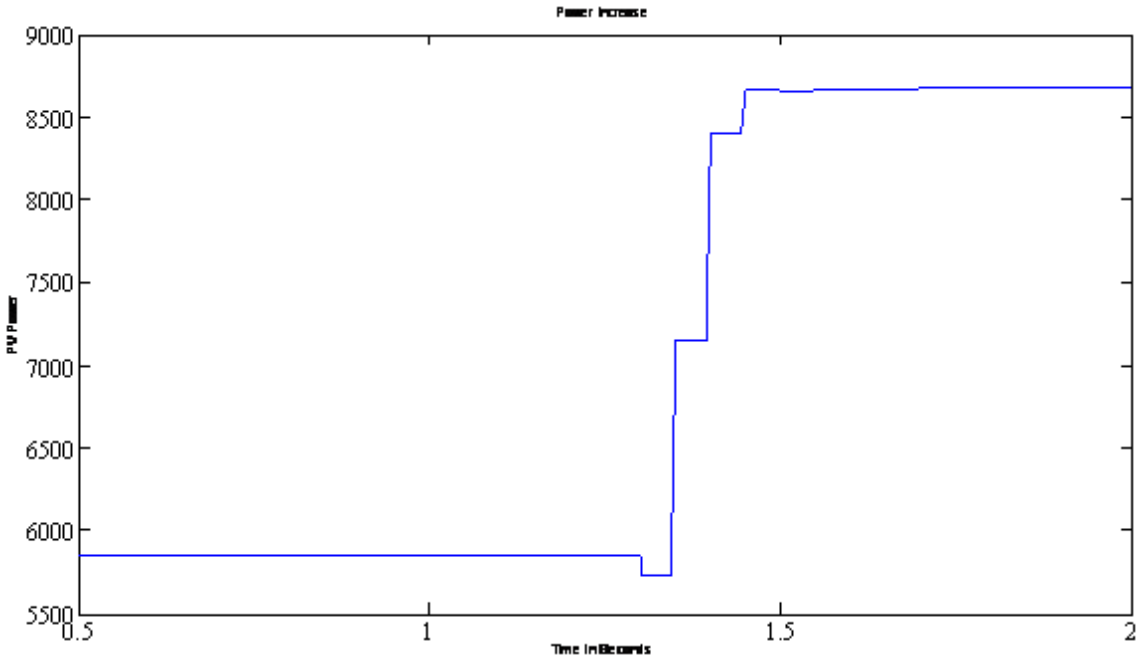

Figure 6.16 PV Power Increase

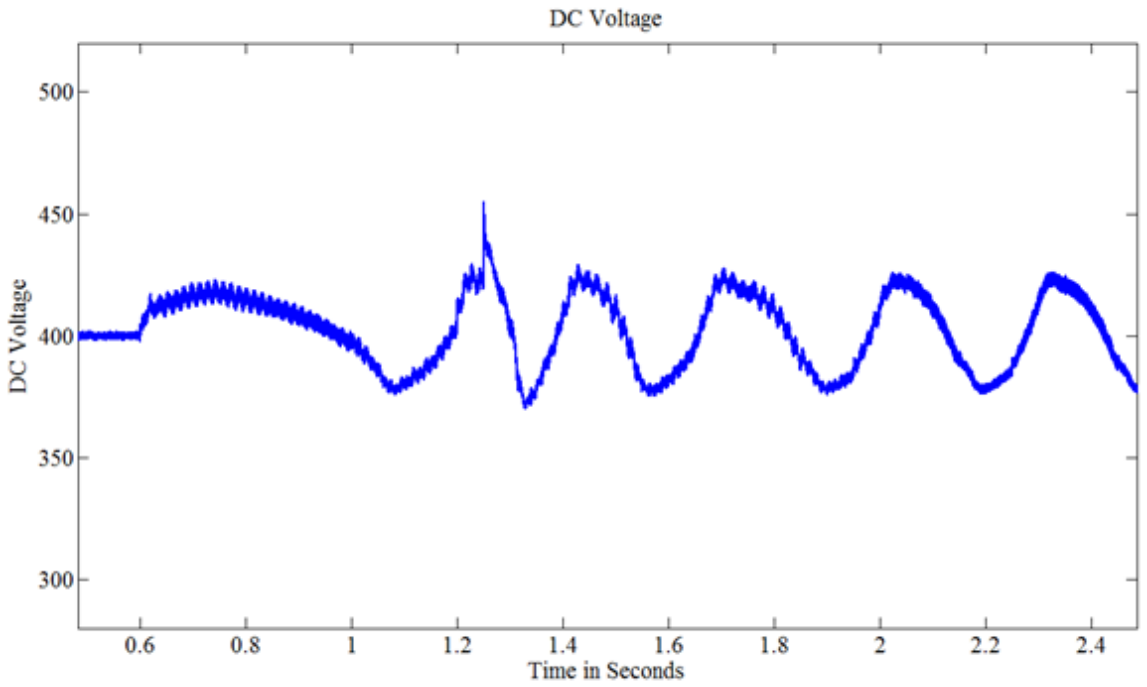

Figure 6.17 DC Bus Voltage with Proposed Method

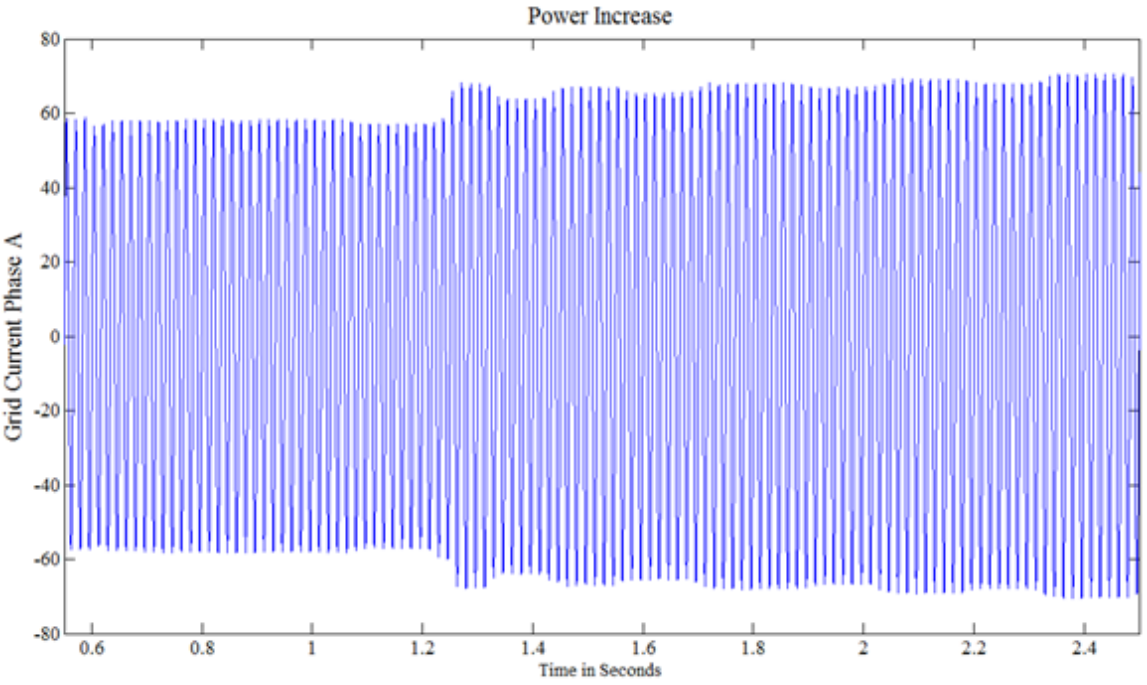

Figure 6.18 Grid Phase Current

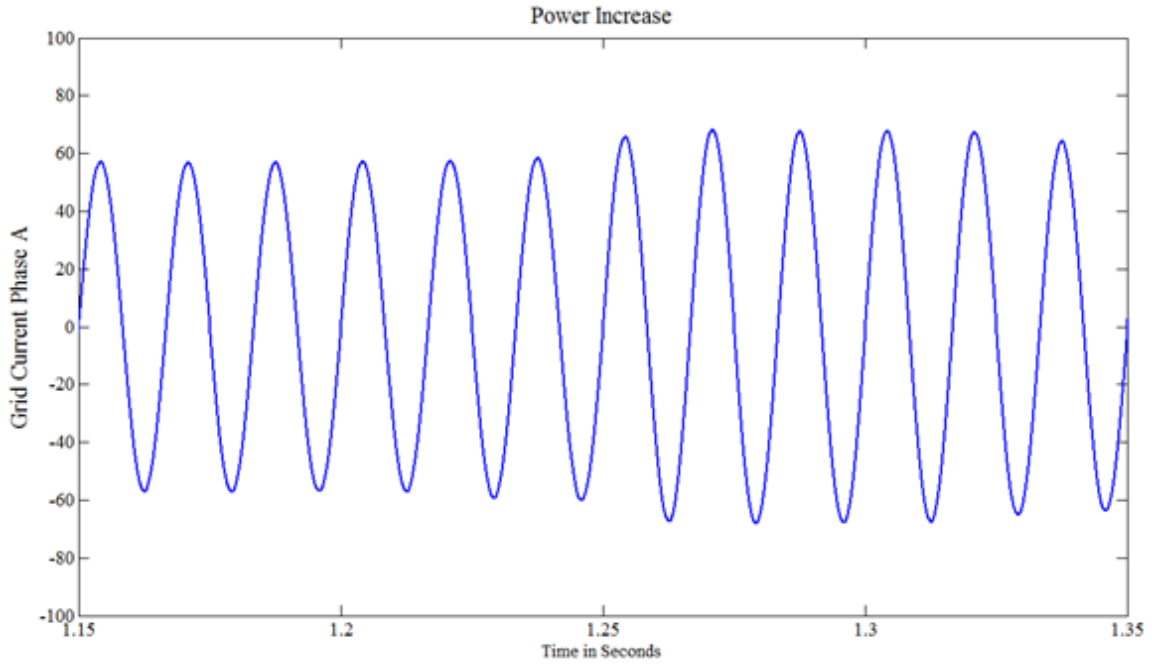

Figure 6.19 Grid Phase A Current

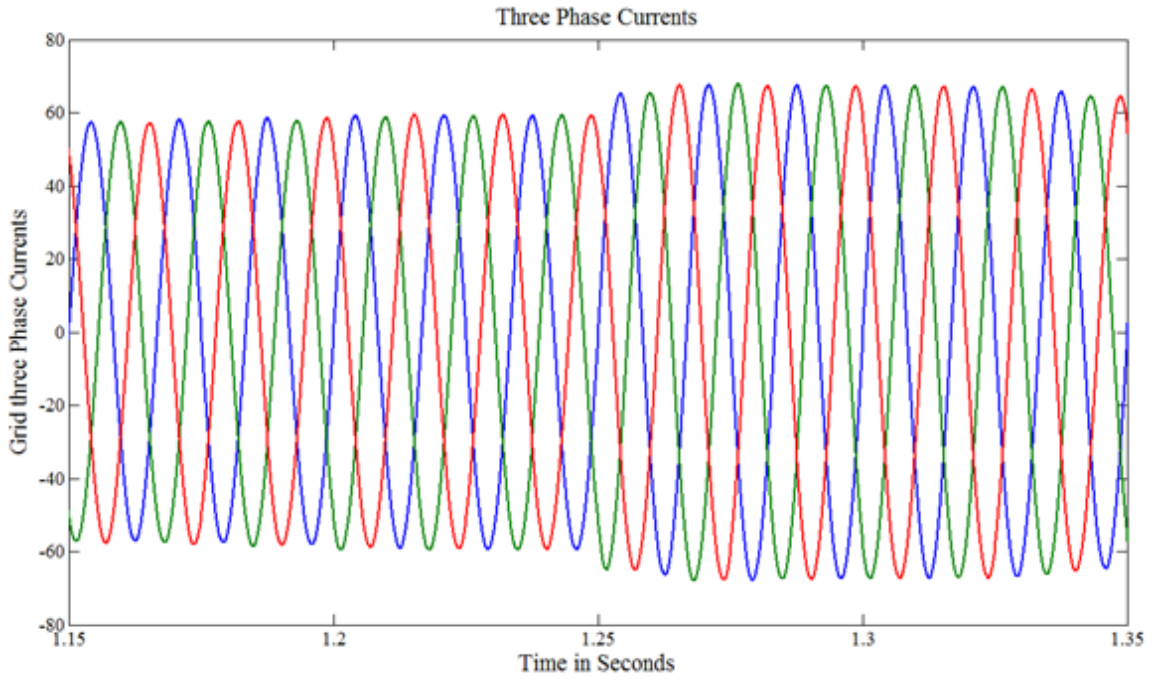

Figure 6.20 Grid Three Phase Currents

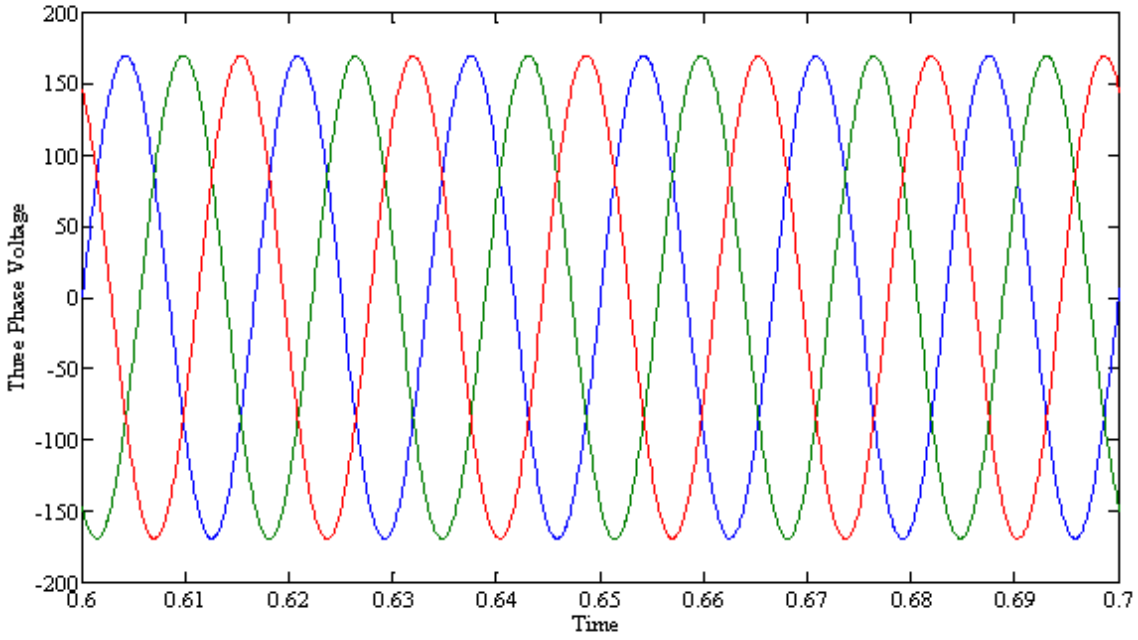

Figure 6.21 Grid Three Phase Voltage

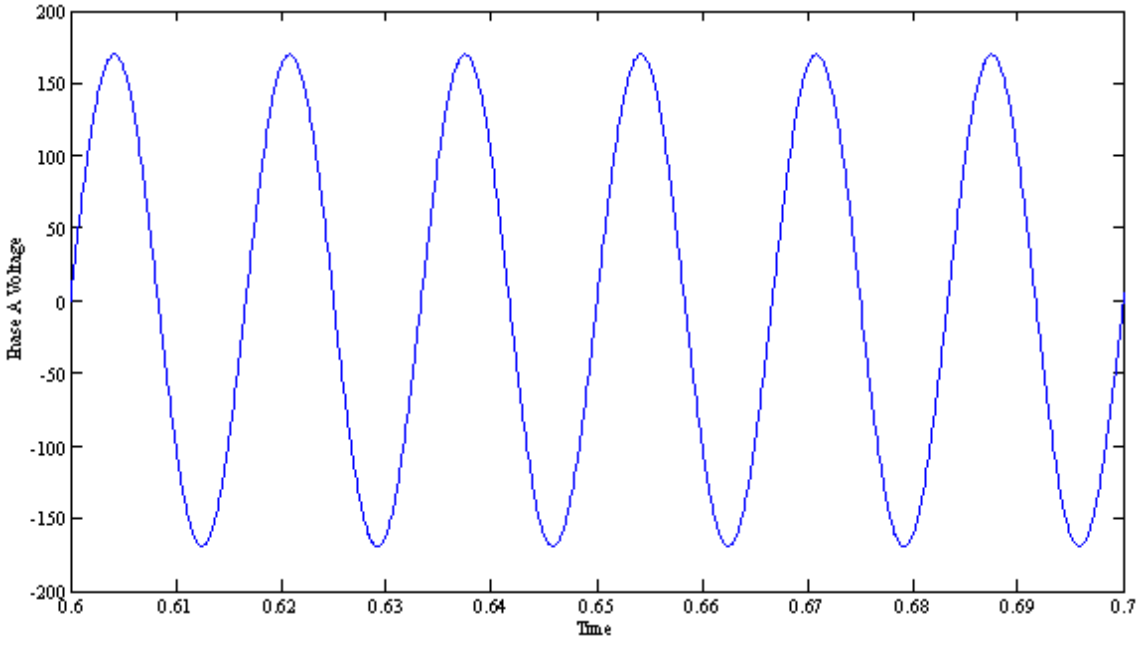

Figure 6.22 Grid Phase A Voltage

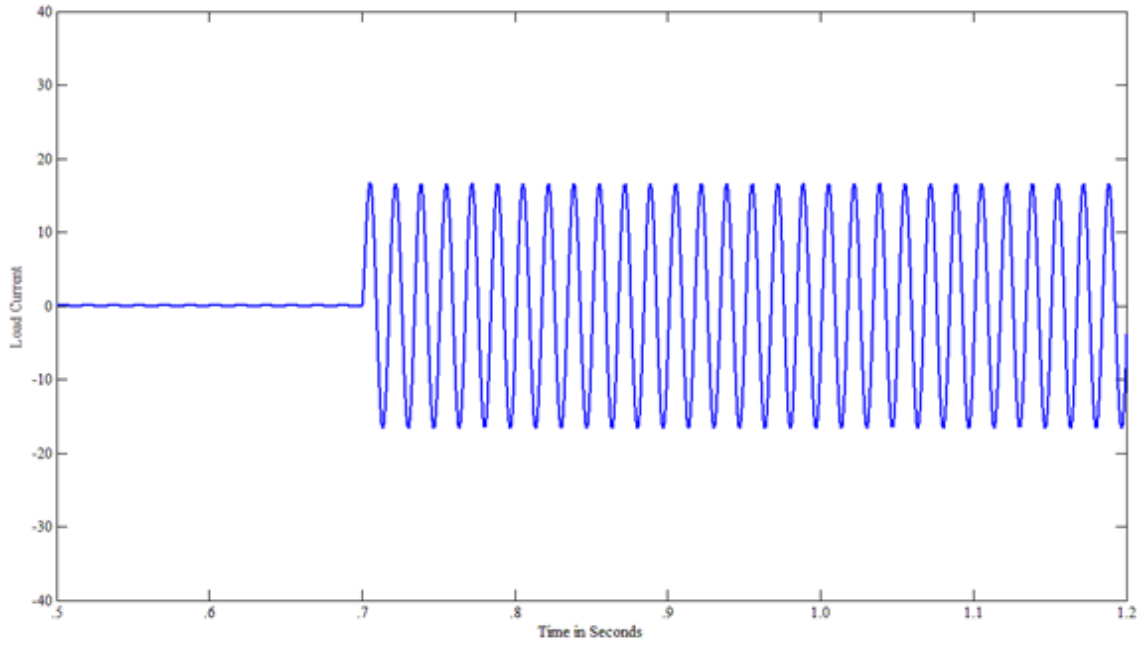

Figure 6.23 Phase A Load Current with load applied at 0.7 sec

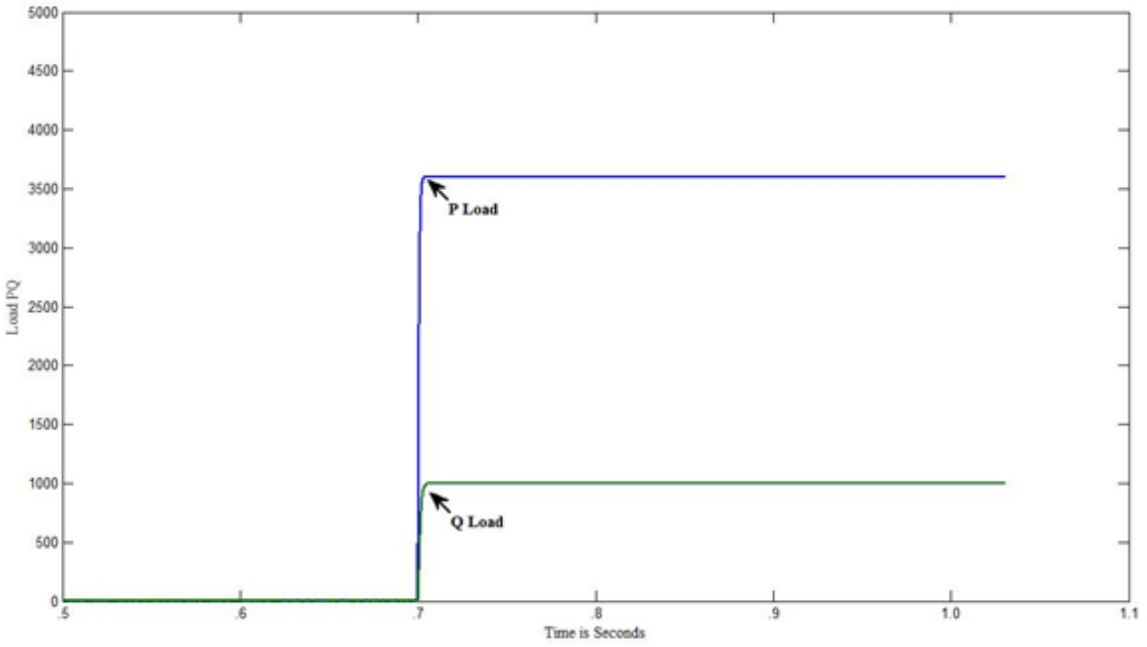

Figure 6.24 Actual Consumed Load P and Q

CHAPTER VII

CONCLUSIONS AND FUTURE WORK

7.1 Conclusions

The ever increasing demand for electricity has driven society toward the installation of new generation facilities. Concerns such as high costs associated with installation of new facilities, environmental pollution, higher transmission and distribution losses, depleting fossil fuels etc. has created a lot of interest in new generation systems at or near the load sites in the distribution systems and in exploring the alternate/renewable energy sources for generation. Accordingly, a lot of emphasis and research efforts have been put on Wind, Photovoltaic and other renewable energy sources. Electricity generation from wind turbines and Photovoltaics is an established technology with power generation ranging from small 1 Kilowatt systems to hundreds of kilowatts at the distribution level. While the efficiency and power generation of the hybrid system depends on several factors like weather conditions, conversion topology and architecture, it was seen that more than 10-15% more power can be obtained from these systems by efficiently controlling them. At the same time, the developed hybrid generation system has to meet the various grid interconnection standards before connecting to distribution network. Due to the random nature of the renewable sources, the power quality concerns are a major problem. Hence a proper design of the system that maximizes the power generation while addressing the power quality concerns and cost is very important.

The dissertation addresses these problems by modeling the Wind and Photovoltaic energy systems, and identifying the appropriate conversion technology and control architecture for the hybrid system. Algorithms are developed to extract maximum power from both the Wind and Photovoltaic energy systems, and it was seen that the proposed algorithms have a better performance and extract more power when compared to the traditional algorithms. Further, in order to improve the power quality, dynamic performance and cost of the system, a new dc bus voltage control strategy has been proposed, and it was seen that the proposed method has improved the power quality when compared to the conventional architectures.

7.2 Future Work

Based on this dissertation, there are several topics for further investigation on design, control, and implementation of power electronic interface for small-scale hybrid Wind Photovoltaic renewable systems. Future works related to this dissertation could be summarized as follows:

1. The devices of power converters used in this dissertation employed are hard switching controls. Instead, soft switching techniques can be explored for the converters for the hybrid renewable energy system control.
2. For a system with multiple energy sources like for example the Combined Heat and Power (CHP) systems, control of various sources in accordance with the load demand, and considering generation efficiencies would improve the overall efficiency of the system, and also reduces the cost thereby acting as an incentive for increasing distributed generation. For

achieving such an objective, there has to be coordination in control of various sources. Multi agent based control approach would be very beneficial in this regard. The system effectiveness could be further improved by employing wireless control.

3. Loss minimization of the permanent magnet generator by improving the power factor of machine, using a new control approach to manage the boost chopper for line current wave shaping.
4. The hybrid renewable energy system was assumed to be operating in a balanced system with a stiff grid. However, the performance of the system needs to be analyzed when there is an unbalanced fault in the system. Further, for minimizing the impact of faults, new protection strategies need to be developed. The existing power distribution network is provided with switches that has only the unidirectional power flow capability. With the increase in distributed generation, it becomes essential to develop novel bi-directional fault tolerant switches.
5. Even though permanent magnet machines are used in wind turbine generation systems, control algorithm can be implemented for this type of machine, but some modifications need to be addressed. For example, the induction machine will need to be connected to a controlled rectifier instead of an un-controlled rectifier. Also, the wind speed and solar radiation profile considered in this dissertation could be refined by considering the actual weather data obtained from weather prediction and forecast.

6. A more detailed cost analysis and developing IEEE 1547 and UL 1741 compliances for connecting the hybrid system to utility grid can be made.
7. Application of Plug-in Hybrid Electric Vehicle as Energy Storage: With the increasing oil prices there has been a growing demand for using more hybrid and all electric vehicles for automotives. In this regard, a lot of research has going on over the years to find novel generation technologies which are ideal for this application. Of the various factors like machine type, type of transmission used etc., that determine the success of the hybrid and all electric vehicle designs and concepts, the energy storage technology is one of the pivotal aspects. The hybrid and electric vehicles typically use battery and ultra capacitors (in addition to the main engine in the case of hybrid vehicles) energy storage devices for providing the required propulsion and other electrical service powers to the automotive.

It would be interesting to note that in many scenarios like when parked at office spaces, shopping malls etc. where the vehicles are typically parked for hours, the batteries could be charged using the power generated through the rooftop hybrid power systems, if the vehicle is plugged into the electrical socket. Any additional power generated from the hybrid system can be utilized to charge the batteries of the vehicles, rather than sending into the grid. This would result in reducing the losses, and increased utilization factor when compared to sending back the additional power to the grid. This method would also help in reducing the peak load demand for charging the vehicles in the mornings or evenings when it would be typically done. In advanced cases, some of the power available in the plugged in cars can be used to meet the intermittent fluctuating loads, thereby reducing the power quality. More research in this regard has to be done.

REFERENCES

[1] Energy Information Agency (EIA), 2008. World Total Electricity Installed Capacity, January 1, 1980 - January 1, 2006

[2] EIA International Energy Outlook Report, 2010

[3] Inventory of U.S. Greenhouse Gas Emissions and Sinks: 1990-2008, USEPA #430-R-10-006

[4] F.Baumgartner, "Performance and Reliability of Photovoltaic Systems", Photovoltaic and Environment Euroconference, November 2003.

[5] P. Gipe, "Soaring to new heights: the world wind energy market," Renewable Energy World, vol. 5, no. 4, pp. 33‑47, Sept./Oct. 2002.

[6] B. Borowy and Z. Salameh, "Dynamic response of a stand alone wind energy conversion system with battery energy storage to a wind gust", IEEE Trans Energy Conversion (1997) (1), pp. 73–78

[7] C. Soras and V. Makios , "A novel method for determining the optimum size of standalone photovoltaic systems". Solar Cells 25 2 (1988), pp. 127–142

[8] F. Valenciaga, P.F. Puleston and P.E. Battaitto, "Power control of a photovoltaic array in a hybrid electric generation system using sliding mode techniques", Proc IEEE 148 (6) (2001), pp. 448–455.

[9] S. K. Kim, J. H. Jeon, C. H. Cho, J. B. Ahn, and S. H. Kwon, "Dynamic modeling and control of a grid-connected hybrid generation system with versatile power transfer," IEEE Trans. Ind. Electron., vol. 55, no. 4, pp. 1677–1688, Apr. 2008.

[10] Y. Chen, Y. Liu, S. Hung, and C. Cheng, "Multi-input inverter for grid-connected hybrid PV/wind power system," IEEE Trans. Power Electron., vol. 22, no. 3, pp. 1070‑1077, May 2007.

[11] "Storage as a Strategic Tool for Managing Variability and Capacity Concerns in the Modern Grid", EAC Energy Storage Technologies Subcommittee 2008

[12] "Flywheel Energy Storage An alternative to batteries for uninterruptible power supply systems", United States Department of Energy, Office of Federal Energy Management, 2005.

[13] Gholamreza Esmaili, "Applications of Advanced Power electronics in Renewable Energy Sources and Hybrid Generating Systems", Doctoral Dissertation, Ohio State University, December 2006.

[14] D. Das , R. Esmaili , L. Xu and D. Nichols "An optimal design of a grid connected hybrid wind/photovoltaic/fuel cell system for distributed energy production," Proc. IEEE IECON, 2005, p. 2499

[15] E. Hau, Wind Turbines: Fundamentals, Technologies, Application, Economics, 2nd edition. Berlin, Germany: Springer, 2006

[16] Z. Lubosny, Wind Turbine Operation in Electric Power Systems, Berlin, Germany: Springer, 2003.

[17] L. H. Hansen, L. Helle, F. Blaabjerg, et.al, "Conceptual survey of Generators and Power Electronics for Wind Turbines",Riso National Laboratory, Denmark, December 2001

[18] Pena,R., Clare,J.C., & Asher,G.M. (1996). Doubly fed induction generator using back-to-back PWM converters and its application to variable speed wind-energy generation. IEE proceedings on electronic power application, 143(3), 231-241.

[19] H.E.Mena.Lopez, Maximum Power Tracking Control Scheme for Wind Generator Systems. Master's Thesis, Texas A&M university, Dec. 2007

[20] D. Das , R. Esmaili , L. Xu and D. Nichols "An optimal design of a grid connected hybrid wind/photovoltaic/fuel cell system for distributed energy production," Proc. IEEE IECON, 2005, p. 2499.

[21] Sawata,T., Kjaer,P.C., Cossar,C., Miller,T.J.E., & Hayashi,Y, "Fault-tolerant operation of single-phase SR generators. IEEE Transactions on Industry Applications., 35(4), 774-781.

[22] Jack L. Stone, "Photovoltaics: Unlimited Electrical Energy From the Sun," Physics Today, September 1993

[23] Available [Online] : http://www.solarpoint.com.au

[24] "Fundamentals of Photovoltaic Materials", National Solar Power Research Institute, Inc, December 1998.

[25] Stanley R. Bull and Lynn L. Billman, "Global Trends: A Glimpse Ahead Renewable Energy: Ready to Meet Its Promise?", The Center for Strategic and International Studies and the Massachusetts Institute of Technology

[26] Available [Online] : http://solarcellcentral.com/cost_page.html

[27] Solar Panels on the roof! Is it worth the investment? Available [Online] : http://www.thegreentechnologyblog.com/2009/solar-panels-on-the-roof-is-it-worth-the-investment/

[28] C.L. Jeong; W.J. Sang; Y.H. Jae; K.K. Seok, S. Jinsoo; Y.H. Kyung; "Si-based thin-film solar cells: process and device performance analysis," Photovoltaic Specialists Conference, Conference Record of the Thirty-first IEEE pp. 1552 – 1555, Jan. 2005.

[29] R. Hezel; C. Schmiga, A. Metz, "Next generation of industrial silicon solar cells with efficiencies above 20%," IEEE Conference Record of the Twenty-Eighth Photovoltaic Specialists Conference, pp.184 – 187, Sept. 2000.

[30] G. Walker, " Evaluating MPPT Converter Topologies Using A Matlab PV Model", AUPEC December 2000

[31] Solarex MSX60 Panel Specifications. Available [Online]: http://www.californiasolarcenter.org/newssh/pdfs/Solarex-MSX64.pdf

[32] Q.Li, "High Frequency Transformer Linked Converters for Photovoltaic Applications", Doctoral Dissertation, Central Queensland University, June 2006.

[33] J. Wiles, "Photovoltaic Power Systems and the National Electrical Code: Suggested Practices," New Mexico State University, March 2001.

[34] F. A. Farret and M. G. Simões, Integration of Alternative Sources of Energy, John Wiley & Sons, Inc., 2006.

[35] A VanderMeulen, J Maurin, " Current Source Inverter vs Voltage Source Inverter Topology", Eaton Corporation, Technical Data TD02004004E, August 2010

[36] K. Tan and S. Islam, "Optimal control strategies in energy conversion of PMSG wind turbine system without mechanical sensors," IEEE Trans. Energy Convers., vol. 19, no. 2, pp. 392–399, Jun. 2004.

[37] D. Das , R. Esmaili , L. Xu and D. Nichols "An optimal design of a grid connected hybrid wind/photovoltaic/fuel cell system for distributed energy production," Proc. IEEE IECON, 2005, p. 2499.

[38] Raza, K.S.M. Goto, H. Hai-Jiao Guo Ichinokura, O. , "A novel speed-sensorless adaptive hill climbing algorithm for fast and efficient maximum power

point tracking of wind energy conversion systems “, IEEE International conference on Sustainable Energy Technologies, No. 2008, pp 628-633

[39] I. Schiemenz and M. Stiebler, “Control of a permanent magnet synchronous generator used in a variable speed wind energy system,” in Proc.IEEE IEMDC, 2001, pp. 872–877.

[40] R. Datta and V.T. Ranganathan, “A method of tracking the peak power points for a variable speed wind energy conversion system”, IEEE Trans Energy Conver 18 (2003), pp. 163–168

[41] Y.-M. Chen, H.-C. Wu and Y.-C. Chen, “DC Bus Regulation Strategy for Grid-Connected PV Power Generation System,” IEEE International Conference on Sustainable Energy Technologies, pp.437-442, Singapore, Nov. 2008

[42] Srighakollapu, N. Sensarma, P.S. , “Sensorless maximum power point tracking control in wind energy generation using permanent magnet synchronous generator “, 34th Annual IEEE Industrial Electronics Conference, Nov. 2008

[43] T. Tanaka, T. Toumiya, and T. Suzuki, “Output control by hill-climbing method for a small scale wind power generating system,” Renewable Energy, vol. 12, no. 4, pp. 387-400, 1997.

[44] Raju AB, Chatterjee K, Fernandes BG, “A simple maximum power point tracker for grid connected variable speed wind energy conversion system with reduced switch count power converters”. In: Proceedings of IEEE PESC’03, vol. 2, June 2003. p. 748–53.

[45] N. Yamamura, M. Ishida, and T. Hori, “A simple wind power generating system with permanent magnet type synchronous generator,” in Proc. IEEE Int. Conf. Power Electronics Drive Systems Hong Kong, vol. 2, Jul. 27\\\–29, 1999, pp. 849-854.

[46] Oghafy, V. Nikkhajoei, H. , “Maximum power extraction for a wind-turbine generator with no wind speed sensor”, IEEE Power and Energy Society General Meeting, July 2008.

[47] E. Koutroulis and K. Kalaitzakis “Design of a maximum power tracking system for wind-energy-conversion applications,” IEEE Trans. Ind. Electron., vol. 53, pp. 486, Apr. 2006.

[48] A.M. De Broe, S. Drouilhet, and V. Gevorgian, “A peak power tracker for small wind turbines in battery charging applications,” IEEE Trans. Energy Convers., vol. 14, no. 4, pp. 1630-1635, Dec. 1999.

[49] G. D. Moor and H. J. Beukes, “Maximum Power Point Trackers for Wind Turbines”, The 35th IEEE Power Electronics Specialists Conference, 2004, Aachen, Germany.

[50] Jia Yaoqin, Yang Zhongqing, Cao Binggang, "A New Maximum Power Point Tracking Control Scheme for Wind Generation," IEEE Con. on Power System Technology, Vol. 1, 13-17 Oct. 2002, pp.: 144-148.

[51] L. Solero, F. Caricchi, F. Crescimbini, O. Honorati, and F. Mezzetti, “Performance of a 10 kW power electronic interface for combined wind/PV isolated generating systems,” in Proc. IEEE PESC'96, 1996, pp. 1027-1032.

[52] K. Buehring and L. L. Freris, “Control policies for wind energy conversion systems,” Proc. Inst. Elect. Eng. C, vol. 128, pp. 253-261, Sept. 1981.

[53] S. Brune, R. Spe\´e, and A. K. Wallace, “Experimental evaluation of a variable-speed, doubly-fed wind-power generation system,” IEEE Trans. Ind. Applicat., vol. 30, pp. 648-655, May/June 1994.

[54] T. Thiringer and J. Linders, “Control by variable rotor speed of a fixed-pitch wind turbine operating in a wide speed range,” IEEE Trans. Energy Conv., vol. EC-8, pp. 520-526, Sept. 1993.

[55] M. Chinchilla , S. Arnaltes and J. C. Burgos “Control of permanent-magnet generators applied to variable-speed wind-energy systems connected to the grid,” IEEE Trans. Energy Convers., vol. 21, pp. 130, Mar. 2006.

[56] M. Ermis, H. B. Ertan, E. Akpinar, and F. Ulgut, “Autonomous wind energy conversion systems with a simple controller for maximum-power transfer,” Proc. Inst. Elect. Eng. B, vol. 139, pp. 421-428, Sept. 1992.

[57] G. E. Peters and A. M. Knight, “Rugged control circuit for efficient operation of a wind turbine,” in Proc. IEEE Canadian Conf. Electrical Engineering, 2002, pp. 262-267.

[58] Ermis, M., Ertan, H.B., Akpinar, E., and Ulgut, F.: ‘Autonomous wind energy conversion system with a simple controller for maximumpower transfer’, IEE Proc. B, Electr. Power Appl., 1992, 139, (5), pp. 421–428

[59] E. Muljadi and C. P. Butterfield, “Pitch-controlled variable-speed wind turbine generation,” IEEE Trans. Ind. Applicat., vol. 37, pp. 240-246, Jan./Feb. 2001.

[60] Jianzhong Zhang, Ming Cheng, Zhe Chen, Xiaofan Fu, “Pitch angle control for variable speed wind turbines”, DRPT2008 6-9 April 2008 Nanjing China

[61] H. Polinder, D. Bang, R.P.J.O.M. van Rooij, A.S. McDonald, and M.A. Mueller, "10 MW Wind turbine direct-drive generator design with pitch or active speed stall control", IEEE Int. Electric Machines and Drives Conf., Antalya, Turkey, May 3-5 2007.

[62] Kosaku, T.; Sano, M.; Nakatani, K., "Optimum pitch control for variable-pitch vertical-axis wind turbines by a single stage model on the momentum theory", IEEE International Conference on Systems, Man and Cybernatics, Oct. 2002

[63] M. G. Simões, B. K. Bose, and R. J. Spiegel, "Fuzzy logic based intelligent control of a variable speed cage machine wind generation system," IEEE Trans. Power Electron., vol. 12, pp. 87-95, Jan. 1997.

[64] A. Z. Mohamed, M. N. Eskander, and F. A. Ghali, "Fuzzy logic control based maximum power tracking of a wind energy system," Renew. Energy, vol. 23, no. 2, pp. 235-245, Jun. 2001.

[65] Abo-Khalil, AG, Lee D-C, Seok J-K. Variable speed wind power generation system based on fuzzy logic control for maximum output power tracking. In: Proceedings of 2004 IEEE 35th annual power electronics specialists conference – PESC 04, Aachen, Germany, vol. 3. p. 2039–4.

[66] Z. Chen , S. Gomez and M. Mc Cornick "A fuzzy logic controlled power electronic system for variable speed wind energy conversion systems," Proc. IEE PEVD Conf., 2000, p. 114.

[67] V. Galdi, A. Piccolo, P. Siano: "Designing an adaptive fuzzy controller for maximum wind energy extraction", IEEE Transactions on Energy Conversion, Vol. 23, June 2008

[68] R. Hilloowala and A. M. Sharaf, "A rule-based fuzzy logic controller for a PWM inverter in a stand alone wind energy conversion scheme," IEEE Trans. Ind. Applicat., vol. IA-32, pp. 57-65, Jan. 1996.

[69] Xin-yan Zhang Jing Cheng Wei-qing Wang, "The intelligent control method study of variable speed wind turbine generator", IEEE International conference on Sustainable Energy Technologies, Nov. 2008, pp 173-177

[70] V. Calderaro, V. Galdi, A. Piccolo, P. Siano: "A fuzzy controller for maximum energy extraction from variable speed wind power generation systems", Electrical Power Systems Research, Elsevier Editorial, vol 78, issue 6, pp 1109-1118, 2008.

[71] Lei Zhang, Haidong Li, Chunliang E, Jianlin Li, Honghua Xu, "Pitch control of large scale wind turbine based on fuzzy-PD method", DRPT2008 6-9 April 2008 Nanjing China

[72] H. Li , K. L. Shi and P. G. McLaren “Neural-network-based sensorless maximum wind energy capture with compensated power coefficient,” IEEE Trans. Ind. Appl., vol. 41, pp. 1548, Nov./Dec. 2005.

[73] Ro, K. Choi, H. h., “Application of neural network controller for maximum power extraction of a grid-connected wind turbine system”,Journal of Electrical Engineering, Vol. 88, 2005, pp 45-53

[74] P. Flores, A. Tapia and G. Tapia, Application of a control algorithm for wind speed prediction and active power generation, Renew Energy 305 (2005), pp. 23–536.

[75] Zhang Xinyan, Wang Weiqing, Cheng Jing, “Analysis on control of variable speed wind turbine using neural network controller”, Journal of Chongqing University, Chongqing of China, 28(11), 2005, pp 65-68.

[76] M.N. Eskander, Neural network controller for a permanent magnet generator applied in a wind-energy conversion system, Renew Energ 26 (2002) (3), pp. 463–477

[77] S. Kelouwani and K. Agbossou, "Nonlinear model identification of wind turbine with a neural network", IEEE Transactions on Energy Conversion, vol. 19, 2004, pp. 607-612.

[78] Wei Qiao, Wei Zhou, J.M Aller, R.G. Harley, “Wind Speed Estimation Based Sensorless Output Maximization Control for a Wind Turbine Driving a DFIG,” IEEE Trans. on Power Electronics, vol. 23, no. 3, pp. 1156 – 1169, May 2008.

[79] G. Venkataramanan, B. Milkovska, V. Gerez, and H. Nehrir, “Variable speed operation of permanent magnet alternator wind turbines using a single switch power converter,” J. Solar Eng., Trans. ASME, vol. 118, pp. 235–238, Nov. 1996.

[80] W. Lawrance, D. Langridge, and D. Johnston, “Low wind generation scheme,” Renew. Energy, vol. 4, no. 5, pp. 489–494, 1994.

[81] Nabil A. Ahmed and Masafumi Miyatake, “A stand-alone hybrid generation system combining solar photovoltaic and wind turbine with simple maximum power point tracking control” Power Electronics and Motion Control Conference, IPEMC '06. CES/IEEE 5th International Aug. 2006 Vol.1, pp. 1-7

[82] Shigeo Morimoto, Tomohiko Nakamura, Yoji Takeda, “Power maximization control of variable-speed wind generation system using permanent magnet synchronous generator”, Electrical Engineering in Japan, Nov. 2004, Volume 150 Issue 2, Pages 11 – 19

[83] G. E. Peters and A. M. Knight, "Rugged control circuit for efficient operation of a wind turbine," in Proc. IEEE Canadian Conf. Electrical Engineering, 2002, pp. 262-267.

[84] A. Mullane, G. Lightbody, R. Yacamini, and S. Grimes, "Adaptive control of variable speed wind turbines.," in 36th Universities Power Enginering Conference, (Swansea, UK), 12-24th September 2001.

[85] F. Valenciaga and P. F. Puleston, ''An adaptive feedback linearization strategy for variable speed wind energy conversion systems'', International Journal of Energy Research, 24:151–161, 2000.

[86] Hui, J. Bakhshai, A. , "A new adaptive control algorithm for maximum power point tracking for wind energy conversion systems", IEEE Power Electronics Specialists Conference, June 2008

[87] Yao Xingjia Wang Xiaodong Xing Zuoxia Liu Jun , "Coordinate control strategy based on expert decision system of wind turbine", IEEE International conference on Sustainable Energy Technologies, Nov. 2008, pp 464-468

[88] Y. D. Song, B. Dhinakaran, and X. Y. Bao, "Variable speed control of wind turbines using nonlinear and adaptive algorithms," Journal of Wind Engineering and Industrial Aerodynamics, vol. 85, pp. 293–308, 2000.

[89] R. Chedid, F. Mrad, and M. Basma, "Intelligent control for wind energy conversion systems," Wind Eng., vol. 22, no. 1, pp. 1-16, 1998.

[90] X. Yao, Y. Liu, and C. Guo. Adaptive fuzzy sliding-mode control in variable speed adjustable pitch wind turbine. Automation and Logistics, 2007 IEEE International Conference on, pages 313–318, August 2007.

[91] Cardenas, R. and Pena, R., "Sensorless vector control of induction machines for variable-speed wind energy applications," IEEE Trans. On Energy Conversion, Vol. 19 , pp. 196 – 205, March 2004.

[92] Q Wang, and L. Chang, "An independent maximum power extraction strategy for wind energy conversion systems," in Proceedings of the IEEE Canadian Conference on Electrical and Computer Engineering, Edmonton, Canada, May 9-12 1999, pp. 1142-1147. 2541

[93] F. Valenciaga , P. F. Puleston and P. E. Battaiotto "Power control of a solar/wind generation system without wind measurement: A passivity/sliding mode approach," IEEE Trans. Energy Convers., vol. 18, pp. 501, Dec. 2003.

[94] A. Koyanagi, et al., "Study on maximum power point tracking of wind turbine generator using a flywheel," in Proc. Power Conversion Conference-Osaka Osaka, Japan, 2002, pp. 322-327.

[95] A. Brambilla, M. Gambarara, A. Garutti, and F. Ronchi, "New approach to photovoltaic arrays maximum power point tracking," in Proc. 30th Annual IEEE Power Electron. Spec. Conf., 1999, pp. 632–637.

[96] K. Irisawa, T. Saito, I. Takano, and Y. Sawada, "Maximum power point tracking control of photovoltaic generation system under non-uniform insolation by means of monitoring cells," in Conf. Record Twenty-Eighth IEEE Photovoltaic Spec. Conf., 2000, pp. 1707–1710.

[97] T.-Y. Kim, H.-G. Ahn, S. K. Park, and Y.-K. Lee, "A novel maximum power point tracking control for photovoltaic power system under rapidly changing solar radiation," in IEEE Int. Symp. Ind. Electron., 2001, pp. 1011–1014

[98] P. Midya, P. T. Krein, R. J. Turnbull, R. Reppa, and J. Kimball, "Dynamic maximum power point tracker for photovoltaic applications," in Proc. 27th Annu. IEEE Power Electron. Spec. Conf., 1996, pp. 1710–1716.

[99] T.Esram, J.W.Kimball, P.T.Krein, P.L.Chapman, P.Midya, "Dynamic Maximum Power Point Tracking of Photovoltaic Arrays Using Ripple Correlation Control", IEEE Transactions on Power Electronics, Vol. 21, pp. 1282-1291, September 2006

[100] J. J. Schoeman and J. D. vanWyk, "A simplified maximal power controller for terrestrial photovoltaic panel arrays," in Proc. 13th Annu. IEEE Power Electron. Spec. Conf., 1982, pp. 361–367.

[101] D. J. Patterson, "Electrical system design for a solar powered vehicle," in Proc. 21st Annu. IEEE Power Electron. Spec. Conf., 1990, pp. 618–622

[102] G. W. Hart, H. M. Branz, and C. H. Cox, "Experimental tests of open loop maximum-power-point tracking techniques," Solar Cells, vol. 13, pp. 185–195, 1984.

[103] Holtz, J. "Pulse width modulation a survey." IEEE Transactions on Industrial Electronics, Oct. 1992, pp. 410 – 420.

[104] T. CY Wang, Z. H. Ye, G. Sinha and X. M. Yuan. "Output Filter Design for a Grid-interconnected Three-Phase Inverter," Proc. Of PESC'03, Acapulco (Mexico), June 2003, vol. 2, pp. 779-784.

[105] Prasad, V H, "Analysis and comparison of space vector modulation schemes for three-leg voltage source inverters," Master dissertation, 1997, Virginia Polytechnic Institute and State University, Blacksburg, VA.

[106] M. Liserre, F. Blaabjerg, and S. Hansen. "Design and Control of an LCL-filter based Three-phase Active Rectifier," Conf. Rec. 36th IAS Ann. Meeting, Chicago, 2001, pp. 297-307.

[107] Liserre M., Blaabjerg F., Dell'aquila A., "Step-by-step design procedure for a grid-connected three-phase PWM voltage source converter," in International Journal of Electronics, vol. 91, n. 8, pp. 445-460, Aug.2004

[108] B. G. Gu and K. Nam, "A DC link capacitor minimization method through direct capacitor current control," in Proc. 2002 IEEE Industry Applications Society Annual Meeting, pp. 811 – 817

[109] Position Statement on Photovoltaic Interconnection, Solar Electric Power Association, October 2000.

[110] DER Interconnection Systems Technology Review, U.S. Department of Energy Quarterly Program Review, July 2002.

[111] "The Interconnection of Photovoltaic Power Systems with the Utility Grid: An Overview for Utility Engineers," Solar Design Associates, Inc., June 1994.

[112] "Distributed Electrical Power Generation - Summary of Alternative Available Technologies," US Army Corps of Engineers, Engineer Research and Development Center, September 2003.

[113] J. Wiles, "Photovoltaic Power Systems and the National Electrical Code: Suggested Practices," New Mexico State University, March 2001.

[114] "Connecting to the Grid – A Guide to Distributed Generation Interconnection Issues," IREC, 2004.

[115] "American National Standard for Electric Power Systems and Equipment Voltage Ratings (60 Hertz) [ANSI C84.1] ," National Electrical Manufacturers Association, 1996.

[116] IEEE Standard 1547-2003: "IEEE Application Guide for IEEE Std 1547, IEEE Standard for Interconnecting Distributed Resources with Electric Power Systems″

[117] IEEE Standard 929-2000: "IEEE Recommended Practice for Utility Interface of Residential and Intermediate Photovoltaic (PV) Systems".

[118] IEEE 519-1992: "IEEE Recommended Practices and Requirements for Harmonic Control in Electrical Power Systems"

[119] [Available Online] : http://www.iaei.org/magazine/05_b/wiles.htm

[120] "Interconnection for Wind Energy and Other Alternative Technologies", United States of America Federal Energy Regulatory Commission 18 CFR Part 35 (Docket No. RM05-4-000), January, 2005

[121] "Standardizing Generator Interconnection", Submitted by Bergey Windpower Co. to United States Of America Federal Energy Regulatory Commission, June, 2002

[122] Randall .S. Swisher, "Bringing Wind Energy up to Code," Public utilities fortnightly, June 2004.

[123] M. Liserre, R. Teodorescu, and F. Blaabjerg, "Stability of Photovoltaic and Wind Turbine Grid-Connected Inverters for a Large Set of Grid Impedance Values," IEEE Transactions on Power Electronics, vol. 21, no. 1, pp. 263- 272, 2006

[124] M. Liserre, A. Dell'Aquila, and F. Blaabjerg, "Stability improvement of an LCL-filter based three-phase active rectifier," in Proc. Power Electronics Specialist Conference 2002, vol.3, pp. 1195-1201.

[125] M. Malinowski, M.P. Kazmierkowski, W. Szczygiel, and S. Bernet, "Simple Sensorless Active Damping Solution for three-phase PWM Rectifier with LCL Filter," in Proc. IEEE Industrial Electronics Conference 2005, pp. 987-991.

[126] M. Prodanovic and T.C. Green, "Control and filter design of three-phase inverters for high power quality grid connection," IEEE Transactions on Power Electronics, vol. 18, no. 1, pp. 373-80, 2003

[127] R. Teodorescu, F. Blaabjerg, M. Liserre, A. Dell'Aquila, "A stable three-phase LCL-filter based active rectifier without damping," in Proc. IEEE Industry Applications Society Annual Meeting 2003, CD-ROM

[128] M. Bojrup, P. Karlsson, M. Alakula, and L. Gertmar, "A multiple rotating integrator controller for active filters," in Proc. European Conference on Power Electronics and Applications 1999, CD-ROM

[129] P.A.Dahono, "A control method to damp oscillation in the input LC filter of AC-DC PWM converters", IEEE Power Electronics Specialists Conference, Feb. 2002

[130] J. Dannehl, F.W. Fuchs, "PWM Rectifier with LCL-Filter using different Current Control Structures", European Conference on Power Electronics and Applications, Aalborg, April 2007

APPENDIX A

GRID INTERCONNECTION STANDARDS

A.1 PV System Interconnection to the Utility Grid

A.1.1 Interconnection Codes and Standards:

A position statement on photovoltaic interconnection released by the Solar Electric Power Association (SEPA) in October 2000 recommended that three national standards, the IEEE 929-2000, the UL Test Procedure 1741, and the NEC Article 690 are sufficient to form a basis for uniform, simplified technical interconnection guidelines. In addition, the IEEE 1547-2003 standard is also advised to be considered.

A.1.2 Considerations for Utility Interconnection and Requirements

A.1.2.1 Electrical System:

1. A Power-Conditioning Unit or PCU ,
2. Balance of System (including wiring and mounting structure), and
3. A means of connecting to the electric grid typically by back-feeding the main electric service distribution panel [112].

To generate high quality power for supply to AC utility system, the following requirements needed to be met.

A.1.2.2 Restrictions on Inverter:

The inverter has to be in accordance with UL 1741 standards and as such are guaranteed to meet IEEE 929-2000 [109]. No additional protection equipment is required to address technical concerns [109]. The following Figure A.1 illustrates a block diagram of a common system for hooking-up a PV system to the grid.

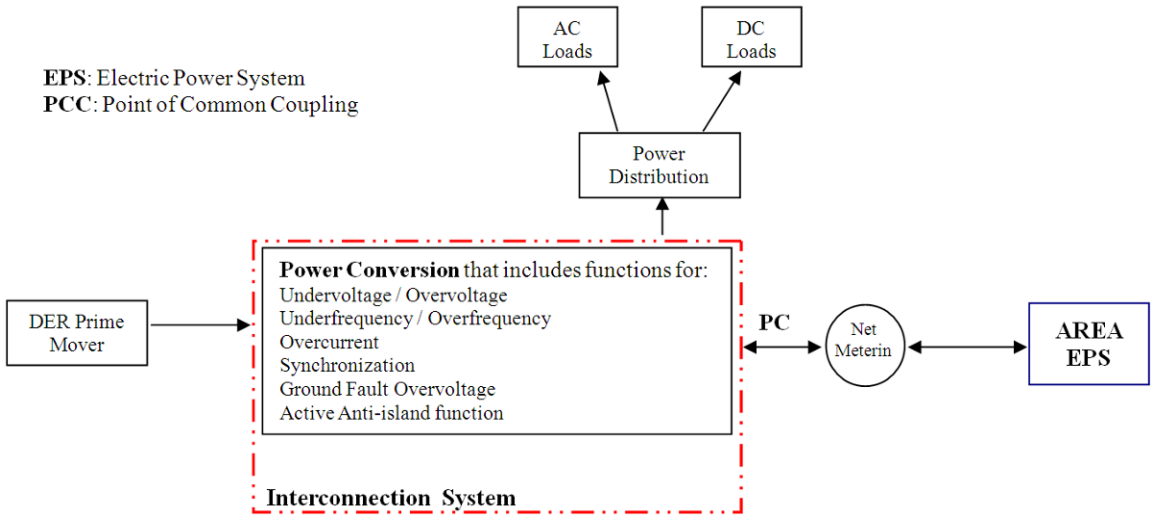

Figure A.1 Common Interconnection System for Small PV System with Net Metering [29]

A.1.2.3 Power Quality:

A.1.2.3.1 Voltage Fluctuation

Maximum allowed voltage variation should be +/-10% of the nominal voltage. On a 120 V base, this variation for small PV systems is specified to be 106-132 volts [116]. Also, voltage at the inverter output should not be more than 5% higher than the voltage at the point of utility [117].

A.1.2.3.2 Power factor

System power factor should be more than 0.85 (leading/lagging) for output greater than 10% of the rating. [117, 118].

A.1.2.3.3 Harmonics

Current THD should be less than 5% of fundamental frequency current at rated inverter output and less than 4% for each individual harmonic. Voltage distortion is not

under the control of the PCU but is more a function of the impedance of the distribution line. UL 1741 draft document on photovoltaic PCUs, specifies no more than 5% total RMS harmonic voltage, and no more than 3% for any one harmonic.

A.1.2.3.4 Frequency

If the line frequency decreases below 59.3 Hz or increases more than 60.5 Hz, the inverter should disconnect from the supply [116].

A.1.2.3.5 DC Current injection and Necessity of Isolation Transformer

The DC injection current is limited to 0.5% of the full rated output current. Also, most 12-48 V PV systems use inverters that have Power frequency/HF transformers to obtain the necessary 120-volt ac output voltage from the lower dc input voltage.

A.1.2.4 Protection-coordination:

A.1.2.4.1 Grounding of PV Arrays and Equipment in PV Systems

As per article 690-5 of the NEC, a ground-fault protection device (Ground Fault Interrupter) is required on all ungrounded PV systems even when the PV array is not mounted on the roof of dwellings where such a device is currently required [119]. Specifically, section 690.47 clarifies the requirements for grounding systems that have both ac and dc grounding requirements. Benefits to a solidly grounded PCU input circuit include; it is far less susceptible to lightning transients if tied to earth ground [33, 35].. Typically, all PV systems with inverters must have both the ac and the dc side of the system grounded since the internal transformer in the inverter isolates the dc grounded

conductor from the ac grounded conductor. Normally the ac part of the PV system is grounded at the ac service disconnect in utility-interactive systems [119].

A.1.2.4.2 External AC Utility-Interface Disconnect Switch

The 2005 NEC 690.14 (A)–(C) states that utility-interactive inverters must have dc and ac disconnects located at the inverter and an additional ac disconnect, usually at the ground level. But, for small PV systems, the additional external, manual, lockable disconnect for isolation from the utility line (shown by arrow in figure 2) is not necessary because of the inverter's built-in automatic AC and DC disconnect features as required by previous versions of NEC 690 [113]. The SEPA statement refers that for UL-listed non-islanding inverters, no additional protective equipment is required [111, 114]. Moreover, the National Electric Safety Code (NESC), which is applicable to equipment on the utility side of the meter states in section 173 that a visible break disconnect switch is mandatory only for circuits of more than 600 V.

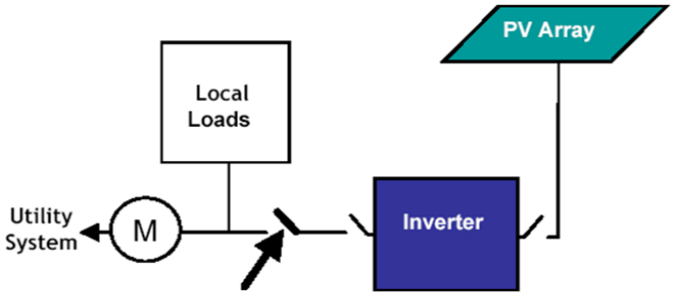

Figure A.2 Manual disconnect requirement in PV system [33]

A.1.2.4.3 Detection of Islanding Phenomenon / Islanding Protection

Islanding protection occurs if the utility line voltage is between 50% and 92% of its nominal value, the inverter should shut down in 2 seconds. A 5-minute delay is needed after utility grid power is restored before reconnection.

No Local Energy Storage: Batteries are not required because the grid supplies any extra demand as well as the low levels of power required at night. [111] Thus the utility effectively becomes an energy-storage bank, receiving energy when a surplus is generated and delivering energy when the load exceeds on-site generation [111].

A.1.2.4.4 Interconnect Location

The actual interconnection from the inverter to the utility service is typically done by back-feeding a circuit breaker on the distribution panel. NEC 690 requires that any back-fed circuit breaker be identified (listed) for that use and be retained by an additional securing device [111]. However, the 2005 NEC 690.64 (B) (5) states that back-fed breakers may not be clamped to the internal load center bus bar where they are connected to a listed utility-interactive inverter and where all circuit breakers in the panel are secured with a front panel [119].

A.2 Wind System Interconnection to the Utility Grid

A.2.1 ~ Interconnection Codes and Standards:

The standards/ regulations, which direct the interconnection of the wind systems to the grid, are:

- *IEEE 1094-1991* - IEEE recommended practice for the electrical design and operation of wind farm generating stations
- *IEC 61400* - Makes special mention of wind turbine specifications, safety and other technical issues related to the interconnection to the grid (Acceptance pending)
- *ANSI C 84.1* - American National Standard for Electric Power Systems and Equipment - Voltage Ratings (60 Hertz)
- *IEEE P1547-2003* IEEE Standard for Interconnecting Distributed Resources with Electric Power Systems

In addition, some standards, which have been developed for the interconnection of PV systems to the grid and general system interconnection, also are generally being used for the wind power systems. These are:

- *Underwriters (UL) 1741*- "Inverters, Converters and Controllers for use in Independent Power systems"
- *IEEE 929- 2000* "Recommended practice for utility interconnection of PV systems to the grid" (This standard is used for wind systems as well)
- *IEEE 519* – IEEE recommended practices and requirements for harmonic control in electrical power systems

A.2.2 ~ Considerations for Utility Interconnection and Requirements for the Facility

A.2.2.1 Electrical System:

1. A power-conditioning unit or PCU ,
2. Balance of System (including wiring and mounting structure), and
3. A means of connecting to the electric grid typically by back-feeding the main electric service distribution panel.

A.2.2.2 Power Quality:

A.2.2.2.1 Voltage Fluctuation

Maximum allowed voltage variation should be +/-10% of the nominal voltage. Also, voltage at the inverter output should not be more than 5% higher than the voltage at the point of utility. However, in the FERC 2005 regulation it was proposed that the voltage range for the wind systems could be +/-5% of the actual voltage base. [117,122]

A.2.2.2.2 Power Factor Design Criteria

A power factor within the range of 0.95 leading to 0.95 lagging has to be maintained at all times. However, the recent FERC 2005 commission proposes to make this specification with certain flexibility regarding whether the location of the reactive support equipment would be at the PCC of the plant rather than at the wind turbine [122].

A.2.2.2.3 Current harmonic distortion limits

Current THD < 5% of fundamental frequency current at rated inverter output and < 4% for each individual harmonic [118].

A.2.2.2.4 Frequency

If the line frequency decreases below 59.3 Hz or increases above 60.5 Hz, the inverter should disconnect from the supply [117].

A.2.2.2.5 DC Current Injection

A DR shall have a dc current injection of less than 0.5% of its rated output current.

A.2.2.3 Protection-coordination

A.2.2.3.1 Grounding

Normally solid grounding or high resistance grounding is employed [121].

A.2.2.3.2 Isolation Device

A readily accessible, lockable, visible-break isolation device shall be located between the DR and the EPS.

A.2.2.4 Other Utility-specific considerations:

- Dedicated/Isolation transformers.
- Direct transfer trip
- SCADA

The modern wind systems should be designed to [121]:

- Ride through system faults and continue to supply energy to the system when those faults clear.
- Contribute reactive power and active voltage control for stability of the grid

- Communicate with grid operators and be able to limit output or rate of change in output, if necessary, for grid reliability.
- The inverters used should have the capability for "Islanding Protection".

A.2.2.4.1 Interconnection issues at the time of starting and stopping of the turbine

Wind turbine controllers are to be programmed to let the turbine run idle without grid connection at low wind speeds because if the systems is grid connected at low wind speeds, it the turbine as a motor. Once the wind becomes powerful enough to turn the rotor and generator at their rated speed, the turbine generator should be connected to the electrical grid. Otherwise there will be only the mechanical resistance in the gearbox and generator to prevent the rotor from accelerating, and eventually over speeding.

Low Voltage Ride-Through Standard: This is not required for smaller systems like the one used in this dissertation, but is proposed for larger systems whose capacity is more than 10 MW [121].

A.3 Summary of Standards and Safety Requirements (PV)

Specification	Requirements	Standards
Voltage Range Required regulation Base Clearing time	 (114 V – 126V) +/- 5% 120-volt 1s for 110< V < 120	ANSI C84.1
Frequency Frequency range Clearing time	 59.3 – 60.5 Hz 0.16s	IEEE 1547 – 2003, IEEE 929 - 2000
Power Quality DC injection current Harmonic current distortion limit ***Individual (odd) harmonics order*** h < 11 11 ≤ h < 17 17 ≤ h < 23 23 ≤ h < 35 35 ≤ h Total demand distortion	Limited to % of full rated output current 0.5% 4.0% 2.0% 1.5% 1.5% 0.3% 5%	 IEEE 1547 - 2003 UL 1741 IEEE 519 - 1992 IEEE 929 – 2000, UL 1741
Voltage distortion limit Individual voltage distortion Total voltage distortion (THD)	% of nominal fundamental frequency voltage 3% 5%	IEEE 519 - 1992
Power factor	> 0.85 (lagging or leading) for output>10% of rating	IEEE 519 - 1992 IEEE 929 – 2000 UL 1741

Voltage variation	+/- 10% of nominal voltage (max)	IEEE 519 - 1992
Inverter voltage	Output < 5% of the voltage at the point of utility. Inverter clearing time 10 cycles (if the110% <utility voltage< 50% of nominal value)	IEEE 929 - 2000
Islanding protection	Utility line voltage – (50% - 92%) of its nominal value, clearing time 2s	IEEE 929 - 2000

A.4 Summary of Standards and Safety Requirements (Wind)

Specification	Requirements	Standards
Voltage Range Required regulation Base Clearing time	 (228V-252V) +/- 5% 120-volt 1s for 110< V < 120	ANSI C 84.1
Frequency Frequency range Clearing time	 59.3 – 60.5 Hz 0.16s	IEEE 1547 – 2003, IEEE 929 - 2000
Power Quality DC injection current Harmonic current distortion limit. Individual (odd) harmonics order h < 11 11 □ h < 17 17 □ h < 23 23 □ h < 35 35 □ h	Limited to % of full rated output current 0.5% 4.0% 2.0% 1.5% 1.5% 0.3%	 IEEE 1547 - 2003 UL 1741 IEEE 519 - 1992
Voltage distortion limit Individual voltage distortion Total Voltage distortion (THD)	% of nominal fundamental frequency voltage 3% 5%	 IEEE 519 - 1992
Power factor	> 0.9-0.95 (lagging or leading) for output>10% of rating	IEEE 519 - 1992 IEEE 929 – 2000 FERC 2005 (proposed)
Inverter voltage	Output <5% of the voltage at the point of utility. Inverter clearing time 10 cycles (if the110% <utility voltage< 50% of nominal value.	IEEE 929 - 2000
Islanding protection	Utility line voltage – (50% - 92%) of its nominal value, clearing time 2s	IEEE 929 - 2000

APPENDIX B

LCL FILTER CODE AND DAMPING MECHANISMS

B.1 LCL Filter Parameter Selection Code

```
% LCL Filter design. Procedure followed from paper
%A novel method of LCL type utility interface for three phase
voltage
% source rectifier" paper. I ripple = 3%, lambda = 2.5%

clear all;
clc;
P = 20e3;   %3 Phase power
Vdc = 400;
fs = 8e3;
ws = 2*pi*fs;   %Switching frequency
f=60;
wf = 2*pi*f;
V = 120; % RMS Phase voltage
lambda = 0.025; % max. fundamental Q absorbed by capacitors wrt
rated power
Iratedpeak = 70;
eta = 100*(wf*wf/(ws*ws));
Iripple = 0.03*Iratedpeak;
Ltotal = Vdc/(8*Iripple*fs)
x = (3*wf*V*V)/(ws*ws*Ltotal*lambda*P);
b = 1.3*(4/(1-2*x));
a = (b-2+sqrt(b*(b-4)))/2;
r = x*(1+a);
L2f = Ltotal/(1+a)   %Grid side filter
L1f = a*L2f       %Converter side filter
Cf = 1/(r*ws*ws*L2f)
fres = sqrt((L1f+L2f)/(L1f*L2f*Cf))*(1/(2*pi));
Rd = 1/(3*2*pi*fres*Cf); %% Passive damping resistor in series
with Cf
```

B.2 LCL Filter Damping

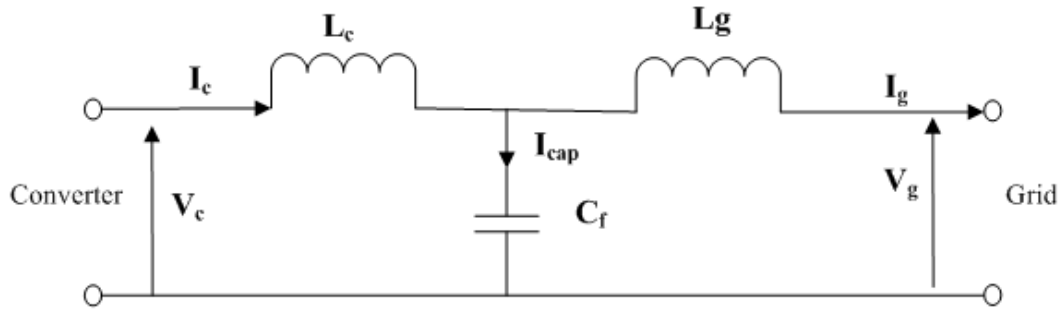

B.3 Comparison of L Filter and LCL Filter Response Characteristics

From Figure A.1, the converter current to voltage transfer function is given by

$$\frac{i_c}{v} = \frac{1}{L_c s}\frac{(s^2 + z_{LC)}^2}{(s^2 + w_{res}^2)} \tag{52}$$

Where:

$$z_{LC}^2 = \frac{1}{L_g C_f} \tag{53}$$

$$w_{res}^2 = \frac{(L_c + L_g) z_{LC}^2}{L_c} \tag{54}$$

and the grid current to converter voltage transfer function is given by:

$$\frac{i_g}{v} = \frac{1}{L_c L_g C_f s^3 + (L_c + L_g)s} \tag{55}$$

For comparison, the Figure B.1 gives the comparison of the L only and LCL filter response for the grid current to converter voltage. As it can be seen, the LCL filter performance is similar to an L-only filter response in the low frequency range, but has a resonance. This resonance causes oscillations in the system and hence adequate damping needs to be provided to the system. As was mentioned in the earlier section, several

damping methods have been proposed over the years with each method having its own merits and demerits.

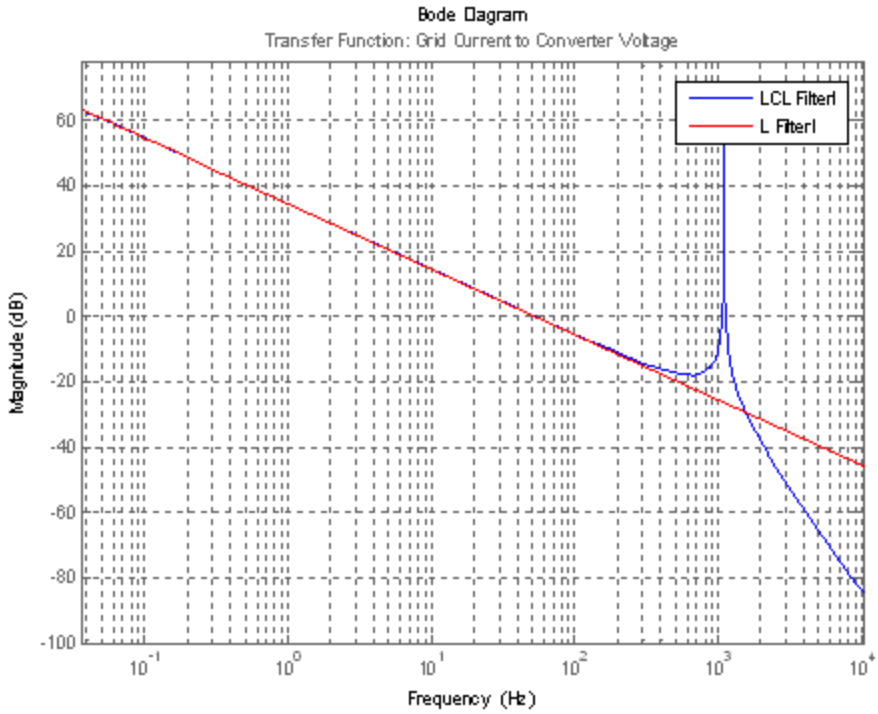

Figure B.1 Comparison of L-Filter and LCL Filter Grid Performance

B.4 Passive Damping

The oscillations caused by the LCL filter resonance can be reduced by increasing the damping in the system using a resistor. The objective of passive damping to insert an impedance at the resonant frequency to avoid oscillation. When a resistor is added in series with the filter capacitor, it introduces one zero and one pole more in transfer function of the system with the additional zero and pole attract the unstable poles into the stability region. The converter current to voltage transfer function with passive damping is given by:

$$\frac{i_c}{v} = \frac{1}{L_c s} \frac{(s^2 + z_{LC}^2)}{(s^2 + w_{res}^2 + (\frac{L_c + L_g}{L_g L_c}))} \tag{56}$$

Where R_d is the damping resistance.

One of the main constraints of the damping resistor is that it must be sufficient enough to avoid oscillation, but the losses but losses cannot be high as to reduce efficiency. Hence, the damping value is set to a similar order of magnitude as the series capacitor impedance at the resonant frequency, and is typically selected to be between 1/4 - 1/3 of the capacitor impedance at resonance. For the system under consideration, the damping resistor is calculated to 1.35 ohms for the resonant frequency and parameter values given in the earlier section.

Figure B.2 shows the performance of the system with and without passive damping. Even though this method is very simple it results in losses in the system. Also, the LCL filter effectiveness is reduced since the ripple injected into the grid increases.

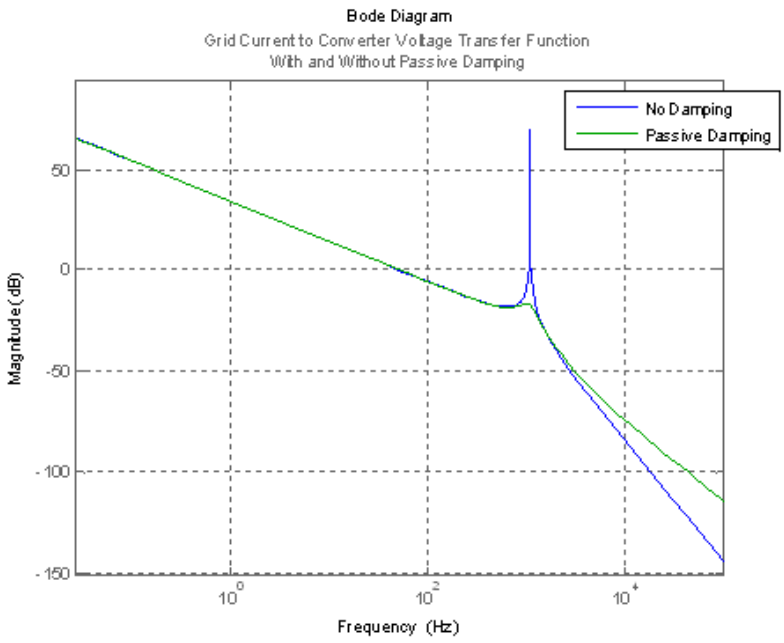

Figure B.2 Filter Performance with and without Passive Damping

B.5 Active Damping

Several other damping methods have been proposed over the years that involve changing the current control architecture of the system thereby reducing the losses as was seen in the case of passive damping. The effectiveness of these various methods depend on the number of additional sensors required complexity of the design and performance with varying grid conditions. In reference [123] the damping is achieved by adding to the current PI controller filter of second order in the open loop. A similar approach is done in reference [124] by the feedback of the voltage across the filter capacitors with lead elements. This method however requires additional sensors for capacitor voltage measurement. In reference [125] a high pass filter is used in the capacitor voltage feedback path and in reference [126] damping was done using the converter current and filter capacitor voltage measurement. Reference [127] uses only the grid current for damping, however, the current THD has increased comparatively and in reference [128] grid current with an additional capacitor current feedback is used for the damping. Reference [129] proposes a virtual resistor method, but it requires an additional voltage sensor or differentiation of the current which induces noise. There are also some approaches where all the three states of the filter are used for the damping and converter control.

Of all these methods, the approach based on grid current with capacitor voltage feedback, converter current with capacitor voltage feedback and the approach based on converter current control with grid voltage feedback are used more. The earlier methods have the advantage of being stable even with the weak grids but require an additional

sensor. Since a practical converter is always provided with a current sensor for protection purposes, and the grid voltage is typically sensed for orientating the control to the grid, the latter method has the advantage of using the already existing sensors used for a typical VSC control application. However, the tuning of the filter is difficult in the conditions when the grid is weak.

B.6 Comparison of Different Methods

B.6.1 Converter Current Sensor with Capacitor Voltage feedback method

A lead compensator was designed following the standard control principles for the converter current sensor with the plant transfer function as given in (53) and is inserted in the with the capacitor voltage feedback loop [124]. Figure B.3 shows performance of the system with this method.

It can be seen that the resonant peak above 0db is successfully damped.

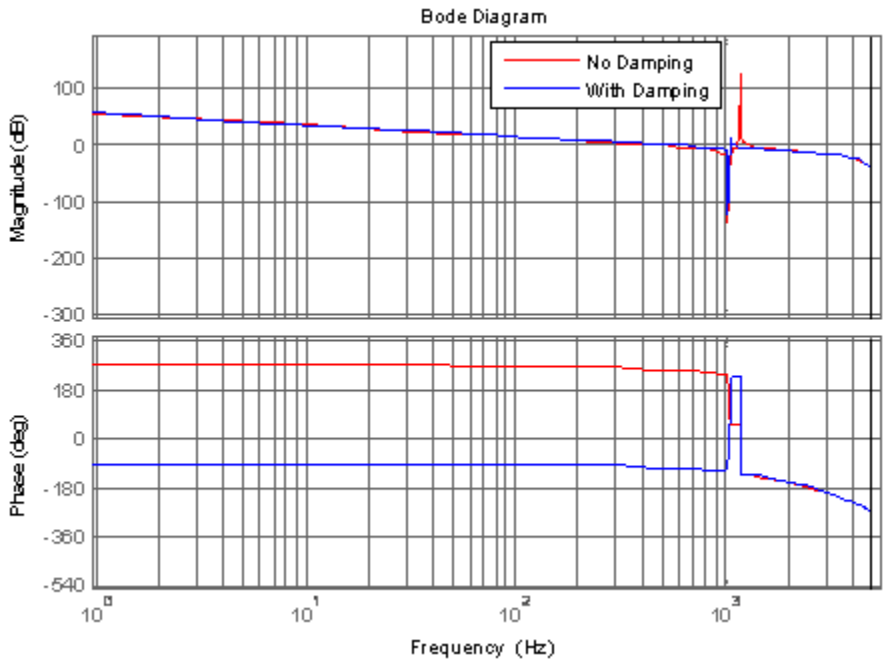

Figure B.3 Filter Performance - Converter Current and Capacitor Voltage Feedback Active Damping

B.6.2 Grid Current Sensor with Capacitor Voltage feedback method

Similar to the above method, a lead compensator is designed, however with the grid current sensor and capacitor voltage. Figure B.4 shows the performance of the system with this method.

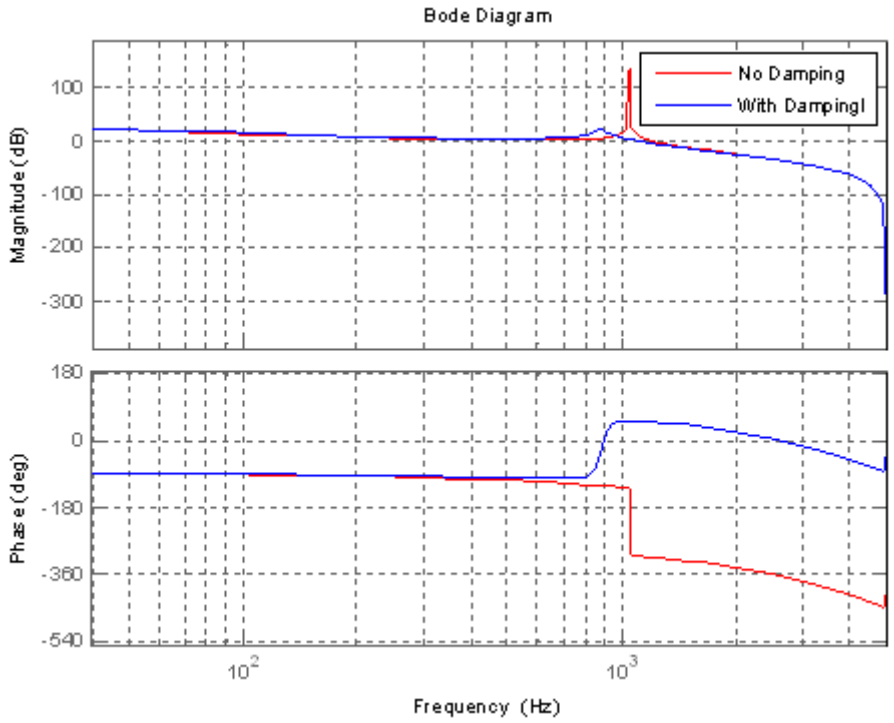

Figure B.4 Filter Performance - Grid Current and Capacitor Voltage Feedback Active Damping

Comparing the Figures B.3 and B.4 it can be seen that the method using the grid current sensor has an improved performance when compared to the converter current. However, as discussed earlier, this method requires extra sensors when compared to the earlier one.

B.6.3 Converter current control with Grid voltage feedback method

One of the main advantages of this method, and hence the popularity in the industrial applications is that it uses the sensors that are already used for the traditional VSC control and does not require any extra sensors. Keeping the cost criteria and the assumption of stiff grid consideration for this work, this method is selected for this work.

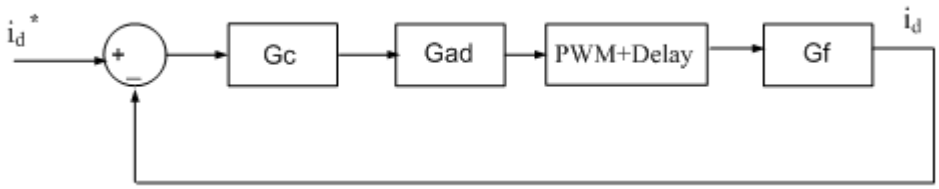

Figure B.5 Control with active damping of LCL Filte

Figure B.5 gives the current control architecture with active damping of the LCL filter. In the figure Gc is the transfer function of the PI controller, Gf is the transfer function of the plant (as given in equation (53)) , and Gad is the active damping transfer function. The damping of the system with converter current sensors can be done by introducing two zeros and two poles more in the system root locus such as to pull the unstable poles into the unit circle. The transfer function of the damping system is given by [124] :

$$\text{Gad} = \frac{K_{ad}(z^2 - z_o^2)}{(z^2) - p_o^2} \tag{57}$$

Where z_o and p_o are the active damping zeros and poles, K_{ad} is the unity dc gain

The choice of selection of the damping poles and zeros for the system is very crucial for this method and determines the performance of the system. The wider the angle between the damping poles and zeros, the more stable the system would be and some papers have adopted using advanced optimization algorithms like genetic

algorithm, particle swarm etc. to determine the optimum location of the poles and zeros. It was observed that the performance of the damping using this method is sensitive for line inductance variations or for weak grids [130] and tuning the filter would be difficult, but for a stiff grid, one of the optimum locations of the damping poles and zeros is at or close to the LCL filter poles and zeros [130]. The damping zeros attract the unstable LCL filter poles into the unit circle and cause damping of the system. Since a stiff grid is assumed in this study, the damping poles and zeros are designed to be close to the LCL filter zeros and poles. Figure B.6 shows the root locus plot of the LCL system without damping, and Figure B.7 shows the root locus plot with damping.

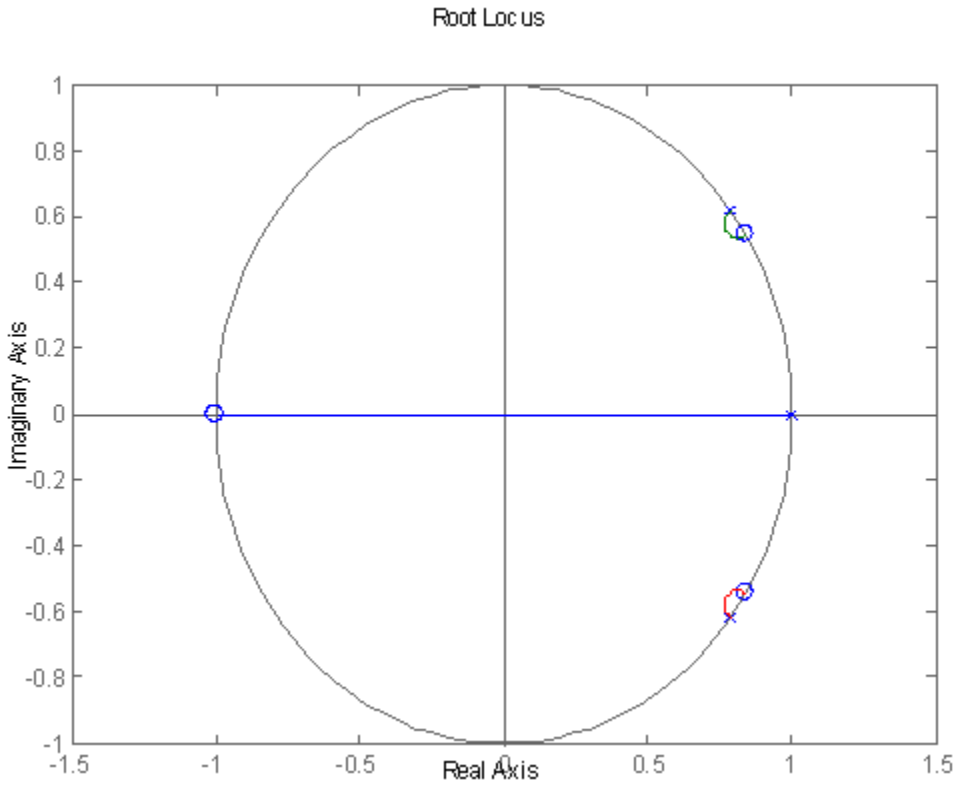

Figure B.6 Root Locus of LCL Filter System without Damping

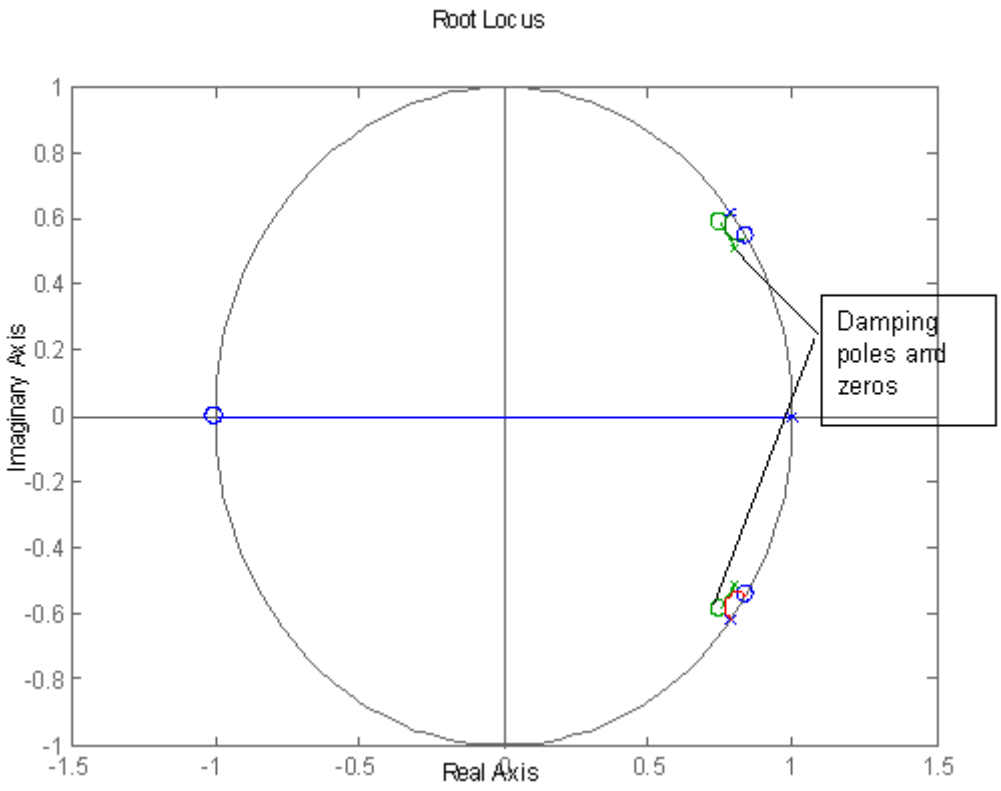

Figure B.7 Root Locus of LCL Filter System with Damping

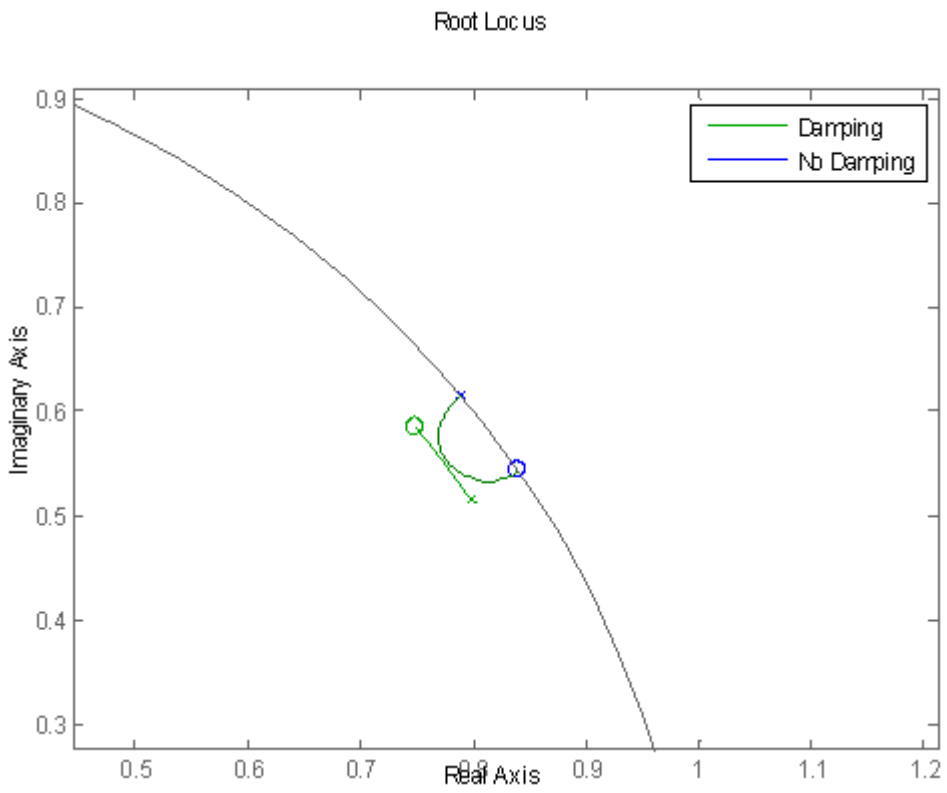

Figure B.8 Root Locus of LCL Filter System with Damping (Zoom in)

It can be seen that the damping zeros pull the unstable LCL filter poles into the unit circle. Figure B.9 shows the bode plot of the active damping filter and Figure B.10 shows the current control loop bode plot with and without damping. The active damping reduces the resonant peak below 0 dB,ensuring the system's stability.

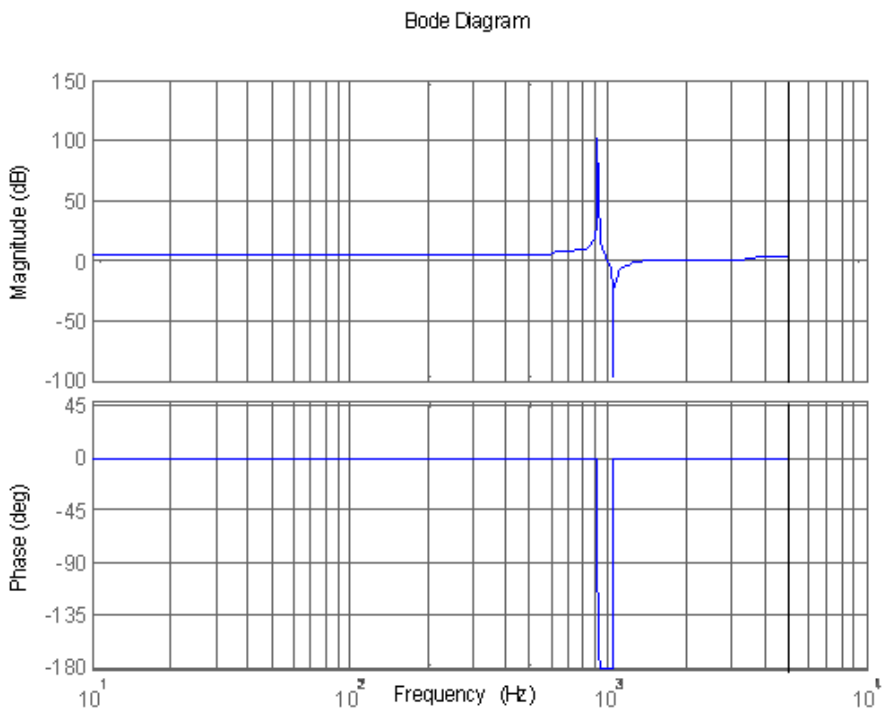

Figure B.9 Bode plot of only the Damping Element

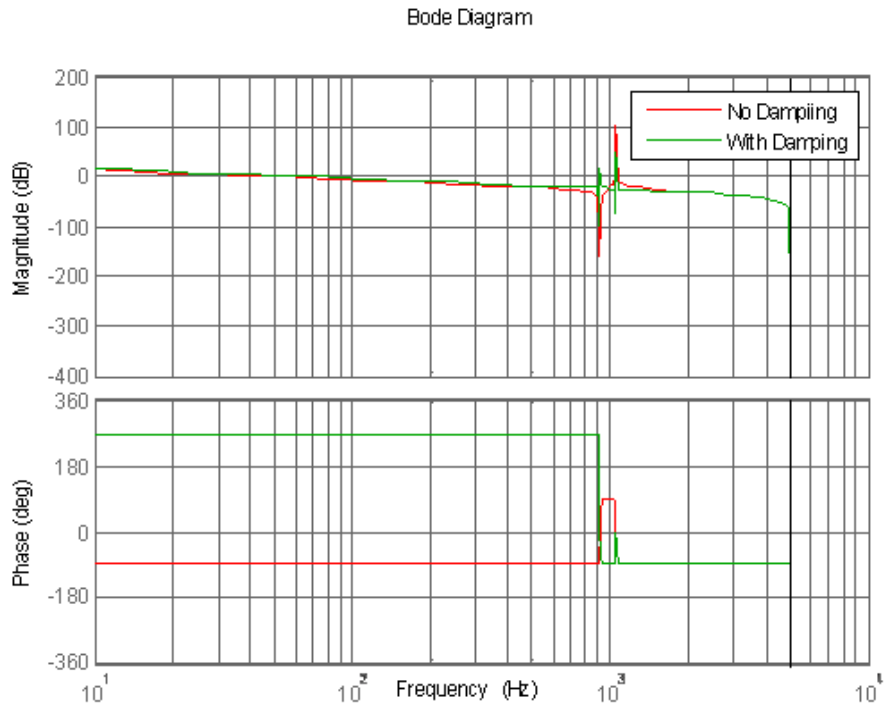

Figure B.10 Bode plot With and Without Damping